The mechanical properties of a liquid-filled porous solid with reference to articular cartilage

M. R. Litchfield

The Mechanical Properties of a Liquid-filled Porous Solid with reference to Articular Cartilage

by

M.R. Litchfield, B.Sc.

Thesis submitted for the degree of Doctor of Philosophy in the Faculty of Science, University of Durham.

September 1974.

Abstract

An investigation is made into the flow of fluids through deformable porous materials with the aim of an application to articular cartilage, which depends on interstitial fluid for some of its mechanical properties.

The law governing flows due to fluid pressure is shown to be valid in a cylinder of material with the same permeability in all directions, both with axial flow only and with axial and radial flow combined, up to Reynolds numbers of about 1. A literature survey shows that there is a large range of values of Reynolds numbers proposed as the limit of the validity of this law, indicating that there is no universal "critical" Reynolds number in flow through porous media.

The variation of permeability with strain is measured, both in directions parallel and perpendicular to the direction of applied strain, in a porous polymeric material.

A model of articular cartilage is proposed which consists of a porous solid matrix, which has a reversible non-linear load/displacement characteristic, with liquid-filled pores. Assuming a simple variation of permeability with strain predicts time-dependent deformations to a good degree of accuracy, agreement being excellent at normal physiological loads. Under oscillating loads, deformations are much larger than those predicted by the model, and it is thought that this is due to the effect of the bulk modulus of the cartilage, which becomes dominant in short term responses.

Acknowledgements

The author would like to express his sincere gratitude to the following:-

Professor G.R. Higginson, for his continued help and encouragement throughout this work.

The technicians of the Engineering Science Department, for their help in the experimental work.

Mrs. J.E. Snaith, for permission to quote several results from her experimental investigations.

Mrs. Gill, for typing my script.

Shell I.P.C. Ltd., for providing the author with financial support.

Contents

Notation

A	cross-sectional area of sample
A_n	$\frac{\text{area of pores}}{\text{area of (pores + solid)}}$
a_t	cross-sectional area of capillary tube
a, b	constants of force-deflection characteristic
C	ratio of mean free path and reciprocal of mean pressure
C_A	constant $\left(= \left(r + \frac{\delta r}{2}\right)\delta\theta\,\delta r\right)$
c	constant of integration
C_v	constant $\left(= \frac{V_o^2 T}{9\pi}\right)$
c_{vc}	coefficient of consolidation
d	length which characterises size scale of porous media (e.g. grain diameter)
D	distance separating two solid surfaces
e	void ratio
e_o	initial void ratio
E	Young's modulus of elastic material
f	porosity of model
f_1, f_2, f_3	function of strain
F	force to be carried
F_a	applied force
F_s	force carried by solid
F_f	force carried by fluid
F_o	sinusoidal force
g	acceleration due to gravity
$G(t), H(t)$	function of time only
h	head, height of fluid above surface of material
Δh	difference in head
H	thickness of material
I	pressure gradient

k_p	permeability
k_ρ	soil mechanics permeability
k_r	radial permeability
k_z	axial permeability
k_x, k_y	permeability in x, y directions
K	bulk modulus
L	characteristic length
L_c	length of a conductor
L_ϵ	length of a conductor at strain
l	length of material
m_{vc}	coefficient of volume compressibility
n	porosity
n_t	number of tubes
N	dimensionless constant ('shape factor')
P_s	load carried by soil
P_w	load carried by pore water
P_T	total load carried
p	fluid pressure
Δp	pressure difference
P	fluid potential $(= p + \rho g H)$
p_m	mean pressure
p_{atm}	atmospheric pressure
$p_{applied}$	applied pressure
q_v	flowrate
Q	total flowrate
Q_m	flowrate at mean pressure
R	external radius
R_c	capillary radius
R_e	Reynolds' number
r	distance from axis of symmetry

Δr	incremental distance in radial direction
δr	size of element in radial direction
r_a	radius of cylinder
t	time
δt	increment of time
T	original thickness of material
u_p	excess pore pressure
u	radial flowrate per unit area
u_x	flowrate per unit area in x-direction
v	initial porosity
V_o	total volume
V	flowrate/unit area
v_y	flowrate/unit area in y-direction
w	axial flowrate per unit area
W_s	mass of fully swollen specimen
W_D	dry mass of specimen
W	mass of specimen at any given time
Y	elastic modulus
z	distance along axis of symmetry
δz	size of element in axial direction
z_o	original thickness of cartilage
z_1	thickness at equilibrium after application of load
δz_o	initial value of δz
α, β	constant indices
δ	deformation from original thickness
δ_o	"instantaneous" response on compression
δ_1	"instantaneous" response after release of load
δ_x	creep deflection
ϵ	strain $(= \delta/z_o)$
$\epsilon_r, \epsilon_\theta, \epsilon_z$	strains in r, θ, z directions

$\dot{\epsilon}_z$	strain rate in z-direction
$\delta\theta$	angle of element
$\text{grad}\,\phi$	potential gradient
ρ	density of fluid
ρ_T	total settlement
$\delta\rho_T$	settlement experienced by thin layer
$\sigma_r, \sigma_\theta, \sigma_z$	stresses in r, θ, z directions
σ	total applied stress
$\dot{\sigma}$	increment of stress
σ'	effective stress
η	dynamic viscosity of fluid
ν	Poisson's ratio
ν_k	kinematic viscosity of fluid
ω	frequency of oscillation

1. Introduction

The aim of this research project was to show how the mechanical properties of porous materials are related to their porous nature. This project arose because of the interest shown at the moment in the functioning of human joints. Attached to the end of each bone in a joint is a thin layer of a substance called articular cartilage which is both porous and deformable, and is crucial to the normal functioning of synovial joints since its presence enables the transmission of high loads whilst maintaining contact stresses at an acceptably low level, and also enables movement with very little frictional resistance.

Amongst engineers it is the lubrication mechanism which has received a lot of attention, and there have been two basic lubrication mechanisms postulated in human joints. It is postulated, in the so-called theory of "weeping" lubrication[1] that when the cartilage is put under load, fluid seeps out of it and replenishes the lubricating fluid film. "Boosted" lubrication has been proposed in two forms, the first[2] is based on the fact that large molecules in the fluid are too large to pass through the pores of the cartilage, so that filtration through the cartilage will cause an increase in viscosity as the concentration increases. The second form[3] argues that, since the permeability (which can be thought of as conductivity to fluid flow) is so low in cartilage, almost all the flow is in the film and the large molecules may have some attraction to the surface of the cartilage, thus being prevented from flowing away from the centre of the film.

It appears, however, that, from a theoretical study of the squeeze-film situation[4][5] the permeability of cartilage is too low to play much part in the lubrication except perhaps at thin films when boundary lubrication regimes will be dominant, either in the "filtration" mechanism or in the

"weeping" mechanism. The main role of permeability in the mechanism of joint lubrication would therefore appear to be in affecting the mechanical stiffness of the cartilage layer. It would appear that no other material is quite so dependent on its porous nature as cartilage for its stiffness, this being due to its low permeability combined with a relatively low elastic modulus when compared with materials (such as rock) with an equally low permeability.

This thesis therefore describes the work performed on other porous materials in formulating a simple mechanical model of articular cartilage which predicts its response to various forms of loading.

Chapter 2 is concerned with the law which governs the transport of fluid through a porous material under fluid pressure, known as Darcy's law. Much work has been done on porous materials in this respect in connection with both soil and rock mechanics and a vast literature has been built up about the validity of Darcy's law.

Chapter 3 looks at the permeability-strain relationship in porous materials when large strains are imposed. For most practical purposes in porous materials the permeability is assumed constant, but bearing in mind that articular cartilage can be subjected to compressive strains of 0.5, this relationship has to be taken into account.

Having established this relationship, the theory for deformable porous materials is then formulated in Chapter 4. The solutions to some special cases are presented, and the numerical work (including computer programs) which is needed to solve some of the other special cases is described. A mention is also made in this Chapter of the theoretical approach made by engineers to the special case of soil mechanics.

Chapter 5 applies this theory to the special case of articular cartilage, making due reservations where necessary. The solutions are

compared to the experimental results already published and to some which have been produced in this Laboratory.

Chapter 6 presents some conclusions from the work described in the thesis.

2. Flow through Undeformed Porous Solids

2.1 Literature Review

The history of the study of the flow of fluids in porous media dates back to 1856, when Henri Darcy, a hydraulic engineer based in Paris, was engaged to enlarge and modernise the waterworks of the town of Dijon in the South of France. He wrote about these experiences in a book,[6] which describes in detail how he went about the task. It appears that during his time in Dijon he was called upon to design a filter bed of sand, and, finding there was no literature or design rules about such things, he set out to perform some experiments.

He built an apparatus consisting of a vertical iron pipe flanged at both ends, and fitted a grillwork inside the pipe which supported approximately 1 metre of sand. Water could be admitted into the apparatus by means of a pipe tapped into the vertical cylinder and could be discharged by a tap near the bottom. The flowrate could be controlled by means of valves at the inlet and exit from the cylinder. Mercury manometers were tapped into the open chambers above and below the column of sand, and these were used for measuring the inlet and outlet pressures. He tested four different types of sand, and was able to conclude that

$$q = -k_b I \qquad (2.1.1)$$

where q is the total flowrate

I is the pressure gradient

k_b is a constant, to be known as the permeability of the sand.

Written another way, Darcy's law can be expressed as

$$q = -k_b \frac{dp}{dx} \qquad (2.1.2)$$

where $\frac{dp}{dx}$ is the pressure gradient in the x-direction, or, generalizing the formula to any direction (see, for instance Scheidegger[7])

$$q = -k_p(\text{grad}\, p - \rho \bar{g}) \qquad (2.1.3)$$

where $\bar{g}$ is the gravity vector (of magnitude g and direction downward) and ρ is the density of the fluid.

The present-day expression of Darcy's law is

$$V = -\frac{k_x}{\eta}\frac{dp}{dx} \qquad (2.1.4)$$

where V is the flowrate per unit area of the porous material (filter velocity)

and η is the viscosity of the fluid.

Carrying out a dimensional analysis of this formula, we find that

$$k_x = Nd^2 \qquad (2.1.5)$$

where N is a dimensionless constant ('shape factor')

d is a length which characterizes the size scale of the pore structure, e.g. mean grain diameter.

For many years this formula was thought to be an empirical one, but several attempts have been made to verify it from first principles. Hubbert[8] has put forward a derivation of it starting from the Navier-Stokes equations, but his relating of microscopic and macroscopic quantities appear rather tenuous and seems to rely on arguments which have not been proved themselves. Both Whitaker,[9] from the momentum equations, and Poreh and Elata,[10] from the Navier-Stokes equations, showed that Darcy's law could be derived by neglecting inertial forces and provided that the correct averaging processes are introduced. Thus, it seems that because relationships between microscopic and macroscopic quantities are involved, a recourse to statistics is required, in order to prove Darcy's law totally (Collins,[11] Scheidegger[12]).

However, despite the absence of totally reassuring theoretical analysis, investigators have extended the results of a steady, one-dimensional, incompressible flow experiment to include transient, multi-

dimensional, compressible flow in anisotropic, compressible and elastic porous media,[13][14][15][12] and it seems to be acknowledged that Darcy's law plays the same role in the theory of the conduction of fluids through porous solids as Ohm's law in the conduction of electricity, or Fourier's law in the conduction of energy by heat.

Darcy's law, as discussed above, appears to give an adequate description of flow through porous media under a wide variety of conditions. However, as in any branch of engineering, it must be expected that there are limitations. Hudson and Roberts,[16] and Leva and co-workers,[17] have reviewed many experiments which demonstrate that Darcy's law is valid only in a certain "seepage" velocity domain outside which more general flow equations must be used to describe the flow correctly.

In order to characterise this seepage velocity domain, it is customary to introduce a Reynolds number as follows:

$$R_e = \frac{\rho V d}{\eta} \qquad (2.1.6)$$

where, in addition to the symbols already defined, d is a microscopic diameter associated with the porous medium ("pore diameter"). The occurrence of the quantity d in the definition of the Reynolds number immediately poses certain problems, in as much as it cannot be properly defined, but it is frequently taken as the grain diameter, as this gives the order of magnitude of the pore size. Nevertheless, many investigations have been attempted to establish a "critical" Reynolds number above which Darcy's law would no longer be valid. As in straight pipe flow, the contention was that there exists a universal critical Reynolds number above which the flow in the pores would become "turbulent". In these investigations, a great discrepancy regarding the universal critical Reynolds number became evident, the values ranging from 0.1[18] to 75,[19] although in the latter case the Reynolds number was based on an interstitial velocity (velocity through

the pores), and converting this to a filter velocity gives a critical Reynolds number of approximately 30. Nevertheless, the great uncertainty in these numbers seems to indicate that Reynolds' numbers being equal does not assure similarity of the flow in two different porous media.

It has generally been contended that the breakdown of Darcy's law is due to the onset of turbulence in the pores as this is known to occur in pipes. However, it is well-known that turbulence in pipes occurs at a Reynolds number of approximately 2000. In porous media, a breakdown of Darcy's law occurs at much lower Reynolds numbers (even if the latter is calculated with the interstitial velocity, rather than the filter velocity) which indicates that an entirely different cause of non-linearity is effective. The cause of non-linearity is that the inertial forces in the fluid become significant with respect to the viscous forces. In view of the Reynolds numbers being so small, it is inconceivable that true turbulence (statistical velocity fluctuations) plays any role at all. However, inertial effects will also become manifest in curved channels in laminar flow and therefore it has been concluded by Scheidegger[12] that the breakdown of Darcy's law is caused by the non-linearity in the flow equations describing laminar flow in curved channels.

The net result of these experiments is that above a "certain" value for the seepage velocity, Darcy's law is no longer valid and a universal characterisation of this value has not been achieved owing to the different structures in various porous media.

The high velocity flow phenomena occurring in porous media have been put into mathematical terms in several ways. Without attempting to understand the physics of the effect, various workers have simply tried to fit curves or equations to the experimental data so as to obtain a correlation between pressure drop and flow velocity. Scheidegger[12] has made a thorough review of all the modifications made to Darcy's law for these high velocities.

McKinley, Jahns, Harris and Greenkorn[20] have shown that Darcy's law can be adapted for flow of a non-Newtonian fluid by introducing a factor involving the square root of the permeability divided by the porosity.

It appears that the coefficient of permeability k_μ is not constant for the flow of liquids and gases through the same porous media. Fancher, Lewis and Barnes[21] and others have observed that air permeabilities are higher than liquid permeabilities in the same porous medium as calculated from Darcy's law. As far as a characterisation of the point where Darcy's law becomes no longer valid for gas flow is concerned, the facts can be summarised by stating that Darcy's law breaks down if the pore diameters become comparable with, or less than, the molecular mean free paths of the flowing gas. Ohle,[22] quoting Klinkenberg,[23] stated that the equation which applies for flow of a gas through a porous medium is

$$k_g = \frac{Q_m \eta L}{A(p_1 - p_2)} + \frac{4C}{p_m R_c} \qquad (2.1.7)$$

where p_m is mean pressure

$(p_1 - p_2)$ is the pressure difference over length L

Q_m is volume flux at the mean pressure

C is ratio between the mean free path and the reciprocal of the mean pressure

η is viscosity of the gas at the mean pressure

R_c is an average capillary radius

It can be seen from the literature on the subject that Darcy's law is widely held to be accurate for most purposes in describing the flow through porous media, but doubts are still held about its theoretical basis.

2.2 Darcy's law in axial and radial flow

As has been stated in 2.1, Darcy's law is widely held to be valid for most purposes describing flow through porous media, but doubts still exist, and so it was thought prudent, in view of the fact that the aim was to use Darcy's law to describe flow both axially and radially, to investigate Darcy's law experimentally both in axial and radial flow.

2.2.1 Definition of Problem

In order to verify Darcy's law in two dimensions, the aim was to allow flow both axially and radially in a porous material, measure the flowrates and compare them with flowrates obtained theoretically assuming Darcy's law to be valid.

It was necessary to assume Darcy's law to be valid in one dimension in order to obtain a coefficient of permeability (by the very definition of Darcy's law), which could be used in the computation, and so it was felt that an investigation into the range of validity of Darcy's law in one dimension should also be made.

The general scheme of the problem, showing boundary conditions, is shown in Figure 1.

2.2.2 Theory

This theory applies for three-dimensional flow of an incompressible fluid in an incompressible porous medium.

If we consider an undeformed porous material with axial symmetry, i.e. $\partial/\partial\theta = 0$ and examine the flowrates per unit area in an element (see Figure 2)

If u is the radial flowrate per unit area

w is the axial flowrate per unit area

Continuity gives

Flowrate in = Flowrate out

$$u.r.\delta\theta.\delta z + w\left(r+\frac{\delta r}{2}\right)\delta\theta\delta r = \left(u+\frac{\partial u}{\partial r}.\delta r\right)(r+\delta r)\delta\theta\delta z + \left(w+\frac{\partial w}{\partial z}.\delta z\right)\left(r+\frac{\delta r}{2}\right)\delta\theta.\delta r$$

$$\therefore \frac{\partial u}{\partial r}\delta r(r+\delta r)\delta\theta\delta z + \frac{\partial w}{\partial z}\delta z\left(r+\frac{\delta r}{2}\right)\delta\theta\delta r + u\,\delta r\,\delta\theta\,\delta z = 0$$

$$\frac{\partial u}{\partial r}\left[r\,\delta r\,\delta\theta\,\delta z + (\delta r)^2\delta\theta\,\delta z\right] + \frac{\partial w}{\partial z}\left[r\,\delta r\,\delta z\,\delta\theta + \frac{\delta z}{2}(\delta r)^2\delta\theta\right] + u\,\delta r\,\delta\theta\,\delta z = 0$$

neglecting terms in $(\delta r)^2$, and dividing through by $r\,\delta r\,\delta\theta\,\delta z$ gives

$$\frac{\partial u}{\partial r} + \frac{\partial w}{\partial z} + \frac{u}{r} = 0 \qquad (2.2.1)$$

If P is the potential, which is defined as

$$P = p + \rho g H$$

where p is the pressure in the fluid

and H is a height above an arbitrary datum level, then Darcy's law, accounting for effects of gravity, can be written as

$$u = -\frac{k_r}{\eta}\frac{\partial P}{\partial r} \qquad (2.2.2)$$

$$w = -\frac{k_z}{\eta}\frac{\partial P}{\partial z} \qquad (2.2.3)$$

where k_r, k_z are coefficients of permeability in the $r-$ and $z-$ directions respectively.

Substituting (2.2.2) and (2.2.3) into (2.2.1) gives

$$\frac{\partial^2 p}{\partial r^2} + \frac{1}{r}\frac{\partial p}{\partial r} + \left(\frac{k_z}{k_r}\right)\frac{\partial^2 p}{\partial z^2} = 0 \qquad (2.2.4)$$

which is a form of Laplace's equation in cylindrical co-ordinates.

Equation (2.2.4) is the governing equation for the potentials in the fluid throughout the porous material, providing the material is undeformed.

2.2.3 Numerical Analysis

The finite difference technique was used to obtain the solution to equation (2.2.4) with the given boundary conditions.

Using Noble,[24] the expressions involved are, in finite difference form,

$$\left[\frac{\partial P}{\partial r}\right]_{r,z} = \frac{[P]_{r-1,z} - [P]_{r+1,z}}{2\Delta r}$$

$$\left[\frac{\partial^2 P}{\partial r^2}\right]_{r,z} = \frac{[P]_{r-1,z} - 2[P]_{r,z} + [P]_{r+1,z}}{(\Delta r)^2} \qquad (2.2.5)$$

$$\left[\frac{\partial^2 P}{\partial z^2}\right]_{r,z} = \frac{[P]_{r,z-1} - 2[P]_{r,z} + [P]_{r,z+1}}{(\Delta z)^2}$$

the nodal points being in the order as shown below,

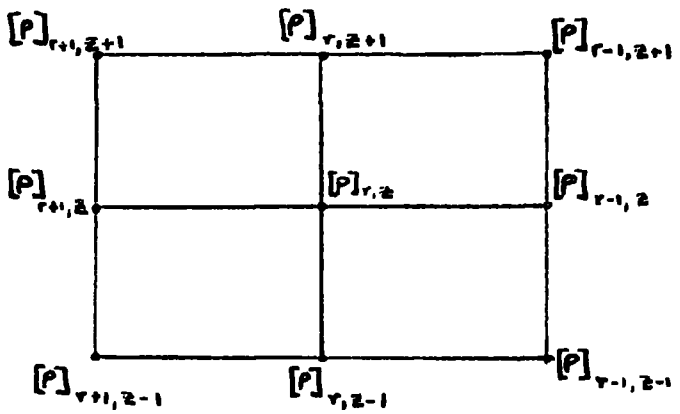

These formulae were substituted into equation (2.2.4) and an expression for $[P]_{r,z}$ was obtained for all parts of the fluid.

The boundary conditions used were:-

$z = 0 \qquad P = P_{applied} \qquad 0 \leq r \leq r_a$

$r = r_a \qquad P = P_{atm} + \rho g z \qquad l > z > 0$

$z = l \qquad P = P_{atm} + \rho g l \qquad 0 \leq r \leq r_a$

where P_{atm} is atmospheric pressure

$P_{applied}$ is applied pressure

l is length of porous material,

although the last condition was modified slightly because it was found that the fluid did not reach all parts of the porous material, and formed its own boundary, a free surface, inside the solid itself. This boundary was therefore, as will be shown later, found by trial and error.

A relaxation process was used to converge the (r, z) mesh of potentials, so that all potentials in the grid eventually conformed to the governing equation, and the applied boundary conditions. From these potentials, the flowrates per unit area could be calculated directly from Darcy's law:-

$$[u]_{r=r_a} = -\frac{k_r}{\eta}\left[\frac{\partial P}{\partial r}\right]_{r=r_a}$$

The evaluation of $\frac{\partial P}{\partial r}$ at the boundary is, however, rather more trouble than the calculation of the potentials. It is well known that numerical differentiation is notoriously unreliable (see Noble[24]) and any calculation of

$$\frac{[P]_{r_a,z} - [P]_{r_a-\Delta r,z}}{\Delta r}$$

will only give an estimate of $\left[\frac{\partial P}{\partial r}\right]$ at $r = r_a - \frac{\Delta r}{2}$. To evaluate $\left[\frac{\partial P}{\partial r}\right]_{r=r_a}$, therefore, a polynomial was fitted to the six values of potential nearest the boundary in the horizontal plane, and this polynomial was then differentiated "by hand" and the value $r = r_a$ substituted into the subsequent polynomial, thus:-

Fitted polynomial is

$$P = Ar^5 + Br^4 + Cr^3 + Dr^2 + Er + F$$

where A,B,C,D,E and F are constants,

$$\therefore \left[\frac{\partial P}{\partial r}\right]_{r=r_a} = 5Ar_a^4 + 4Br_a^3 + 3r_a^2C + 2Dr_a + E$$

This expression proved to give a much better estimate than any finite difference expression, although the calculated values of $[P]$ helped in

the respect that they were always smoothly decreasing as the value of the radius increased.

Once reliable figures had been obtained for $\left[\frac{\partial P}{\partial r}\right]_{r=r_a}$, the flowrates were evaluated by integrating the flowrates per unit area over the areas considered using the trapezoidal rule.

Several problems were encountered in the computing, especially in specifying the boundary conditions.

As can be seen from the boundary conditions, for an infinitely small step length, the potentials at the inlet corner are P_{atm} and $P_{applied}$ separated by the infinitely small step length, thus causing an infinite flowrate. Because the nodal points used in calculating a potential are horizontal and vertical, as opposed to the diagonal method, the value of the potential at the corner is never, in fact, used for the calculation of the potentials. As the mesh size was decreased, the flowrates at the corner became larger and larger and, in the limit, would have become infinite, so it was felt that the solution of the potentials and flowarates was complete (i.e. no more nodal increases needed) when the flowrates had converged in the rest of the mesh, and the flowrates per unit area at ($r_a, 0$) were extrapolated from the values of the other flowrates by means of curve fitting. This was a problem both in the axial inlet and radial outlet regions, but it was found that by using this method the values of the flowrate per unit area at ($r_a, 0$) in both directions were within 3%.

Another problem arose in the value of $[P]$ at $r = 0$. Substitution of $r = 0$ into equation (2.2.4) gives a value to $\frac{1}{r}\frac{\partial P}{\partial r}$ of infinity. The values at these points were therefore found by assuming the pressure distribution at the centre of the cylinder to be parabolic about $r = 0$:-

$$P_r = L + Mr^2$$

Symmetry is preserved by the fact that $\left[\frac{\partial P}{\partial r}\right]$ is zero at the centre of the cylinder,

$$P_{r=2\Delta r} = L + M(2\Delta r)^2$$

$$P_{r=\Delta r} = L + M(\Delta r)^2$$

Thus $$P_{r=0} = L = \frac{4P_{r=\Delta r} - P_{r=2\Delta r}}{3}$$

giving a value of the potential at the centre of the cylinder.

The last problem concerned the position of the free surface at the top of the cylinder, as has already been mentioned. Initially, the boundary was taken as being at the top of the cylinder, but negative output flowrates there showed this to be an unreal situation. The solution lay in the consideration of the equipotentials and streamlines (see Streeter[25]) of the flow in the porous material. The position of a free surface was assumed, and the potential mesh was then iterated to convergence. Lines joining points of the same potential (equipotentials) were drawn, and if these equipotentials cut the free surface orthogonally, then the free surface that had been assumed was taken as the boundary inside the material.

2.2.4 Experimental Work

For a diagram of the apparatus used in this experimental work, see Figure 3.

In order to verify Darcy's law axially and radially, it was necessary to investigate the law in one dimension and then use the coefficient of permeability obtained from this experiment to calculate from the computer program the theoretical flowrates in both axially and radially. Therefore it can be seen that a material was needed which was isotropic in all three dimensions.

Because of this last requirement, it was decided to construct a material from small beads of uniform size. In order to ensure that they were almost undeformable and unlikely to be corroded by a fluid such as oil or water, it was decided to obtain beads made from glass. The beads obtained from manufacturers were claimed to be spherical and by systematic sieving had diameters which were within the range of 0.89 to 1.0 mm.

The beads were contained in a cylindrical gauze cage (600 micron mesh size) of dimensions 100 mm diameter by 130 mm length. In order to obtain as close a packing as possible the beads were vibrated using a rod connected to an oscillator. When the cylinder was completely full of close-packed beads, a gauze lid was fixed to the cylinder so that the "solid" could not be deformed in any way.

2.2.4.1 Axial flow only

Around this gauze cage was fixed a perspex cylinder of dimensions 150 mm diameter by 250 mm length which had trays at 10 mm intervals leading out of the side of the gauze. The inlet to the cage was at the bottom and the only outlet at the top. For one-dimensional flow, pipes were fixed in each tray to allow the connection of stand pipes to measure pressure at any level in the porous material. Thus, with this arrangement, flow from the

inlet through the solid to the outlet would be one-dimensional.

To enable to range of Reynolds numbers to be studied, distilled water, two types of mineral oil (HVI 55 and HVI 160s), and air were used as percolating fluids.

The liquids were pumped through the apparatus by either a screw-thread action pump (for low flowrates) or a helical gear pump (for higher flowrates), connected to a variable speed gearbox. For the flow of liquids, potential (head) differences were read from identical glass standpipes of 5 mm inside diameter, which was thought large enough to make any surface tension effects negligible. Three standpipes were used to give two readings of head difference for each value of flowrate. Readings were taken by starting with a slow motor speed giving a low applied pressure and waiting for conditions to stabilize, steady conditions being shown both by constant head differences in the standpipes and flowrates being constant. Flowrates were measured by collecting the outflow during a measured time and weighing the contents. An increase in pressure was obtained by increasing the speed of the motor, conditions were again allowed to stabilize and readings taken. Temperatures of the liquids were read after exit from the apparatus in order to obtain the viscosities of the percolating fluids. Densities of the liquids at this temperature were also evaluated by weighing in a relative density bottle.

For gas flow, two of the pressure tappings were connected to a water manometer. Outlet from the apparatus was connected to a "Rotameter" which measured gas flowrate on the principle of balancing the weight of an aluminium float inside a tapered tube against the drag exerted by the gas on the float. These are not very accurate devices and in order to obtain a reasonably accurate range for the air flowrate, two Rotameters were

used, one for low flowrates and one for higher ones. The air to the inlet was taken through a valve from a compressed air supply, changes in pressure being made by opening of the valve.

2.2.4.2 Axial and Radial Flow

Once the tests had been concluded satisfactorily in the one-dimensional case, the apparatus was altered to make it amenable to axial and radial flow simultaneously. This involved the cutting out of a 60^{o} piece from the perspex cylinder in the top four trays. This was so that flow could pass out of the sides of the cylinder at each of the four heights, and then be collected and weighed. It was thought at the time that these outlets were sufficiently large not to hamper the flow coming out of the gauze cylinder and cause a resistance to flow. Any larger cuts might well have endangered the stability of the perspex cylinder.

The tests were then performed by pumping de-aired distilled water into the cylinder and allowing it to flow out radially from the cylinder of beads into the top four trays. Measurements of pressure were taken by means of the standpipes fixed to the tappings lower down the cylinder, so that the inlet pressures to the "radial flow" part of the fluid could be evaluated. Again the pressures were controlled by means of a variable speed gearbox connected to a helical pump. Flowrates were again measured by means of weighing the outflow during a given time interval.

2.2.5 Experimental Errors

In all experiments on porous materials involving liquids, the one practical hazard which occurs is that of air coming out of solution. The liquid is often passing through very small and tortuous channels and cavitation effects are easily obtained. The air then stays trapped in the pores thus causing a smaller area through which the flow can pass. Hence, for a constant pressure, smaller flowrates are observed as time passes. This problem was overcome by de-airing the liquids beforehand and measuring the flowrate to see that it was not decreasing with time for a constant applied pressure. This was not as much a problem as feared because pore sizes ranged from about 0.1 to 0.5 mm , which for a porous material is fairly large.

Flowrates were measured for liquids by weighing the outflow over a given time and the errors in these were as follows:-

HVI 160s

Weight	500 ± 1 gm	error ± 0.2%
Time	100 ± $^1/_5$ sec.	error ± 0.2%
	error in flowrate = ± 0.4%	

HVI 55

Weight	500 ± 1 gm	error ± 0.2%
Time	50 ± $^1/_5$ sec.	error ± 0.4%
	error in flowrate = ± 0.6%	

Water

Weight	600 ± 1 gm	error ± 0.2%
Time	20 ± $^1/_5$ sec.	error ± 1%
	error in flowrate = 1.2%	

Flowrate for air was measured by means of Rotameters. The manufacturers state that the error of an instrument of this sort is of the order of 5% at full scale displacement of the float and thus errors are greater for smaller displacements. With the flowrates used, the maximum error was never less than ± 3%.

Temperatures were measured to 0.2°C, and therefore errors in viscosities calibrated from these temperatures would be of the order of 1%. With the same figure for errors in density measurement, total errors for Reynolds numbers were as follows:-

HVI 160s ± 2.4%

HVI 55 ± 2.6%

Water ± 3.2%

Air ± 3% → ± 15%

Differences in head were read from identical glass standpipes, and it was thought that as differences were being measured, any errors due to the apparatus, such as surface tension effects, would be cancelled out, and the only errors which are not negligible are those associated with reading the heights.

HVI 160s

Δh 10 → 30 ± 0.1 cm error ± 1% → ± 0.3%

HVI 55

Δh 3 → 30 ± 0.1 cm error ± 3% → ± 0.3%

Water

Δh 1.5 → 5 ± 0.1 cm error ± 6.5% → 2%

Air

Δh 1.4 → 20 ± 0.1 cm error ± 7% → 0.5%

2.2.6 Experimental Results

2.2.6.1 Axial flow

Graphs are plotted as a non-dimensional filtration velocity (Reynolds number) versus difference in head per unit length.

Figures 4, 5, 6 and 7 show the variation of Reynolds number with differences in head for various ranges of Reynolds numbers.

Figure 4 is for mineral oil HVI 160s giving Reynolds numbers of the order of 0.002.

Figure 5 is for mineral oil HVI 55 giving Reynolds numbers of the order of 0.02.

Figure 6 is for distilled water giving Reynolds numbers of the order of 5.

Figure 7 is for air giving Reynolds numbers of the order of 20.

Discussion

Figure 4

Low Reynolds numbers are obtained by using an oil whose density (882 Kg/m^3) is of the order of that of water, but which has a dynamic viscosity of 230 cP. Darcy's law is shown to be valid by the linear proportionality of Reynolds number to head difference.

Figure 5

Slightly larger Reynolds numbers are encountered by using an oil of density 816 Kg/m^3 and a dynamic viscosity of 36 cP. Darcy's law is again shown to be valid.

Figure 6

Using water (density 1000 Kg/m^3, dynamic viscosity 1 cP), the gradual dominance of inertial forces is shown by the gradual tailing off of the graph, so that eventually an increase in applied pressure will give no increase in flowrate. From the graph it is very difficult to evaluate

at which point the line starts to deviate from linearity, but perhaps the graph is best left to show the increasing dominance of inertial effects as the applied pressure is increased.

Figure 7

High flowrates are obtained using air (density 1.23 Kg/m^3, dynamic viscosity 0.01 cP), the readings from the two Rotameters agreeing fairly well. Again the increase in inertial dominance is shown.

From these graphs we can examine the value of the coefficient of permeability for the material independent of the fluid passing through it.

From equation (2.1.4)

$$V = -\frac{k_x}{\eta}\frac{dP}{dx} = -\frac{Nd^2}{\eta}\frac{dP}{dx}$$

but $$\frac{dP}{dx} = \rho g \frac{dh}{dx}$$

where $\frac{dh}{dx}$ is the difference in head per unit length.

$$\therefore V = -\frac{Nd^2 \rho g}{\eta}\frac{dh}{dx}$$

$$\text{or } R_e = \frac{\rho V d}{\eta} = -\left[\frac{\rho}{\eta}\right]^2 [gd][Nd^2]\frac{dh}{dx}$$

where $\left[\frac{\rho}{\eta}\right]$ represents the fluid properties

and $[Nd^2]$ is the permeability of the material.

Now $R_e / \frac{dh}{dx}$ is the slope of the graph in each case

$$\therefore [Nd^2] = \frac{\text{Slope} \times [\nu_k]^2}{[gd]}$$

where ν_k is kinematic viscosity ($= \eta/\rho$).

As stated before, the slopes of Graphs 6 and 7 are rather hard to ascertain, but the largest one apparent in each case has been taken.

	$[\nu_k]$ m^2/s	Slope	$[Nd^2]$ m^2
HVI 160s	261 x 10^{-6}	0.285 x 10^{-3}	1.98 x 10^{-9}
HVI 55	44.3 x 10^{-6}	9.85 x 10^{-3}	1.97 x 10^{-9}
Water	1.0 x 10^{-6}	14.0	1.43 x 10^{-9}
Air	6.46 x 10^{-6}	0.041	1.74 x 10^{-9}

As can be seen, the values of the coefficient of permeability are all of the same magnitude and for values of small Reynolds numbers where slopes can be evaluated easily, the values for the two types of mineral oil are equal within experimental error.

For water and air, as has been stated, the slopes are extremely difficult to evaluate and it is quite possible that the figures for the slopes of the linear parts of the graphs may be higher than those quoted.

The value of 1.98×10^{-9} m^2 was used in the theoretical analysis as the coefficient of permeability of the material, and proved reasonably satisfactory.

2.2.6.2 Experimental Results for axial and radial flow

Figures 8 and 9 show the comparison of theory and experiment for three-dimensional flow of water. The three lines and points in Figure 8 refer to the flow in each layer, layer 1 being the lowest layer and layer 3 the highest, whereas Figure 9 shows the comparison of theory and experiment for the total flow involved.

Discussion

For the individual layers, agreement is poor for increasing applied pressures and this could be put down to one of two things. Inertial effects may be becoming increasingly significant, and although this would account for flow in Layer 1 diverging away from the theoretical line, it would not account for observed flowrates in Layer 2 being greater than theoretical values. The other reason might have been that the perspex spout used for catching the flow was causing a resistance to the flow and consequently fluid inside the material was pushed up into the next layer. This would account for observed flowrates in this layer being greater than theoretically calculated.

Figure 9 lends a great deal of support to the latter conclusion inasmuch that there is fairly good agreement between total and observed flowrates and theoretically calculated ones at both low and high values of inlet pressure. Therefore using Figure 9, it is clear that it is quite valid to use Darcy's law to evaluate flowrates in axial and radial flow simultaneously.

2.3 Conclusions on validity of Darcy's law

A literature survey and a series of experiments have shown Darcy's law to be valid in one-dimensional flow for low values of Reynolds number, ranging from zero to approximately unity and can be used with safety between these limits.

It has also been shown that Darcy's law can be used with some confidence to predict the flowrates in three-dimensional flow.

3. Variation of Permeability due to Deformation of Solid

When large strains are involved in the compression of a porous material, the constant of proportionality from Darcy's law, the permeability, can no longer be regarded as constant with variation in strain, although it is constant for a constant strain provided the range of Reynolds Numbers is within the limits mentioned in Chapter 2.

A study, both of the literature and by experiment, with a theoretical consideration, has therefore been made of the variation of permeability with strain.

3.1 Definitions

Throughout this work the following definitions have been used:

ϵ = strain = $\frac{\text{change in length from original length}}{\text{original length}}$

where compression is positive

n = porosity = $\frac{\text{volume of pores}}{\text{volume of pores + solid}}$

e = void ratio = $\frac{\text{volume of pores}}{\text{volume of solid}}$

Now consider a cube of side a,

let v = initial porosity

Volume of solids = $a^3(1-v)$

If we compress the cube to a height H (with no lateral expansion)

Then $\epsilon = \frac{(a-H)}{a}$

and, assuming all deformation is due to the closure of the pores, then

new volume = a^2H

and volume of pores = $a^2H - a^3(1-v)$

$= a^3(v-\epsilon)$

Porosity $n = \frac{(v-\epsilon)}{(1-\epsilon)}$

and Void Ratio = $\frac{(v-\epsilon)}{(1-v)}$

3.2 Review

3.2.1 Theoretical Work

The most widely used expression for estimating the coefficient of permeability from measured parameters is that derived by Kozeny[26] and later modified to add a further element of generality by Fair and Hatch.[27]

It is not possible to derive a relationship between permeability and porosity on very general grounds, and one must be satisfied with discussing particular idealized models of a conducting body. Most models of this type are based on the flow of fluids in cylindrical tubes or between parallel plane surfaces.

If q is the volume of fluid flowing per second through a tube of radius r along which is imposed a potential gradient, $\text{grad}\ \phi$, then Poiseuille's equation gives

$$q = -\frac{\pi \rho g r^4}{8\eta} \text{grad}\ \phi$$

or the corresponding equation for flow per unit width of a plane slit between solid surfaces which are separated by a distance D is

$$q = -\frac{\rho g D^3}{12\eta} \text{grad}\ \phi$$

With a concentration of n_t tubes per unit area of total cross-section of the body, the total flowrate

$$Q = n_t q = -\frac{n_t \rho g \pi r^4}{8\eta} \text{grad}\ \phi$$

Because, for this model the porosity f is equal to the area of conducting channel per unit area of cross-section, i.e. $n_t \pi r^2$ the above equation may be rearranged and written:

$$Q = -\frac{\rho g f r^2}{8\eta} \text{grad}\ \phi$$

and comparison with Darcy's law (equation (2.1.4.)) for one-dimensional flow gives

$$k_x = \frac{\rho g f r^2}{8} \qquad (3.2.1)$$

Let it now be supposed that, with either of the above models conducting fluids in the direction of a principal axis, one adds an extra set of plane slits, each with its plane perpendicular to the direction of the potential gradient. Each of these slits will lie in an equipotential surface and there will therefore be no tendency for them to facilitate the movement of fluid, except that insofar as, at junctions between intersecting slits, that slit which is the effective conducting element will have a locally increased width and will therefore make a slightly enhanced contribution to the permeability. On the whole, however, that part of the porosity which is contributed by the equipotential slits is ineffective and may, for the purpose of assessing permeability, be regarded as dead space. In any static measurement of total porosity, however, this dead space is indistinguishable from the effectively conducting channels, and the permeability will only be proportional to the total porosity if, fortuitously, the dead space increases in the same proportion as the effective space.

It is possible to give Equation (3.2.1) a far more general appearance and thereby to hide the fact that it is, by its derivation, applicable only to the capillary tube model, by writing

$$k_x = \left(\frac{\rho g f^3}{2\eta}\right)\left(\frac{1}{n_c 2\pi r}\right)^2$$

and assigning the symbol A_S to the specific surface area developed by the conductor, namely the total surface area of the solid part divided by the volume of that solid part,

$$A_S = \frac{n_c 2\pi r}{(1-f)}$$

and

$$k_x = \left(\frac{\rho g}{2\eta}\right)\left(\frac{1}{A_S^2}\right)\left[\frac{f^3}{(1-f)^2}\right] \qquad (3.2.2)$$

which is known as Kozeny's equation.

It is mainly used in evaluating the permeability of powders and when used for a geometry for which it was not derived, the constant 2 is usually replaced by an empirically determined "pore shape factor" which is commonly in the range from 2 to 2.5.

3.2.2 Experimental Work

There appears to be a fair amount of literature comparing permeability and porosity, especially in the fields of soil mechanics and powder metallurgy (see, for instance, Mitchell, Hooper and Campanella,[28] or Grootenhuis and Leadbeater[29]). But all this work seems to be applied to the permeability and porosity of different materials or powders with varying porosities. No work appears to have been performed on the same material as it is being compressed, which is what is required here. Morgan[30] states that for the same material there is an approximately linear relationship between log (permeability) and log (porosity) which means

$$k \propto (n)^{\beta}$$

with β constant.

This would seem reasonable in the sense that zero permeability would result from zero porosity, but the factor β is not defined. Taylor[31] states that for fine-grained soil the relationship between void ratio and log (permeability) is a linear one, but this only covers a small range in void ratio.

These relationships all tend to bear out Fraser's statement:[32] "No correlation can safely be made between two samples on the basis of their porosity, unless it is certain that all their physical properties are identical."

However, it would seem more reasonable to expect some sort of correlation of permeability and strain from a material which is being compressed and therefore does not differ in physical content, only in pore shape and size.

3.3 Experimental Work Performed

From the literature survey, it appeared that no experimental work had been performed of the type that was required, i.e. the measurement of the change of coefficient of permeability in the axial and radial directions as a porous material was compressed, and that no theoretical model could be produced which would simulate these characteristics. Therefore an experiment was designed to measure these coefficients as an increasing applied compressive strain was applied to the material.

A diagram explaining the orientation of axial and radial directions with respect to the direction of the applied strain is shown in Figure 10.

3.3.1 Material

The requirements for the material to be used in the experiments were

(i) to be reasonably thick so that large strains could be measured accurately with dial gauges

(ii) to have as low an elastic modulus as possible so that the force needed to compress a large area of the material to an appreciable strain would be within the range of a testing machine in the laboratory

(iii) to have as large a permeability as possible so that measurement of flowrate would be less susceptible to error

(iv) to have as large a porosity as possible, so that large strains could be accomplished before total closure of the pores

(v) to be "solid", in that strains would be transmitted equally through the material and not just, as in a sponge, near the parts of the material where the load was being applied

(vi) that the cut edges of the material could be capable of being sealed, so that no fluid would pass through.

To fulfil requirement (ii), it was obvious that sintered metal was not the answer, and that a plastic of some sort would be needed. Requirement (i) was also a problem insofar as most sintered plastic is made in thin sheets (of the order of 1 to 5 mm thickness) because it is mainly used as a man-made substitute for leather in the shoe industry. The information also was that any attempt to manufacture the material in the laboratory to any reasonable thickness and area would probably result in a very uneven permeability and porosity from layer to layer and complete closure of the pores on one side of the material. Eventually, two filter tiles were obtained from Schumacher Filters Ltd. These tiles were of thickness approximately 20 mm and 1 m x 1 m area. Their quoted porosities were 40-45 per cent. One was a type intended for use in pneumatic fluidisation and pneumatic conveyance of powders and granular products, and the other a filter element for liquids and gases. Manufacturer's literature quoted the elements as being made from a polyolefine base and totally resistant to absorbing moisture. The material also had the advantage of appearing to be made from sintered fibres, which as shall be seen later, resembles articular cartilage in that respect.

3.3.2 Measurement of Initial Permeability

In order to have some data on the coefficient of permeability for the filter tiles, some experiments were initially performed on the undeformed material.

The method of measuring permeability was the method of falling head. A diagram of the apparatus is shown in Figure 11. A cylindrical plug of the material of 10 mm diameter was wrapped with tape to stop flow out of the sides, and fitted into the bottom of a copper tube. In order to evaluate the head in the tube, a glass tube was fitted into the side of the apparatus, so that the level in the copper tube could be measured.

Water was allowed to fall through the material under gravity and readings of head and time were taken. Difficulty was found in air coming out of solution when passing through the small pores (of the order of 50μ diameter). The air was found to collect on the face of the material, giving a smaller area for the water to flow through. This gave the effect of decreasing the flowrate and could be seen clearly from a subsequent deviation in the linearity of the graph plotted from the results. These problems seemed to disappear when de-aired water was used.

The method of a falling head is probably the most accurate for measuring the coefficient of permeability insofar as neither pressures nor flowrates are measured directly and the consequent errors in their measurement are absent. Providing the heights read are accurate and the cross-sectional areas of the tubes (and the specimen) are known, then very little accuracy should be lost in measurement.

The coefficient of permeability was evaluated by using the theory shown below:-

Referring to Figure 11,

Darcy's law states that, for the x-direction

$$V_x = -\frac{k_x}{\eta}\frac{dp}{dx}$$

as for Equation (2.1.4)

and in this case

$$\frac{dp}{dx} = \frac{\rho g h}{T}$$

where h is the head of fluid above the sample

and T is the thickness of the sample

and $$V_x = \frac{(A+a_t)}{A}\frac{dh}{dt}$$

where t is time

A is cross-sectional area of copper tube

a_t is cross-sectional area of glass tube

$$\frac{(A+a_t)}{A}\frac{dh}{dt} = -\frac{k_x}{\eta}\frac{\rho g h}{T}$$

$$\therefore \log_e h = -\frac{k_x \rho g A}{\eta T (A+a_t)}t + c \qquad (3.3.1)$$

where c is a constant.

Thus a graph of $\log_e h$ vs. t will be linear with a slope of $\left[-\frac{k_a \rho g A}{\eta T(A+a)}\right]$

Both axial and radial permeabilities of the tile were measured in this way, and in the former case proved perfectly adequate. However, radial plugs involved passing water through surfaces which had been cut by hand, and in many cases the measured permeability was substantially lower than in the normal case. It was discovered by investigation under a microscope that, in the course of the cutting, the heat generated had welded most of the material together, and almost sealed up the faces, and in cutting much more gently and slowly and using cooling water, the results were much more satisfactory.

It was found that the material was not homogeneous on the scale that was measured, but over large areas these differences were found to average out to an overall permeability.

Typical graphs of head and time are shown in Figures 12 and 13 for the axial and radial directions respectively. Figures 14 and 15 show the variation of $\log_e h$ and t, and the linearity from which the permeability can be calculated.

Slope of Graph = 1.35×10^{-3} sec^{-1}

Slope of Graph = 1.12×10^{-3} sec^{-1}

in the axial case T = 20 mm

in the radial case T = 26 mm

Axial permeability = 0.275×10^{-11} m^2

Radial permeability = 0.295×10^{-11} m^2

These values were typical of permeability in the unstrained material.

3.3.3 Measurement of Initial Porosity

Measurement of porosity was obtained by initially weighing a cube of known volume of the porous material and then placing it under water and under vacuum until it was thought that all the air had been extracted from the material. The cube was then taken from the water, any surface water wiped away, and the whole specimen weighed again. This process was repeated twice more to ensure that the specimen was full of water, and all air had been extracted.

It was found that because of the fineness of the pores, once water had entered the centre of the specimen, it stayed there until evaporation occurred, and so it was thought that errors caused by the draining of part of the interstitial water were minimal.

This method ensured that only the effective porosity (i.e. pores interconnected with each other and finally to the boundaries) was measured. The other method of measuring porosity is by compressing the material until all pores are closed, and this therefore measures total porosity (effective and ineffective pores).

The porosity was calculated from the results below:-

Volume of material $= 31.2 \times 10^{-6} \pm 0.3 \times 10^{-6}\ m^3$

Mass of material dry $= 17.45 \times 10^{-3} \pm 0.05 \times 10^{-3}$ kg

Mass of material + water $= 29.90 \times 10^{-3} \pm 0.05 \times 10^{-3}$ kg

Mass of water $= 12.45 \times 10^{-3} \pm 0.1 \times 10^{-3}$ kg

Temperature $= 20^{\circ}C$

Volume of water $= 12.45 \times 0.998 \times 10^{-6}\ m^3$

$= 12.43 \times 10^{-6}\ m^3$

$$\text{Porosity} = \frac{\text{Volume of voids}}{\text{Total Volume}} = \frac{12.43}{31.2} = 0.40 \pm 0.01$$

3.3.4 Apparatus

A diagram of the overall apparatus for measuring permeability with variation in applied strain is shown in Figure 16.

The purpose of the experiment was to pass water under a constant, measured head through the porous plastic material and collect the outflow, whilst a compressive strain was applied to the material. For the construction of the porous specimens see below. The apparatus basically consisted of a reservoir on either side of the porous material through which water passed under gravity. Next to the specimen was placed a steel plate with 256 5mm diameter holes bored through it into a reservoir. Led out of the reservoir were two copper pipes connected at a T-junction to either another reservoir at the inlet or atmosphere at the outlet side. A constant head at the inlet was maintained by a simple overflow device. Compression was effected by loading the apparatus in a 500KN Denison testing machine.

Porous Specimens

Diagrams of the porous specimens are shown in Figures 17(a) and 17(b).

Axial Permeability

A 150 mm x 150 mm square of porous plastic was cut and placed between two 6 mm plates of Porosint bronze filter (Grade A) of the same size. The whole of the outside edge of this "sandwich" was then coated with araldite in order to prevent leakage around the sides. The bronze discs had a much larger permeability than the plastic, so that no constriction of flow was produced, and achieved a two-fold purpose. They provided a firm base for the porous plastic to be strained equally across the area, and not just where the steel plates were solid, and the discs also served to diffuse the flow before it reached the plastic, so that flow took place over the whole area, and not just in the places where the flow passed through the

steel plate. In both these objectives the bronze discs seemed to prove highly successful. Gaskets could not be used for sealing, because of their finite deformation and the problems of its measurement in relation to the subsequent measurement of deformation of the plastic, so the bronze discs were pushed up against the steel plates and then plasticene was used to seal the boundary.

Radial Permeability

Two 30 mm x 150 mm plates were cut from the bronze discs, and these were glued to two 120 mm x 150 mm x 6 mm brass plates. These were then placed as shown in Figure 17(b), and the sandwich made up with araldite as in the axial permeability case. The only passage for the flow was then axial at the inlet and outlet and radial flow everywhere else. In this manner, flow never passed through any cut surfaces and the consequent problems mentioned in Section 3.3.2 were absent.

3.3.5 Measurements

The measurements taken were of flowrate, deformation and load.

Flowrate, as in Section 2.2.4, was measured by means of collecting the outflow and weighing it.

Deformation was measured by means of dial gauges fixed to the lower, stationary part of the testing machine.

Load was measured by the testing machine. This load was measured only so that a repeated experiment without the porous plastic would give the deformations of the bronze discs alone and therefore deformations of the plastic alone could be calculated by subtraction at the same value of load.

It was found at the start of the experiment that the air in the plastic material tended to block some of the flow of water, similar to the

experience noted in Section 2.2.5. However, flow was facilitated at the start by the use of a vacuum pump connected to the outlet side of the apparatus which drew much of this air out initially, and results were then found to be steady after the removal of the pump. It was always found at the start of an experiment that flowrates tended to increase slightly for small increases in load, and it was thought that this initial action was dislodging any bubbles which may have formed on the surface. De-aired water was again used throughout the experiment for the same reasons as noted before.

Almost every range of strain was covered at least twice, this being done by releasing the load and then allowing a certain amount of relaxation of the strain before applying the load once more.

The experiment was repeated identically without the porous plastic so that the permeability and deformations of the apparatus alone could be evaluated. It was found that the bronze discs deformed elastically in the range tested, and flowrates only changed to a very slight degree when these discs were deformed.

3.3.6 Computation for permeability-strain relationships

In both the normal and tangential flow cases, there are pressure drops due not only to the porous plastic but also due to the rest of apparatus, this being mainly due to the bronze discs. Therefore consideration has to be made of their combined effect in producing the flow.

Consider the situation for a given flowrate

The pressure drop across the porous plastic = p_1

and the pressure drop across the apparatus = p_2

Total Pressure drop $\Delta p = p_1 + p_2$

P_1 is given by Darcy's law:-

$$\frac{Q}{A} = \frac{k_z}{\eta} \frac{P_1}{H}$$

P_2 is given by a constant of proportionality

$$Q = C_A P_2 \qquad \text{where } C_A \text{ is a constant}$$

$$\therefore \quad \Delta P = Q\left[\frac{\eta H}{k_z} + \frac{1}{C_A}\right]$$

or

$$k_z = \frac{\eta H}{\left(\frac{\Delta P}{Q} - \frac{1}{C_A}\right)} \qquad (3.3.2)$$

Axial Permeability

It can therefore be seen that the permeabilities can be easily calculated from the varying flowrates and thicknesses measured for increasing strain by using equation (3.3.2).

Radial Permeability

As can be seen from Figure 18(b), flow in this case was two-dimensional, and in order to obtain the permeability for a given flowrate and thickness, resort had to be made to numerical methods.

In order to formulate the equations governing the flow, consider the continuity equation in Cartesian co-ordinates:-

$$\frac{\partial u_x}{\partial x} + \frac{\partial v_y}{\partial y} = 0$$

where u_x is the flowrate per unit area in the x-direction

and v_y is the flowrate per unit area in the y-direction.

Substitution of Darcy's law gives Laplace's equation to two dimensions:-

$$k_x \frac{\partial^2 P}{\partial x^2} + k_y \frac{\partial^2 P}{\partial y^2} = 0$$

As in Section 2.2.3, writing $\frac{\partial^2 P}{\partial x^2}$ and $\frac{\partial^2 P}{\partial y^2}$ in finite difference form gives an expression for the potential at a point

$$P_{I,J} = \left[\frac{k_x\left(P_{I+1,J} + P_{I-1,J}\right)}{(\Delta x)^2} + \frac{k_y\left(P_{I,J+1} + P_{I,J-1}\right)}{(\Delta y)^2}\right] \Big/ \left(2\left[\frac{k_x}{(\Delta x)^2} + \frac{k_y}{(\Delta y)^2}\right]\right)$$

Iteration of this expression throughout a mesh gives the potentials and hence the flowrates (from Darcy's law) for given boundary conditions.

In this case, referring to Figure 18(b), the boundary conditions are

$$y = 0 \qquad 0 \leq x \leq 3 \text{ cm.} \qquad P = 0$$

$$y = H \qquad 12 \leq x \leq 15 \text{ cm.} \qquad P = 2250 \text{ N/m}^2$$

Thus for a given strain (i.e. a given thickness) a value of k_y, the axial permeability, could be read from Figure 21, and then a value of radial permeability could be found which satisfied the given output flowrate.

3.3.7 Results

Results of variation in flowrate for a range of thicknesses of the porous material are shown in Figure 19 for the exial flow case and Figure 20 for the radial flow case.

Figures 21 and 22 show the consequent variation in permeability with strain calculated from the median line drawn through the flowrate results for axial and radial flow respectively.

3.4 Theoretical Considerations

In order to gain some insight into the mechanism of permeability and its consequent variation with strain, simple consideration has been made of a model of a porous material consisting of tubes similar to the approach by Kozeny already mentioned,[26] but variations in the length of a conductor, previously ignored, have now been taken into account.

Poiseuille's equation for the flowrate through a cylindrical conductor is[25]

$$q = -\frac{\rho g \pi r^4}{8\eta} \operatorname{grad} \phi$$

$$= -\frac{\pi r^4 \Delta p}{8\eta L_c}$$

where q is the flowrate

r is the radius of the conductor

Δp is the pressure drop along the length of the conductor

L_c is the length of the conductor

Thus, if there are n_t conductors,

$$Q = -\frac{n_t \pi r^4 \Delta p}{8\eta L_c}$$

where Q is the total flowrate

Darcy's law is

$$Q = -\frac{k}{\eta}\frac{\Delta p}{L}$$

where L is the thickness

$$\therefore \quad k = \frac{n\pi r^4 L}{8 L_c} \qquad (3.4)$$

Then if the total volume at zero strain is V_o (solids + voids)

Volume of voids = $V_o . v$

where v is the porosity.

Assuming that, in compressing the material to a strain ϵ, the volume change is due only to the closure of the voids, the total volume will then be

$$V_o(1 - \epsilon)$$

and thus the volume of voids now is

$$V_o v - [V_o - V_o(1-\epsilon)] = V_o(v-\epsilon)$$

Still considering the solid consisting of n_t tubes, the volume of each tube is now $\frac{V_o(v-\epsilon)}{n_t}$

and the cross-sectional area of each hole is

$$\frac{V_o(v-\epsilon)}{n_t L_\epsilon}$$

where L_ϵ is the length of the conductor at strain ϵ

$$\therefore \pi r^2 = \frac{V_o(v-\epsilon)}{n_t L_\epsilon}$$

$$\therefore \pi r^4 = \left[\frac{V_o(v-\epsilon)}{n_t L_\epsilon}\right]^2 \frac{1}{\pi}$$

referring back to the "equivalent" expression for permeability (equation (3.4)), substituting L_ϵ for L_c , we obtain

$$k = \frac{V_o^2}{8\pi} \frac{(v-\epsilon)^2 L}{L_\epsilon^3}$$

$\frac{V_o^2}{8\pi}$ is constant with ϵ and if T is the original thickness of the specimen at zero strain, then $L = (1-\epsilon)T$

and $$k = \frac{C_v (v-\epsilon)^2 (1-\epsilon)}{L_\epsilon^3} \qquad (3.4.1)$$

where C_v is a constant $\left(= \frac{V_o^2 T}{8\pi}\right)$

A graph of the form

$$k \propto (v-\epsilon)^2 (1-\epsilon) \qquad (3.4.2)$$

is shown in Figure 23, and compares reasonably with the experimental results. Equation (3.4.2) conforms to the reasonable assumption that, when the strain is equal to the initial porosity, which if it is assumed that all volume change is due to the closure of the pores, means that, with no lateral expansion, all the pores are then closed, the permeability has the value of zero and no flow of the fluid will take place.

Comparing equation (3.4.2) with (3.4.1) gives the condition that the length of a conductor remains constant with strain. This can only be accomplished if the flow passages are increasing in length with respect to the overall thickness, due to the continual closing of passages, in the same proportion to the decrease in the overall thickness.

If we now consider flow in the radial direction, referring to Figure 18, Darcy's law becomes

$$q = -\frac{k}{\eta}\frac{\Delta p}{L}.H.L$$

where H is the thickness of the material at strain

and L is the width and breadth.

Again comparing with Poiseuille's equation gives

$$k = \frac{\pi}{8}\frac{r^4}{L_\epsilon H}$$

now from before

$$\pi r^2 = \frac{V_o(v-\epsilon)}{n_\epsilon L_\epsilon}$$

and

$$k = \frac{V_o^2}{8\pi n_\epsilon}\frac{(v-\epsilon)^2}{H \times L_\epsilon^3} \qquad (3.4.3)$$

if T is again the original thickness

$$H/T = (1-\epsilon)$$

A curve of the form

$$k \propto \frac{(v-\epsilon)^5}{(1-\epsilon)} \qquad (3.4.4)$$

is shown in Figure 24, and again conforms to the condition that the permeability becomes zero when the strain is equal to the initial porosity. Comparing equation (3.4.4) with (3.4.3) gives the variation of the length of a conductor,

$$L_\epsilon \propto (v-\epsilon)^{-1}$$

which satisfies the condition that as $\epsilon \longrightarrow v$ then $L_\epsilon \longrightarrow \infty$.

It would seem reasonable in the radial flow case to expect the path length to increase with strain, as the overall horizontal distance over which the fluid has to travel remains constant.

The considerations are only meant to give an idea of how permeability might vary with strain, and the assumptions deduced regarding the "length of a conductor" can only be examined from a quantitative viewpoint.

In the case of axial flow, the actual thickness is decreasing, but although the flow is predominantly uniaxial, on a microscopic level some flow must take place radially and consequently an axial compression will cause the area of the holes for radial flow to decrease perhaps to zero, which will, in turn, cause the flow path to change and consequently increase. We can perhaps say that the "length of a conductor" may stay reasonably constant.

However, in the radial flow case, the macroscopic length over which the fluid has to flow remains constant with variation in strain, and because of the diminishing area of flow causing increasing path length, as has already been mentioned the "length of a conductor" must increase with increasing strain.

However dubious the assumptions may appear, we can compare the experimental results of Figures 23 and 24 with those of the fictitious model porous material by adjusting the constant of proportionality so that the permeability at zero strain is equal to the initial permeability. It can be seen in both cases that the variation of the experimental permeability can be reasonably represented by relationships of the form equations (3.4.2) and (3.4.4), when large variations in strain are encountered. Probably a better fit for small strains, however, to the axial flow results is by the expression

$$k \propto (v-\epsilon)^3 \qquad (3.4.5)$$

which differs slightly from equation (3.4.2) throughout the whole range and whose variation is shown by Figure 25.

Finally, if one thinks qualitatively about the variation of permeability with strain, it would appear that axial permeability would always be less affected than radial permeability, because, in the latter case, macroscopic flow is perpendicular to the direction of applied strain, and flow channels are likely to be more affected in the plane of flow.

3.5 Conclusions

From the experiments it has been shown that the variation of permeability with strain can be represented to a fair degree of accuracy for the porous plastic material tested by simple relationships of the following forms:

In the axial flow case,

$$k \propto (v-\epsilon)^3$$

and in the radial flow case,

$$k \propto \frac{(v-\epsilon)^5}{(1-\epsilon)}$$

Although the comments that there can be no definitive statement about the variation of permeability and porosity have been noted, this will be true for permeabilities of different materials. For any material whose porosity is being altered by an applied strain, especially one which has the same basic form as that used in the experiments (i.e. sintered fibres), it would seem reasonable to assume that the relationships above can be used to a fair degree of accuracy.

4. Theoretical and Numerical Analysis of the Load/Deformation/Time Characteristic of a Porous Solid

The theory will now be put forward for evaluation of the deformation-time characteristics at certain loads, and, with the aim of applying this theory to articular cartilage, certain restrictions have been made, the main one of which is that deformation is uniaxial and that there is no lateral strain. This restriction will be justified later in the case of articular cartilage, but with this restriction and the other assumptions noted, this theory can be applied to the case of any deformable porous material.

4.1 Theory

Assume initially therefore that the deformation is uniaxial

that the fluid is incompressible

that the solid is incompressible.

These assumptions mean that all volume change is effected by fluid transfer in and out.

Now consider an element of a porous material which has axial symmetry, and which contains a fluid (Figure 2).

The element has dimensions (in cylindrical co-ordinates) of δr, $\delta\theta$, δz as shown.

u is the flowrate/unit area in the radial direction

w is the flowrate/unit area in the axial direction.

Because axial symmetry is considered, $\delta\theta$ remains constant and because only uniaxial deformation is considered, δr also remains constant.

Thus δz is varying, let the initial value of δz be δz_0.

Consider the continuity equation:-

Flow In = Flow Out + rate of volume increase.

$$u r \delta\theta \delta z + w\left(r+\frac{\delta r}{2}\right)\delta\theta\delta r = \left(u+\frac{\partial u}{\partial r}\delta r\right)(r+\delta r)\delta\theta\delta z + \left(w+\frac{\partial w}{\partial z}\delta z\right)\left(r+\frac{\delta r}{2}\right)\delta\theta\delta r + \dot{V}_e \qquad (4.1.1)$$

where V_e is the volume of the element.

Now $$V_e = \left(r+\frac{\delta r}{2}\right)\delta\theta\delta r\delta z$$

$$= C_A \cdot \delta z$$

where $C_A\left[=\left(r+\frac{\delta r}{2}\right)\delta\theta\delta r\right]$ is constant

$$\therefore \dot{V}_e = C_A \frac{d}{dt}(\delta z)$$

$$\delta z = \delta z_0(1-\epsilon_z)$$

where ϵ_z is defined as "engineering strain" and the convention taken

such that compression is positive.

$$\therefore \epsilon_z = -\left(\frac{\delta_z - \delta_{z_o}}{\delta_{z_o}}\right)$$

$$\frac{d}{dt}(\delta_z) = -\delta_{z_o}\dot{\epsilon}_z = -\frac{\delta_z}{(1-\epsilon_z)}\cdot\dot{\epsilon}_z$$

$$\therefore \dot{V}_e = -\left(r + \frac{\delta_r}{2}\right)\delta\theta\,\delta_r\,\delta_z\frac{\dot{\epsilon}_z}{(1-\epsilon_z)} \qquad (4.1.2)$$

Cancelling equal terms and neglecting terms of the order $\frac{\partial u}{\partial r}\delta_r^2\delta\theta\delta_z$, equation (4.1.1) gives the continuity condition:-

$$\frac{\partial u}{\partial r} + \frac{u}{r} + \frac{\partial w}{\partial z} - \frac{\dot{\epsilon}_z}{(1-\epsilon_z)} = 0 \qquad (4.1.3)$$

If Darcy's law is now used

$$u = -\frac{k_r}{\eta}\frac{\partial p}{\partial r}$$

$$w = -\frac{k_z}{\eta}\frac{\partial p}{\partial z}$$

where k_r, k_z are radial and axial permeabilities respectively, and η is the dynamic viscosity of the fluid.

$$\frac{\partial u}{\partial r} = -\frac{k_r}{\eta}\frac{\partial^2 p}{\partial r^2} - \frac{1}{\eta}\frac{\partial k_r}{\partial r}\frac{\partial p}{\partial r}$$

and

$$\frac{\partial w}{\partial z} = -\frac{k_z}{\eta}\frac{\partial^2 p}{\partial z^2} - \frac{1}{\eta}\frac{\partial k_z}{\partial z}\frac{\partial p}{\partial z}$$

and substituting these expressions into equation (4.1.3) gives

$$k_r\frac{\partial^2 p}{\partial r^2} + \frac{\partial k_r}{\partial r}\frac{\partial p}{\partial r} + \frac{k_r}{r}\frac{\partial p}{\partial r} + k_z\frac{\partial^2 p}{\partial z^2} + \frac{\partial k_z}{\partial z}\frac{\partial p}{\partial z} + \frac{\eta\dot{\epsilon}_z}{(1-\epsilon_z)} = 0 \qquad (4.1.4)$$

which is the equation governing the fluid pressures in axi-symmetric porous materials.

The other equations which are needed to solve for the pressures are:-

$$k_r = f_1(\epsilon_z) \qquad (4.1.5)$$

and

$$k_z = f_2(\epsilon_z) \qquad (4.1.6)$$

where f_1 and f_2 indicate functions of ϵ_z, but assume both permeabilities remain constant with variations in hydrostatic pressure and time.

The next step in the formulation of the problem is to assume that, at any time, the load applied will be carried by the force in the solid mesh of fibres and the force generated by the hydrostatic pressure in the fluid inside the pores.

i.e. $$F = F_s + F_f \qquad (4.1.7)$$

where F is the force to be carried

F_s is the force carried by the solid

and F_f is the force due to the hydrostatic pressure in the fluid, and this statement is taken to be true at all times at every layer in the porous material.

Now $$F_s = f_{fs}(\epsilon_z) \qquad (4.1.8)$$

and the function f_{fs} can be calculated from the variation of F with ϵ_z when $F_f = 0$. This latter condition is satisfied when the fluid pressure throughout the porous material is equal to the external fluid pressure (zero gauge pressure) which means that there are no pressure gradients throughout the fluid, which in turn means that no flow is taking place, which, from the initial assumptions, means that no deformation of the material is taking place with increase in time. Thus a variation of F_s with ϵ_z can be obtained by applying a constant load F_s and allowing the deformation to become constant, at which point the strain ϵ_z can be calculated.

F_f can be calculated by a summation of the fluid pressures in a layer, each pressure being multiplied by its respective area. In a formulation of this sort, the pores must be assumed to be randomly distributed throughout the porous material, and therefore the area of the pores in each layer can be calculated, and considering this area to be distributed equally throughout the layer. Taking the assumption that the deformation is uniaxial, which means that the total area of the porous material

(pores and solid) remains constant, the volume of the pores can be measured by considering the porosity at a strain ϵ_z (see Section 3.1)

$$\text{porosity, } n = \frac{\text{volume of pores}}{\text{volume of (pores + solid)}}$$

Now consider the ratio,

$$A_n = \frac{\text{area of pores}}{\text{area of (pores + solid)}} ,$$

in one particular layer this will, in some way, be related to the porosity (i.e. volume instead of area)

$$A_n = n^{\alpha} \qquad (4.1.9)$$

where α is a constant

$$\text{Now} \quad \frac{\text{volume of solid}}{\text{volume of (pores + solid)}} = (1 - n)$$

and therefore,

$$\frac{\text{area of solid}}{\text{area of (pores + solid)}} = (1 - n)^{\alpha}$$

but, by definition, $\dfrac{\text{area of solid}}{\text{area of (pores + solid)}} = (1 - A_n)$

$$(1 - A_n) = (1 - n)^{\alpha}$$

$$A_n + (1 - A_n) = 1$$

$$\therefore \quad n^{\alpha} + (1 - n)^{\alpha} = 1 \qquad (4.1.10)$$

to which the only solution for all n is $\alpha = 1$, and thus the ratios A_n and n are directly proportional.

From Section 3.1, the porosity at a strain ϵ_z is given by

$$n = \frac{(v - \epsilon_z)}{(1 - \epsilon_z)}$$

and thus the ratio of the areas of a layer at strain ϵ_z will vary by the same relationship. Thus with a constant cross-sectional area being implicit in a uniaxial deformation, the area over which the fluid pressures act can be calculated from a knowledge of the cross-sectional area, the

original porosity, and the strain in the increment at that particular time.

4.2 Special Cases

Having formulated the general equations and assumptions, it now remains to produce solutions to some of the special cases which can occur in testing the properties of a porous material.

4.2.1 Radial Flow Only

The case of radial flow alone means that flow cannot take place in the axial direction, the load being applied through flat impermeable plates. The effect of gravity on the flow is ignored.

Referring to Figure 26(a), ~~changes~~ variations of permeability and pressure in the z-direction are zero ($\partial/\partial z = 0$), and k_r is a function of time only, not of radius or of height.

Thus, equation (4.1.4) reduces to

$$k_r \frac{\partial^2 p}{\partial r^2} + \frac{k_r}{r}\frac{\partial p}{\partial r} + \frac{\eta \dot{\epsilon}_z}{(1-\epsilon_z)} = 0$$

or
$$\frac{\partial}{\partial r}\left(r \frac{\partial p}{\partial r}\right) = -\frac{\eta \dot{\epsilon}_z r}{(1-\epsilon_z) k_r} \qquad (4.2.1)$$

ϵ_z and $\dot{\epsilon}_z$ are independent of r, so integration gives

$$r \frac{\partial p}{\partial r} = -\frac{\eta \dot{\epsilon}_z}{(1-\epsilon_z)} \frac{r^2}{2} + G(t)$$

where $G(t)$ is a function of time only, and using the boundary condition at $r = 0$, $\frac{\partial p}{\partial r} = 0$ because of symmetry,

$$G(t) = 0$$

and
$$\frac{\partial p}{\partial r} = -\frac{\eta \dot{\epsilon}_z}{(1-\epsilon_z) k_r} \frac{r}{2}$$

$$\therefore \quad p = -\frac{\eta \dot{\epsilon}_z}{(1-\epsilon_z) k_r} \frac{r^2}{4} + H(t)$$

where $H(t)$ is also a function of time only,

at $r = R$, $p = 0$

$$\therefore \quad H(t) = \frac{\eta \dot{\epsilon}_z R^2}{4 k_r (1-\epsilon_z)}$$

$$\therefore \quad p = \frac{\eta \dot{\epsilon}_z}{4 k_r (1-\epsilon_z)} (R^2 - r^2) \qquad (4.2.2)$$

where R is the radius of the cylinder.

To calculate the total fluid force, assume a random porosity (n) and integrate over an incremental area $2\pi r\,\delta r$

$$F_f = \int_0^R \frac{\eta n \dot{\epsilon}_z (R^2 - r^2) 2\pi r\,dr}{4k_r(1-\epsilon_z)}$$

$$= \frac{\eta n \dot{\epsilon}_z R^4}{8k_r(1-\epsilon_z)} \qquad (4.2.3)$$

The porosity can be expressed as

$$n = \frac{(v-\epsilon_z)}{(1-\epsilon_z)}$$

and making the assumption that k_r varies with ϵ_z in the same way as the porous plastic material of Section 3.3.6,

$$k_r = \frac{k_o(v-\epsilon_z)^5}{v^5(1-\epsilon_z)} \qquad (4.2.4)$$

substituting into (4.2.3)

$$F_f = \frac{\eta \pi R^4 \dot{\epsilon}_z v^5}{8k_o(1-\epsilon_z)(v-\epsilon_z)^4}$$

substituting into (4.1.7) gives the total force applied

$$F = F_s + \frac{\eta \pi R^4 \dot{\epsilon}_z v^5}{8k_o(1-\epsilon_z)(v-\epsilon_z)^4} \,, \qquad (4.2.5)$$

for a constant applied force F_a and a Hookean solid $\left(\frac{F_s}{\pi R^2} = Y\epsilon_z\right)$ this becomes

$$F_a - \pi R^2 Y \epsilon_z = \frac{\eta \pi R^4 \dot{\epsilon}_z v^5}{8k_o(1-\epsilon_z)(v-\epsilon_z)^4}$$

the solution to which is

$$t = \frac{\eta \pi R^4 v^5}{8k_o(\pi R^2 Y - F_a)}\left[\frac{\log_e\left(\frac{1-\epsilon_z}{1-\epsilon_z/v}\right)}{(v-1)^4} - \frac{\log_e\left(\frac{1-\frac{\pi R^2 Y \epsilon_z}{F_a}}{1-\epsilon_z/v}\right)}{\left(v-\frac{F_a}{\pi R^2 Y}\right)^4}\right.$$
$$+\left(\frac{1}{(v-1)^3} - \frac{1}{\left(v-\frac{F_a}{\pi R^2 Y}\right)^3}\right)\left(\frac{1}{v-\epsilon_z} - \frac{1}{v}\right)$$
$$+\frac{1}{2}\left(\frac{1}{(v-1)^2} - \frac{1}{\left(v-\frac{F_a}{\pi R^2 Y}\right)^2}\right)\left(\frac{1}{(v-\epsilon_z)^2} - \frac{1}{v^2}\right)$$
$$\left.+\frac{1}{3}\left(\frac{1}{(v-1)} - \frac{1}{\left(v-\frac{F_a}{\pi R^2 Y}\right)}\right)\left(\frac{1}{(v-\epsilon_z)^3} - \frac{1}{v^3}\right)\right] \qquad (4.2.6)$$

which conforms to the boundary condition $\epsilon_z = 0$ when $t = 0$.

and k_o is initial permeability.

However, when strains approaching the initial porosity of the material are imposed, most porous materials, at equilibrium, exhibit grossly non-linear force-strain characteristics, and tend towards an asymptote when the strain is equal to the initial porosity, beyond which all pores are closed, and any load applied is then compressing the solid material only. It appears that a good approximation in most instances to these force-strain characteristics is of the form

$$\frac{F_s}{A} = \frac{a\epsilon_z}{1-b\epsilon_z} \qquad (4.2.7)$$

where a and b are constants, and this characteristic is assumed to be totally reversible.

If this is substituted into (4.2.5)

$$F_a - \frac{a\epsilon_z \pi R^2}{(1-b\epsilon_z)} = \frac{\eta \pi R^4 \dot{\epsilon}_z v^5}{8k_0(1-\epsilon_z)(v-\epsilon_z)^4} \qquad (4.2.8)$$

the solution to which is

$$t = \frac{\eta \pi R^4 v^5}{8k_0(X-F_a)}\left[\frac{(1-b)}{(v-1)^4}\log_e\left(\frac{1-\epsilon_z}{1-\epsilon_{z/v}}\right) - \frac{\left(1-\frac{bF_a}{X}\right)}{\left(v-\frac{F_a}{X}\right)}\log_e\left(\frac{1-\frac{\epsilon_z X}{F_a}}{1-\epsilon/v}\right)\right.$$
$$+\left(\frac{(1-b)}{(v-1)^3} - \frac{\left(1-\frac{bF_a}{X}\right)}{\left(v-\frac{F_a}{X}\right)^3}\right)\left(\frac{1}{v-\epsilon_z} - \frac{1}{v}\right)$$
$$+\frac{1}{2}\left(\frac{(1-b)}{(v-1)^2} - \frac{\left(1-\frac{bF_a}{X}\right)}{\left(v-\frac{F_a}{X}\right)^2}\right)\left(\frac{1}{(v-\epsilon_z)^2} - \frac{1}{v^2}\right)$$
$$\left.+\frac{1}{3}\left(\frac{(1-b)}{(v-1)} - \frac{\left(1-\frac{bF_a}{X}\right)}{\left(v-\frac{F_a}{X}\right)}\right)\left(\frac{1}{(v-\epsilon_z)^3} - \frac{1}{v^3}\right)\right] \qquad (4.2.9)$$

where $X = bF_a + \pi R^2 a$, and the initial condition is $\epsilon_z = o$, when $t = o$.

If the load is taken off, equation (4.2.8) becomes

$$-\frac{a\epsilon_z \pi R^2}{(1-b\epsilon_z)} = \frac{\eta \pi R^4 \dot{\epsilon}_z v^5}{8k_0(1-\epsilon_z)(v-\epsilon_z)^4} \qquad (4.2.10)$$

the solution to which is

$$t = \frac{\eta R^2 v^5}{8k_0 a}\left[\frac{1}{v^4}\log_e\left(\frac{\epsilon_0}{\epsilon_z}\right) - \frac{(1-b)}{(v-1)^4}\log_e\left(\frac{1-\epsilon_0}{1-\epsilon_z}\right) - \left(\frac{1}{v^4} - \frac{(1-b)}{(v-1)}\right)\log\left(\frac{v-\epsilon_0}{v-\epsilon_z}\right)\right.$$
$$-\left(\frac{1}{v^3} - \frac{(1-b)}{(v-1)^3}\right)\left(\frac{1}{(v-\epsilon_z)} - \frac{1}{(v-\epsilon_0)}\right)$$
$$-\frac{1}{2}\left(\frac{1}{v^2} - \frac{(1-b)}{(v-1)^2}\right)\left(\frac{1}{(v-\epsilon_z)^2} - \frac{1}{(v-\epsilon_0)^2}\right)$$
$$\left.-\frac{1}{3}\left(\frac{1}{v} - \frac{(1-b)}{(v-1)}\right)\left(\frac{1}{(v-\epsilon_z)^3} - \frac{1}{(v-\epsilon_0)^3}\right)\right] \qquad (4.2.11)$$

the initial condition being that $\epsilon_z = \epsilon_0$ when $t = o$.

The addition of an oscillatory force $F_o \sin \omega t$ to the constant applied force F_a causes equation (4.1.7) to be modified to

$$F_a + F_o \sin \omega t = F_s + F_f \qquad (4.2.12)$$

assuming that any deformations are slow and inertia forces can be neglected. This causes all subsequent equations involving strain and time to be non-linear, separation of the variable is therefore not possible, and resort has to be made to numerical methods for the solution.

4.2.2 Axial Flow only

Because flow cannot take place radially, the effect is an axial one alone and the problem becomes one-dimensional.

Referring to Figure 26(b), variations of pressure and permeability in the radial direction are zero,

i.e. $\partial/\partial r = 0$

and the equation (4.1.4) reduces to

$$k_z \frac{\partial^2 p}{\partial z^2} + \frac{\partial k_z}{\partial z} \cdot \frac{\partial p}{\partial z} + \frac{\eta \dot{\epsilon}_z}{(1-\epsilon_z)} = 0 \qquad (4.2.13)$$

Again, the assumption is made that the axial permeability varies in the manner shown by the porous plastic in Section 3.3.6,

$$k_z = \frac{k_o (v - \epsilon_z)^3}{v^3} \qquad (4.2.14)$$

The solutions to the equations have to be obtained by numerical methods (described later), and the assumption of how the total force is carried (equation (4.1.7)), and the force-strain relationship (equation (4.2.7)) are again utilized.

4.2.3 Axial and Radial Flow Together

If compression between flat plates is assumed (Figure 26(c)), then every element in a horizontal layer would be expected to experience the same strain at the same time, and this means that the radial permeability along a layer is constant.

$$\therefore \frac{\partial k_r}{\partial r} = 0$$

and equation (4.1.4) reduces to

$$k_r \frac{\partial^2 p}{\partial r^2} + \frac{k_r}{r} \frac{\partial p}{\partial r} + k_z \frac{\partial^2 p}{\partial z^2} + \frac{\partial k_z}{\partial z} \cdot \frac{\partial p}{\partial z} + \frac{\eta \dot{\epsilon}_z}{(1-\epsilon_z)} = 0 \qquad (4.2.15)$$

which again must be solved numerically with equations (4.1.7) (4.2.7) (4.2.4) and (4.2.14).

4.3 Soil Mechanics Approach

At this juncture it may be interesting to note the approach and assumptions made by engineers in evaluating the consolidation of soil (see for instance [33]).

Consider the configuration for axial flow only of Figure 26(b).

Defining P_T as the total load carried

P_S as the load carried by the soil

P_W as the load carried by the pore water

then the effective stress $\sigma' = P_S/A$

and the excess pore pressure $u_p = P_W/A$

the total applied stress $\sigma = \sigma' + u_p = P_T/A$ (4.3.1)

where A is the cross-sectional area of the cylinder.

The boundary conditions are as follows:-

in loading, $t = 0$, $\sigma' = 0$, $u_p = \sigma = P_T/A$

$t = t_1$, $\sigma = \sigma' = (\sigma - u_p)$ σ' increasing with time

$0 > u_p > 0$ u_p decreasing with time

$t = \infty$ $\sigma' = \sigma = P_T/A$

$u_p = 0$

and the total settlement of the piston is ρ_T

unloading, $t = 0$, $\sigma' = P_T/A$, $u_p = -\sigma'$, $\sigma = (\sigma' + u_p) = 0$

$t = t_1$, $P_T/A > \sigma'$, σ' decreasing with time

$-P_T/A < u_p (= -\sigma') < 0$, u_p increasing with time

$t = \infty$ $\sigma' = 0 = u_p$

and the piston has risen by ρ_T .

Referring to Figure 27(a), consider a suitably thin horizontal layer of the soil specimen and investigate its condition at some instant during the consolidation process. Assume that the process is entirely

one-dimensional (with no lateral variations) so that the velocity and pressure of the pore water are only functions of the depth z measured vertically downwards from the surface of the specimen, and of the time t. Imagine that two small probes are inserted so that the pore-pressures of the top and bottom surfaces of the layer are known. The sign convention requires that the artificial velocity v_a is taken as positive downwards in the direction of z ; also a positive increment of excess head δh is shown which will cause an upward velocity, i.e. negative v_a .

The loading increment $\dot{\sigma}\,(=\delta\sigma)$ applied to the specimen is such that the initial and final equilibrium states are E_0 and E_1, shown in Figure 27(b). At the present time t after the start of the consolidation process, the state of the thin layer will be represented by some point T between E_0 and E_1. The conventional assumption introduced by Terzaghi in his classic theory of primary consolidation is that T always lies on a straight line joining E_0 and E_1. The slope of this straight line which will change for different states E_0, is defined as

$$-\frac{de}{d\sigma'} = (1+e_0)\,m_{vc} \qquad (4.3.2)$$

where m_{vc} is the coefficient of volume compressibility,
and e is the void ratio.

This definition allows a relation between settlement and effective stress. Let $d\rho_T$ be the settlement experienced by the thin layer during time δt . The reduction in volume of the layer will be $A\,d\rho_T$ which can be expressed as $A\,\delta z\left(-\frac{\delta e}{1+e_0}\right)$

$$\therefore \frac{\delta\rho}{\delta z} = -\frac{\delta e}{1+e_0} = -m_{vc}\,d\sigma' \qquad (4.3.3)$$

Because of continuity, the reduction in volume of the thin layer must be exactly matched by the volume of water expelled, which during time δt will be $\left(\frac{\partial v_a}{\partial z}\right) A \delta z \, \delta t$. Hence in the limit

$$\frac{\partial v_a}{\partial z} = -\frac{1}{1+e_o}\frac{\partial e}{\partial t} = m_{vc}\frac{\partial \sigma'}{\partial t} \qquad (4.3.4)$$

Since the loading increment is a fixed one of $\dot{\sigma} = \delta\sigma$ we have $\delta\sigma' + \delta u_p = \dot{\sigma} = \text{const.}$ so that

$$\frac{\partial \sigma'}{\partial t} = -\frac{\partial u_p}{\partial t} \qquad (4.3.5)$$

and equation (4.3.4) can be taken a step further to give

$$\frac{\partial v_a}{\partial z} = -m_{vc}\frac{\partial u_p}{\partial t} \qquad (4.3.6)$$

Finally another relationship can be obtained between v_a and u by employing Darcy's law,

$$v_a = -\frac{k_p}{\rho g}\frac{\partial u_p}{\partial z} \qquad (4.3.7)$$

Differentiating this with respect to z and combining with (4.3.6) gives

$$\frac{k_p}{\rho g}\frac{\partial^2 u_p}{\partial z^2} = -\frac{\partial v_a}{\partial z} = m_{vc}\frac{\partial u_p}{\partial t}$$

usually written as

$$\frac{\partial u_p}{\partial t} = c_{vc}\frac{\partial^2 u_p}{\partial z^2} \qquad (4.3.8)$$

where $c_{vc} = \frac{k_p}{\rho g m_{vc}}$ is the coefficient of consolidation.

Considering the boundary conditions and configuration of Figure 26(b), the solution can be obtained by employing Fourier analysis:-

$$u_p = \sum_{m=1,2}^{\infty} \frac{2\dot{\sigma}}{m\pi}(1-\cos m\pi)\sin\left(\frac{m\pi z}{2H}\right)e^{-m^2 M t} \qquad (4.3.9)$$

and the proportion of the total settlement,

$$U = 1 - \sum_{1,2}^{\infty} \frac{4}{m^2\pi^2}(1-\cos m\pi)\left(1-\cos\frac{m\pi}{2}\right)e^{-m^2 M t} \qquad (4.3.10)$$

where $M = \frac{\pi^2 C_{vc}}{4H^2 t}$

where H is the total thickness.

Biot has put forward a general theory of three-dimensional consolidation[34] in the subject of soil mechanics. The theory was later extended to include the case of anisotropy[35] and viscoelasticity,[36] and solutions to the case of isotropy were produced.[37] The basic properties of the soil that were assumed in this work were:-

1. Linearity of stress-strain relations,
2. Small strains,
3. The water contained in the pores is incompressible
4. The water flows through the skeleton according to Darcy's law.

In soil mechanics, it is the first condition which is most suspect, although Biot argues that Terzaghi's theory, the main parts of which are shown in this Section, has been found quite satisfactory for the practical requirements of engineering. In problems involving strains approaching the porosity of the material, however, it is (1), (2) and (4), where the constant of Darcy's law, the permeability, is changing, that cannot be assumed, and therefore although the theory satisfies the soil conditions, it will not satisfy the case of larger deformations of other porous materials.

4.4 Numerical Method

As in Section 2.2.3, a relaxation technique was used to produce solutions to the governing equations which could not be solved analytically for given boundary conditions.

Because in all configurations, the load was applied through flat plates, it was assumed that the strains in the material in any horizontal plane were equal, and thus the fluid pressures in any one layer could be integrated to give the total fluid force in that plane.

It was found easier in the formulations to start off with fixed points in the porous material and calculate the fluid pressures, forces and strains at those points with respect to a fixed datum, rather than divide each new thickness into a number of equally spaced nodes spread throughout the material. Therefore the step length δz was not constant either with variations in time, or with variations in distance from the datum at a certain time, so the finite difference expressions used are modified forms of those used in Section 2.2.3:-

$$\left[\frac{\partial \rho}{\partial z}\right]_I = \frac{\rho_I - \rho_{I-1} + \frac{\Delta z_{I-1}}{\Delta z_I}(\rho_{I+1} - \rho_I)}{2\Delta z_I}$$

$$\left[\frac{\partial^2 \rho}{\partial z^2}\right]_I = \frac{(\Delta z_{I-1} + \Delta z_I)}{2\Delta z_{I-1}\,\Delta z_I}\left[\frac{\rho_{I-1}}{\Delta z_{I-1}} + \frac{\rho_{I+1}}{\Delta z_I} - \rho_I\left(\frac{1}{\Delta z_{I-1}} + \frac{1}{\Delta z_I}\right)\right]$$

which become the same expressions as equation (2.2.5) when adjacent step lengths are equal.

Substitution of these formulae into the equations to be solved (either (4.2.13) or (4.2.15)) gives an expression for $\rho_{I,J}$ in terms of the pressures surrounding it in a rectangular mesh. The general method of solution is then to position equally spaced fixed points throughout the column or area at time $t = 0$, and make guesses at the strain at each of these points for a certain increment of time $t = t + \Delta t$. The axial and radial permeabilities can then be calculated and an iteration of the fluid

pressures throughout the mesh can then take place, using the given boundary conditions. These fluid pressures in any one layer can be integrated by the trapezoidal rule and multiplied by their respective fluid areas to give the total fluid force in that layer. The force in the solid is then obtained by subtraction, and the strain thus evaluated from the force-strain relationship. These calculated strains are then used as the guesses and the step lengths Δz at this time can also be evaluated from these strains. This process continues until convergence of the calculation and guess occurs, and deformations in each layer are then evaluated by multiplication of the average strain in the increment by the step length, and the total deformation calculated by the addition of these.

Boundary Conditions

In the one-dimensional axial flow only case, the configuration used was that in Figure 26(b), and one boundary condition used was that the pressure at the surface where the load is applied is zero gauge pressure. The other condition used was that there is no flow per unit area at the very bottom of the material, i.e. from Darcy's law

$$z = 0 \quad , \quad \frac{\partial p}{\partial z} = 0$$

This can be explained if one considers a configuration of a porous material being simultaneously compressed by a porous piston at either end, then by symmetry there can be no flow across the centre plane. The configuration of Figure 26(b)is one half of this condition, and therefore there can be no pressure gradient at the cylinder wall. The fact that there is (or can be) a strain at the bottom of the cylinder is not inconsistent with this condition, because on a molecular scale there will be flow out of the next layer above this, and so in that small layer, which tends to a plane, there will be a strain which is non-zero.

This condition of zero pressure gradient is represented numerically, by exactly the method used in Section 2.2.3, i.e. fitting a quadratic function to the two nodal points next to the boundary, only with varying step lengths:-

$$p(1) = \frac{(\Delta z_1 + \Delta z_2)^2 p(2) - p(3)\cdot \Delta z_1^2}{(2\Delta z_1 \Delta z_2 + \Delta z_2^2)}$$

In the axial and radial flow case, the configuration was as in Figure 27(c), and the conditions of no flow from the impermeable surface together with the pressure being zero both at the surface where the load is applied and at the edges of the cylinder, were

$$p = 0 \quad \text{for} \quad r = R \quad \text{for all} \quad z$$

$$\frac{\partial p}{\partial z} = 0 \quad \text{for} \quad z = 0 \quad \text{for all} \quad r$$

A block diagram of the computer program used to evaluate the deformations from the given data is shown in Figure 28.

5. Application to Articular Cartilage

Having formulated the theory together with some experimental observations of deformable porous materials, it now remains to apply this theory to the special case of articular cartilage, making suitable reservations where necessary.

5.1 Literature Review of Articular Cartilage

5.1.1 Description

Despite the observation by Hunter[38] that fibres ran from the subchondral bone to the surface in articular cartilage, the general consensus of opinion in the nineteenth century was that cartilage was a completely homogeneous structure, and both Hassell[39] and Schäfer[40] based this belief on light microscopy of cartilage specimens. However, Hultzkranz[41] deduced from pricking the surface with a blunt-ended awl and producing splits, that the formation of these splits was due to fibre orientation on the surface. Ramon and Cajal[42] reported that cartilage was a ground substance with numerous collagen fibres embedded in it, and pointed out that collagen and ground substances have similar refractive indices and thus could not be separated when viewed by ordinary light. Benninghof[43][44][45] suggested that these collagen fibres in cartilage are made up from a three-dimensional network of fibrils grouped together to form thick fibres, and this seems to be the description of articular cartilage which is generally accepted today.

Benninghof also suggested that these fibres are connected to the underlying bone and pass radially towards the centre zone. When approaching the surface of the cartilage, these fibres bend and run parallel to the articular surface back to the bone layer. The effect was to produce a series of arcades, and cells were observed to be located between the sides of these arcades. Each cell was seen to be surrounded by a layer of concentrically disposed fibrils, which, Benninghof suggested, were arranged so as to support tensile forces whilst the ground substance supported the compressive forces. MacConaill[46] agreed with most of Benninghof's proposed structure, but disagreed with this arrangement of arcades and suggested that the fibres ran in oblique directions between the cartilage surface and the bone, and

proposed that this arrangement was effective in supporting the stress distribution under physiological loading. However, Zarek and Edwards[47] have questioned the validity of this stress distribution, and the question of the structure of cartilage and its relation to the stress distribution applied appears a complex one.

Investigations into the orientation of the fibres at different layers in the cartilage have been made by several workers (Little et al,[48] Davies et al,[49]) but perhaps the clearest differences in the orientation have been shown by McCall.[50] In a normal adult joint, three zones exist: superficial, intermediate and deep. The superficial zone is the bearing surface and is composed of parallel bundles of fibres which run in directions parallel to the surface. Most of the cartilage thickness is comprised of the intermediate zone which consists of coiled S-shape fibres arranged in an open meshwork with large spaces in between. The deep zone is composed of a tighter meshwork of thicker fibres arranged in a direction perpendicular to the surface. McCall also showed that in an osteoarthritic specimen the zoning which predominates in the normal cartilage has been lost and is replaced by a closely packed network of thick, coarsened fibres, all running in a direction perpendicular to the surface.

5.1.2 Synovial Fluid

The fluid in the cavities of freely movable joints of the body is known as synovial fluid, which is a dialysate of blood plasma with the addition of a high molecular weight molecule known as hyaluronic acid. A review article of its composition and properties has been written by Davies[51] and its only property that will be mentioned here is the one principally concerned in lubrication and deformation of articular cartilage, the dynamic viscosity. Early investigators did not realise that the fluid

was grossly non-Newtonian, but both King[52] and Davies[51] have shown that the dynamic viscosity of synovial fluid is sharply dependent on the shear rate. However, this viscosity characteristic is thought to be due to the presence of the hyaluronic acid molecule in the fluid.

5.1.3 Mechanical Properties of Cartilage

5.1.3.1 Compression

The most convenient method of studying the compressive properties of articular cartilage is the indentation test, because it enables tests to be performed without removal from the bone. Bär,[53] Göcke[54] and Hirsch[55] performed these tests on human articular cartilage and all showed the main features of indentation tests under constant load, namely an "instantaneous" response followed by a time dependent one. They also exhibited incomplete recovery after removal of the load, the so-called "imperfect" elasticity which was investigated by Elmore et al[56] and shown to be the effect of performing the tests in air and thus not allowing the cartilage to take in fluid which had been expelled during compression and consequently return to its original shape and size. Sokoloff,[57] using the same apparatus as Elmore, produced figures of 101 lbs/in^2 for the Young's modulus of articular cartilage, and 402 lbs/in^2 and 724 lbs/in^2 for the costal cartilage of young (9-22 years) and old (42-66 years) people respectively. He also demonstrated that there was no significant correlation between the magnitudes of the indentations and the age of the individual concerned, and that indentations varied considerably with position on the patella. The topographical variation of the compressive properties of human articular cartilage have been reported in a series of papers[58][59][60] and the indentation-time curves exhibit the same basic characteristics as demonstrated earlier, i.e. an "instantaneous" response followed by a time dependent one.

In formulating his theory of "weeping" lubrication in human joints, McCutchen[1] performed experiments by placing cartilage between two porous glass sheets and squeezing them together with a series of increasing loads load-deformation curves were plotted by allowing 30 minutes after the application of the load to allow for wring-out and then reading the deformation. From these experiments McCutchen obtained values for Young's modulus of 5.8×10^6 dynes/cm^2 for water-soaked cartilage and 3.2×10^6 dynes/cm^2 for salt-soaked cartilage. Young's modulus for the immediate deflection on application of the load was calculated to be 111×10^6 dynes/cm^2.

Edwards[61] performed tests on cylindrical pieces of cartilage from dogs which were confined so that no movement, either of liquid or material could take place sideways. Graphs of thickness versus applied pressure and liquid content versus time were plotted for a series of different loads. Edwards also allowed the specimens to recover in normal saline and found that the original dimensions were recovered after about 30 minutes.

Camosso and Marotti[62] looked at the behaviour of articular cartilage when subjected to compressive stresses. They performed compression tests on cubes both of cartilage and bone intact and bone only and measured deflections for different loads. It was noted that the rate of deformation decreased for increasing load for the cartilage and bone together whereas the deformation rate increased for increasing load in the bone only case. The authors, however, seemed to confuse the terms plastic and viscoelastic as they are used in the engineering sense.

Linn and Sokoloff[63] studied the movement and composition of the extracellular water of cartilage. They performed tests on costal cartilage confined only to move in the vertical direction and produced graphs similar to those of Edwards. They also studied the amount of extra-cellular water in costal and articular cartilage and found that about 50% by volume could

be expressed from articular cartilage as opposed to 20% in costal cartilage at 500 lbs/in^2. It was found that the rate at which cartilage imbibed water was similar to the rate at which the deformation recovered although there was an immediate linear deformation which was too large.to be accounted for in its entirety on the basis of lateral fluid displacement from a vertically compressed matrix, and therefore it was presumed that a rubber-like lateral displacement of the matrix was involved.

Hayes and Mockros[64] studied the viscoelastic properties of human articular cartilage and evaluated creep compliances for torsion and uniaxial strain tests. In their strain experiments, cartilage was compressed between pervious and impervious load pads and deflections noted. The results led the authors to the conclusion that, even for load times of several minutes, flow processes are not dominant in deforming normal cartilage. Cartilage with an intact surface layer seemed to deform similarly with and without a free draining boundary, whereas for degenerative tissue, deviations in the mechanical behaviour occurred which could be attributed to fluid flow from the matrix.

5.1.3.2 Tension

Experiments have also been performed to measure the tensile properties of articular cartilage by Swanson et al[65]. Load-extension tests were performed on specimens cut from the joints in such a way that some were orientated with their collagen fibres in the direction of pull and some at right angles. The results showed that the tensile strength of the specimens tested parallel to their collagen fibre orientation was between 100 and 200 kg/cm^2 whereas the specimens tested at right angles to their fibre orientation had a tensile strength of 40 to 100 kg/cm^2. Stiffness too varied according to the direction of loading from 500-1700 kg/cm (parallel to the fibres) to 200-500 kg/cm (across the fibres).

Clearly the cartilage was stronger and stiffer when pulled in the same direction as the fibre orientation, which would appear entirely logical since in this case the fibres themselves were being stretched whereas in the case on transverse loading the fibres were simply being separated from each other.

5.1.4 Permeability

Owing to difficulties in its measurement, because of the small flowrates involved, only three investigators have reported figures for the coefficient of permeability in cartilage. McCutchen[1] measured the permeability by forcing fluid through a disk of cartilage under a known pressure difference and observing the rate of rise of fluid in the upper column. McCutchen quotes a figure of 5.8×10^{-13} cm^4/dyne sec as the permeability in the normal direction. The tangential permeability was measured indirectly by squeezing a disk of cartilage and measuring the force exerted by it during wring out. A mathematical analysis, assuming constant permeability, enabled McCutchen to calculate the permeability from the rate of deformation for a constant load. A figure for the tangential permeability of 5.45×10^{-13} cm^4/dyne sec. is quoted although the deformation is finite, the permeability is reduced and the matrix carries some of the load, causing this figure to be too small, perhaps, says McCutchen, by a factor of 2, although he does not rule out isotropic permeability. It is also stated that the normal permeability varies with depth, being greatest near the surface. The quoted figures are 7.65×10^{-13} cm^4/dyne sec. for the top disk, and 4.3×10^{-13} cm^4/dyne sec. for the lower disk.

Edwards,[61] in performing the confined tests on articular cartilage also carried out tests of permeability on his specimens. Using a similar apparatus to McCutchen, he obtained normal permeability coefficients of 1.09×10^{-13} cm^4/dyne sec. for saline and 3.3×10^{-13} cm^4/dyne sec. for

Ringers solution. The pressure gradient used in both cases was 70 lbs/in^2 which is important because not only does it force more fluid through but it may compress the cartilage and make the pores smaller, thus reducing the permeability. Edwards relates the flow out of cartilage and its subsequent deformation to the consolidation of a soil but includes the comment that, at equilibrium, the applied load is carried partly by elastic stresses in the fibrous framework and partly by osmotic forces generated mainly in the ground substance.

Maroudas also carried out permeability tests in applying an ion exchange theory to articular cartilage. In measuring the permeability in a similar fashion to both McCutchen and Edwards, Maroudas measured the fixed charge density and varied the depth from which the layer of cartilage came. As well as finding that the fixed charge density increases considerably with the distance from the articular surface, Maroudas produced graphs of permeability coefficient with variation in the distance from this surface. In Maroudas' first paper on this subject,[66] this variation appeared to be an approximately linear one, decreasing from a maximum value near the surface, but no data was given in a region within approximately 2 x 10^{-2} cm of the articular surface because of experimental difficulties involved in dealing with slices of small cross-sectional area obtained near the surface. However, these difficulties were overcome and a second paper[67] showed an unexpected decrease in the permeability in this layer. This was put down to the fact that the bearing surface is made up of thickly packed smaller fibres as has already been noted in this review.

5.1.5 Theoretical Predictions of Mechanical Properties

Several workers have put forward predictions of how cartilage behaves under load, but unfortunately most of these theories seem to have little theoretical backing except in the method of curve-fitting.

Yannas[68] suggested that the fluid transfer in and out of the cartilage accompanying deformation could be represented by a linear relaxation process where the amount of fluid expelled depended on the time and increment of load but was independent of the weight of fluid displaced by any previously applied load. Thus the individual increments could be summed to produce the total fluid expelled or imbibed at any given moment in time. By taking the work of Edwards and using it to give the boundary conditions, Yannas produced a theoretical curve for the uptake of fluid in Edwards experiments and found exceptionally good correlation.

Hayes and Mockros,[64] in their investigation of the viscoelastic properties of cartilage, applied linear viscoelastic theory to their creep results by determining three exponential terms and four bulk compliance coefficients for a spring and dashpot representation of a generalised Kelvin solid to fit their experimental results for torsion and uniaxial strain.

Fantuzzo and Graziati[69] also presented a rheologic theory in which a combination of a spring, a dashpot, and a spring and dashpot in parallel, were put in series and the response of an equivalent electric circuit studied. The model was claimed to satisfactorily interpret the behaviour of cartilage under dynamic stress, as observed experimentally, although unfortunately the authors do not state what this behaviour is.

Kempson et al[58] produced values for the Young's modulus of cartilage by using the equations formulated by Waters[70][71] for the indentation of thin sheets of rubber, and substituting the recorded deformations after two seconds of application of the load. Hayes et al[72] also produced a mathematical analysis for indentation tests based on the model of articular cartilage as being an infinite elastic layer bonded to a rigid half space. The problem was formulated as a mixed boundary value

problem of the theory of elasticity and the solutions were suggested as being useful in the determination of an elastic shear modulus of intact articular cartilage.

5.2 Reynolds Numbers of Fluid Flow in Cartilage

To see whether it is valid to use Darcy's law for the flows in articular cartilage, the Reynolds numbers can be estimated by calculating the fluid velocities and using estimates for the pore diameter in articular cartilage.

Assume a diameter of a "pore" to be 60×10^{-10} m.

The maximum deformation rate seems to be of the order of 1 mm in 100 seconds, and as this is accomplished mainly by fluid flow out,

the flowrate/unit area $= 1 \times 10^{-5}$ m/sec.

$$\text{Reynolds number} = \frac{\rho V d}{\eta}$$

$$= \frac{10^{3} \times 1 \times 10^{-5} \times 60 \times 10^{-10}}{10^{-3}}$$

$$= 60 \times 10^{-9}$$

It therefore appears that when flow is occurring in articular cartilage, Darcy's law can be thought of as being entirely valid. Where oscillating deformations take place, and deformation rates are higher than those used above, it will be shown that very little extra flow above that of flow due to the d.c.force is thought to be taking place.

5.3 Some General Comments on Experimental Observations

The main experimental observations from work on the mechanical properties of articular cartilage up to now have been:-

1. Same measurements of porosity and permeability.
2. The articular cartilage is mounted with good adhesion on a bone backing which is very much stiffer than the layer itself.
3. The layer is capable of compressive strains in excess of 40%, followed by complete recovery.
4. Under load, the deformation consists of an "instantaneous" component followed by a creep component, and similarly for the removal of load.
5. The response is very time-dependent.
6. The long term, i.e. equilibrium, load-displacement curve is non-linear but reversible.
7. Osmotic pressures of the order of one atmosphere are postulated.

In the case of an articulating joint, it would appear that the cartilage surfaces on either bone-end are highly conforming, and therefore, when dealing with expanses of the order of (square centimetres) and thicknesses of the order of millimetres, it would appear that any large strains that are imposed will be predominantly uniaxial. From this point of view, indentation tests, although being highly valuable in looking at the topography of the surface, and being able to be performed directly on the femoral head, probably cause the same order of magnitude of strain in the radial as in the axial direction.

In testing of materials, the case where no radial strain is allowed is known as a confined test, and that where no constraint is put on the radial strain as an unconfined test. As was noted in the assumptions for the section on the theory of the deformation of porous materials, only axial

deformation has been assumed in formulating the theory, and therefore in theoretical terms only the confined test is considered, but, as will be seen later, some experimental work has been performed on unconfined tests and the relationship of these tests to the theoretical curves will be commented upon. But because flow of fluid may take place in different directions, no restriction has been placed on the flow.

It may be useful to consider the relationship between the deformations in a confined and unconfined test for a Hookean elastic solid. Using cylindrical co-ordinates and applying linear elastic theory, Hooke's law gives

$$\epsilon_z = \frac{1}{E}\left[\sigma_z - \nu(\sigma_r + \sigma_\theta)\right]$$
$$\epsilon_\theta = \frac{1}{E}\left[\sigma_\theta - \nu(\sigma_r + \sigma_z)\right]$$
$$\epsilon_r = \frac{1}{E}\left[\sigma_r - \nu(\sigma_\theta + \sigma_z)\right]$$

where $\epsilon_z, \epsilon_r, \epsilon_\theta$ are the strains in the z, r, θ directions respectively

$\sigma_z, \sigma_r, \sigma_\theta$ are the stresses in the z, r, θ directions respectively

ν is Poisson's ratio

and E is Young's modulus

For an unconfined test, $\sigma_r = \sigma_\theta = 0$

and $\epsilon_z = \frac{\sigma_z}{E}$

and for a confined test, $\epsilon_\theta = \epsilon_r = 0$

$$\epsilon_z = \frac{1}{E}\left[\sigma_z - \nu \cdot \frac{2\sigma_z}{(1-\nu)}\right]$$
$$= \frac{\sigma_z}{E}\left[\frac{(1+\nu)(1-2\nu)}{(1-\nu)}\right]$$

For a material such as rubber, ν is very near to 0.5 and its resistance to volume change is very large, so compression in a confined test will yield very small strains compared with the results in an unconfined test.

The bulk modulus can be defined as the elastic modulus applied to a body having uniform stress distributed over the whole of its surface, and is related to Young's modulus by the expression

$$K = \frac{E}{3(1-2\nu)}$$

where K is the bulk modulus.

Liquids have no shear at rest but a bulk modulus can still be defined for them, the bulk modulus of water being 2×10^9 N/m^2.

In a confined test, assume that the solid and fluid are equally compressed by the bulk modulus effect, the deformation due to which, as will be shown, is very small compared to the deformation due to fluid flow in and out. Because the articular cartilage can be thought of as composed of 70-80 per cent liquid, assume that the bulk modulus of both solid and fluid is of the same order as that of the fluid (water) alone. Therefore under a normal physiological stress of 1×10^6 N/m^2, the strain due to the bulk modulus effect is of the order of 10^{-3}. Compared to total strains of 0.3 and above, this strain due to elasticity of the cartilage is negligible, when referring to confined tests. It is thought that it is the deformation due to the lateral expansion in an unconfined test which would account for the instantaneous deflections noted by other workers. However, when referring to the performance of articular cartilage under an oscillating load, it will be seen that the strains due to the bulk modulus effect cannot be neglected either in confined or unconfined tests.

To sum up, therefore, it is thought that, under load, the deformation of articular cartilage does consist of an instantaneous component, followed by a creep component, but that this instantaneous component is due to the lateral expansion in unconfined tests, which can be neglected in confined tests under constant load. Experimental evidence for this will be shown later. The creep component, present in both types of tests, is due to fluid flow in and out of the matrix.

5.4 Results from Axial Flow Only

As can be seen from the literature survey, most of the experiments performed on cartilage have been indentation tests or unconfined, and in only two cases have results been reported from confined tests, Edwards on articular cartilage,[61] and Linn and Sokoloff on costal cartilage.[63]

In the former case, curves are presented of

1. Specimen thickness at equilibrium as a function of applied pressure,
2. percentage liquid exchange as a function of time for four differing loads,
3. percentage liquid exchange as a function of applied pressure,

where liquid exchange is defined as $\frac{W_s - W}{W_s - W_D}$

W_s is the fully swollen mass of the specimen,

W is the mass of the specimen at a given time,

W_D is the dry mass of the specimen.

A comparison between curves 1. and 3. show that the relationship between the change in specimen thickness and liquid exchange is approximately constant, showing that the deformation could be accounted for solely by fluid flow out of the matrix. The weighing measurements were taken by removing the cartilage from the apparatus after a certain time of loading, and if there were any significant elastic response in loading, this would recover immediately on removal of the load, so if the specimen thicknesses were measured when the cartilage was out of the apparatus, all that would be measured would be a deformation due to fluid flow out, which will be proportional to the percentage liquid exchange. Curve 2. showed both the variation of liquid content after application of the load, and also, after equilibrium had been obtained, the load was released to show the swelling curves. All results were for articular cartilage from the femoral head of a dog, and the consolidation and swelling curves were for cartilage in

normal saline solution at 20°C.

Edwards also gives values of permeability for the cartilage used in the experiments using both normal saline solution and normal Ringer's solution as the filtration liquid. The values quoted are:-

	Specimen Thickness mm	Pressure Potential lbs/in^2	K cm^4/dyn.s.
Normal Saline	0.51	70	1.09×10^{-13}
Normal Ringers	0.38	70	3.3×10^{-13}

Taking into account a viscosity of approximately 0.001 Ns/m^2, values are obtained of 1.09×10^{-19} m^2 and 3.3×10^{-19} m^2 respectively, the first one of which is certainly very low compared with other values of permeability measured (see literature survey). There may be two reasons for this. One is that the pressure potential of 70 lbs/in^2 which was used to force the fluid through the cartilage will cause a decrease in the area of the pores, although in a complicated way, varying through the thickness.

The other reason for the low permeability may be that the thickness of 0.51 mm is probably not the total thickness and this thickness may have been taken from the deeper parts of the cartilage layer where the fibres are thicker and the permeability (as shown by Maroudas) is lower than the average throughout the thickness.

Edwards does not quote an initial porosity as such, but he does give figures from which this value can be deduced:-

Initial dimensions of specimen = 6.6 mm diameter x 0.48 mm thick

Fully swollen mass of specimen = 16.2 mg.

Dry mass of specimen = 4.6 mg.

These figures give an initial porosity of 71%.

A computation of the experiments Edwards performed was therefore set up to predict deformation with time under the loads that were used in

the experiments. The curve given by Edwards of deformation versus applied pressure at equilibrium is shown in Figure 29. A fit to this curve of the form $\sigma = \frac{a\epsilon}{1-b\epsilon}$ which was used in the computation is also shown. The graphs of percentage liquid exchange were converted to direct deformations, the value of 1.09×10^{-16} m^4/N sec as measured by Edwards was used for the coefficient of permeability divided by the dynamic viscosity, and 0.71 as the value for initial porosity. Effects on the deformations of varying these parameters will be shown later, but the graphs for the four different applied loads shown by Edwards, both for compression and expansion, are shown in Figures (30) - (33).

Agreement at the two lower loads is good, but this agreement tends to decrease as the applied load is increased. In all the graphs after the release of load the agreement is good. Also shown on the graphs is the difference that an assumption of constant permeability with strain would make, and it appears that this makes far more difference in the compression of the cartilage than in the expansion.

Applying dimensional analysis to the system gives

$$\left(\frac{\delta}{z_0}\right) = f_n\left[\left(\frac{k_z}{z_0^2}\right), \left(\frac{\sigma t}{\eta}\right), (\nu)\right]$$

where δ is the deformation

and σ the applied pressure.

For two constant applied pressures of 1.02×10^6 N/m^2 and 2.04×10^6 N/m^2, Figures (34) and (35) show the variation of $\left(\delta/z_0\right)$ with $\left(\frac{\sigma t}{\eta}\right)$ for various values of $\left(k_z/z_0^2\right)$ and Figures (36) and (37) show the variation for various values of (ν). The variation of initial porosity makes some difference to the response, and this effect increases as the strain becomes nearer to the initial porosity. To extrapolate this to the situation of the initial porosity equalling the final strain means that, as soon as the load is applied, the pores at the surface are closed up and

no fluid flow through the surface can then take place.

However it is the coefficient of permeability which governs to a large extent the deformation-time characteristic as would be expected, and there is an inverse linear relationship between the time to reach a certain strain and $\left(k_z/z_0^2\right)$ for a given constant load.

At high loads the solution is more prone to instability, because small changes in the fluid pressures will be accompanied by large changes in strain, and the process does not converge when high fluid pressures cause low strains which cause low fluid pressures. This instability does not occur at the lower loads.

It is thought that from these curves it is reasonable to state that it is probably not the initial values of the permeability or porosity which cause the discrepancy at high loads. Because the agreement is so good at the lower loads, it is thought that this descrepancy may lie in the variation of permeability with strain when strains nearing the initial porosity are encountered. This variation is not so important after release of the load, when the difference between the curves assuming variable and constant permeability is very slight, and therefore the predictions after release of load are very near the experimental results. It appears that the variation of permeability with strain is approximately correct at low strains, but is more severe than the one postulated at high strains. However the simple relationship used gives good results for normal physiological walking stresses[73] of 150-300 lbs/in^2 (1 - 2 x 10^6 N/m^2).

The way the deformation is accomplished with time is shown by the way the strain varies with the depth from the surface as the time is increased. Figure 38 shows this variation under a constant pressure of 1.02 x 10^6 N/m^2. Because one of the boundary conditions is that the fluid pressure at the surface is zero, all the loading at the surface must be taken by the solid, so immediately upon application of the load the strain

at the surface has the value of the final strain, and everywhere else the strain is zero. As time increases, the strains in the lower layers are gradually increased as fluid seeps out of them. Eventually, at an infinite time in theory, the whole material is at the same strain, the final strain, and no more deformation will then take place. The vertical lines on the graph show the positions of various points in the solid with respect to the surface as the whole surface deforms with time. Figure 39 shows the magnitude of the fluid pressures throughout this deformation, the pressures bearing most of the load at the start of the deformation except at the surface where the gauge pressure must be zero, and decrease as the strain in the material and time increases.

Figure 40 shows the position after the constant stress of 1.02×10^6 N/m^2 has been removed. Immediately after release of the load the strain at the surface returns to zero, and the other layers then gradually imbibe fluid and return to the original dimensions, when the strain throughout the cartilage is zero. Figure 41 shows the magnitudes of the fluid pressures in this situation. It should be noted here that during the re-establishment of the original dimensions after the release of load, the fluid pressures predicted by the theory are negative. In practice, a fluid under tension may cavitate, and in this situation the fluid will not sustain the negative pressures. Thus the cartilage dimensions will return far more quickly to the initial conditions than the theory here predicts. It is perhaps an indication of the theory predicting the release of load to some degree of accuracy that the fluid does not cavitate inside the cartilage under the conditions prevailing.

Experiments have also been performed in this Laboratory[74] on the variation of deformation with time for various loadings on bovine cartilage using the same configuration as the experiments performed by Edwards.

The experiments were performed on the total thickness of cartilage attached to the bone end, the diameter of the specimens being 5.5 mm. The load was applied axially so that flow could take place axially through a permeable bronze disc which had a permeability coefficient of about 10^8 times as big as that of cartilage, so flow would not be impeded. Deformation was read from an ultra-violet recorder to which was fed the signal of the average of two displacement transducers positioned an equal distance on either side of the applied load.

Initially it appeared that there was an instantaneous deformation of about 0.2 mm, but it transpired that the p.t.f.e. liner in which the cartilage was contained had deformed permanently under the constant loading to which it was subjected. This deformation meant that there was room for the cartilage to expand laterally, initially giving an axial deformation of about 0.2 mm. It was thought that after this lateral expansion the cartilage was in effect confined and could therefore be treated as such. Unfortunately, reliable measurements of permeability have not yet been obtained, the difficulties having been noted in the literature review. Because the total thickness of a layer of cartilage was used, an average coefficient of permeability of 5.0×10^{-19} m^2 has been used, as this figure seems a mean of measurements taken by other workers when working on the whole layer. Strains in excess of 0.75 could be achieved by applying very large stresses, so an initial porosity of 0.8 was used. As can be seen from Figures (42) and (43) the agreement is again quite good.

An effect which has not been taken into account in deformation is that of osmosis. Flow under osmosis will be into the cartilage due to the concentration of large molecules inside the cartilage, and thus when compression occurs in a laboratory rig, flow will only take place under a difference in fluid pressure from the equilibrium osmotic pressure. Thus osmosis will tend to keep the fluid inside the cartilage whilst under

pressures, due to the osmotic pressure in the fluid outside causing the effective gauge pressure to be altered.

The application of a sinusoidal load (which will subsequently be called the a.c. load) together with that of a constant load (subsequently called the d.c. load) has also been investigated, as joints are very seldom under static loads for very long. It appears that the deformations due to the a.c. load oscillates about the d.c. deformation, although the two deformations cannot be superimposed in theory because the d.c. stiffness affects the a.c. deformation. However it will be shown that in practice the two effects can be treated separately.

In theoretical terms, assuming that inertia effects can be neglected and that the force on the solid is equal to the addition of the constant and sinusoidal forces at its appropriate time in the cycle, the deformations predicted differ very little from those in the constant load case. The frequency used in the cases of oscillating loads was 60 cycles/minute (approximating to that of a walking cycle), but because of computational difficulties in the axial flow case, only the results from two cycles were produced. These showed that for an a.c. stress of 1×10^6 N/m^2, an a.c. strain of 6.25×10^{-6} was produced, giving a modulus of 1.6×10^{11} N/m^2. The phase difference was difficult to ascertain to any degree of accuracy because the deformations computed were only for the first two cycles.

In practice it appears that in sinusoidal loading the bulk modulus effect that has already been mentioned becomes significant, unlike the d.c. loading case. The experimental results show that, in the confined, axial flow type test, the response is of a sinusoidal deflection superimposed upon the deformation due to the constant load alone. This a.c. response appears to lag the applied a.c. load slightly and has a modulus of $0.25 - 1.0 \times 10^9$N/m^2 depending from where on the cartilage surface the specimen is taken. The

deflection appears to stay approximately constant with variation in time providing the a.c. load is kept constant. The frequency of oscillation mainly used was 50 cycles/minute, although it was found that altering the frequency made very little difference to either the phase lag or modulus. Figure 44 shows a typical hysteresis loop for one cycle at 50 cycles/minute, and gives a phase lag of about 15°. To ascertain if this phase lag was significant in talking about the elasticity of articular cartilage, the same oscillating experiment was performed on a cylinder of rubber of the similar dimensions. The results of stress versus strain for one cycle are shown in Figure 45 and this shows a hysteresis loop with a phase lag of about 11°, approximating to that of cartilage. Therefore it would appear that the a.c. response of articular cartilage in a confined configuration can be regarded as reversible as that of rubber, the modulus of which is of the same order as the bulk modulus of water, i.e. all that is happening on a short time cycle is that the fibres and water together which make up the articular cartilage are being alternately compressed and relaxed due to the bulk modulus effect.

It may be interesting to note the findings of Hayes and Mockros,[64] who compressed human articular cartilage in a confined test with pervious and impervious load pads. Their findings indicated to them that flow processes were not dominant in the deformation, because deflections in both cases were similar. This would therefore indicate a bulk modulus for the cartilage of the order of 10^{6} N/m^{2}, three orders of magnitude different from that of water, and also very different from the bulk moduli of most liquids or solids. These results seem totally at variance with other findings, and the explanation may be that there was fluid flow around the sides of the impervious load pad, the total sealing of a test of this kind being difficult.

5.5 Results from Radial Flow Only

The theoretical results for radial flow only in a confined case both for a constant load and also with the addition of a sinusoidal load are much easier to produce, but are probably not so useful from the experimental standpoint. In practice, to produce radial flow only means making no restriction on the flow at the sides of the cylinder which then makes the test unconfined.

However, looking at the theoretical results from a confined radial flow test can show several salient points. Because the boundary conditions are now different, the deformation in general takes longer to accomplish than in the axial flow case. Figure 48 shows the variation of deformation with time using the same thickness of specimen as in Edwards' experiment, but now it is the radius of the cylinder which will make a large difference.

Dimensional analysis gives

$$\left(\frac{\delta}{z_0}\right) = f_n\left[\left(\frac{k_r}{R^2}\right), \left(\frac{\sigma t}{\eta}\right), (\nu)\right]$$

where R is the radius of the cylinder.

Figure 46 shows that for a given deformation, the time is inversely proportional to $\left(k_r/R^2\right)$ (as given by Equation (4.2.9)). Figure 47 shows the effect of variation of initial porosity on the non-dimensional deflection-time curve. It is interesting to note that, as shown by Figure 48, on release of load, the rate of recovery of the deformation is very much slower than in the axial flow case, and that all these curves corresponding to no load are a constant distance apart, the distance depending on the strain at which the load was released. This latter point also appears from the solution to the conditions at no load (Equation (4.2.11)).

Figures (49) - (52) show the effect of an a.c. load superimposed upon a d.c. load at different times during the deformation. These clearly show that these a.c. strains, which, from the initial assumptions, are due

to fluid flow in and out of the matrix, are very small compared to those experienced when including the bulk modulus effect. These oscillations lag the applied load by approximately 50°, and, as can be seen from Figures (49) and (52) reduce in magnitude as the d.c. load causes a deformation, due to the decrease in the permeability and increased stiffness in the matrix. Initially the amplitude of the oscillations is of a strain of about 0.0001 for an a.c. stress of 1×10^{6} N/m^{2} giving a modulus of 10^{10} N/m^{2}. Towards the end of the displacement the modulus is of the order of 10^{11} N/m^{2}.

It is also interesting to note in a confined radial flow test, the behaviour when a constant strain rate is applied to the surface and calculating the total force exerted by the specimen. This variation is shown in Figure 53. Because the fluid force is directly proportional to the strain rate, this force becomes dominant at high strain rates. Of course, the case of a strain rate of zero corresponds to the stress-strain curve at equilibrium.

In the practical case of radial flow, the specimen is now unconfined and there is no resistance to sideways motion, except for friction of the specimen on the plates through which the load is transmitted. This effect causes the specimen to become barrel-shaped under loading. The experiments in this Laboratory on unconfined tests,[74] have shown that, for a given load, there is a larger final strain than in the confined case, which can be attributed to the lateral expansion due to Poisson's ratio mentioned earlier at the start of this Section. Figure 54 shows a typical curve of deflection with time under a constant load, showing an instantaneous displacement followed by a time dependent response, and on release of load there is an instantaneous recovery followed by a slow relaxation as shown by the theory. The instantaneous deflections on compression and relaxation

are not equal in magnitude, the deflection on release of load always being smaller. This can be explained by considering articular cartilage as being a complete material for the moment. At the beginning of compression there is physically more material than when fluid has been squeezed out at the end of the time dependent deformation. Considering constant cross-sectional area A and a constant elastic modulus Y,

Initially on compression

$$Y = (\sigma/A)/(\delta_0/z_0)$$

where σ is the applied stress

At relaxation $$Y = -(\sigma/A)/\left(-\frac{\delta_1}{(\delta_1 + z_1)}\right)$$

where δ_0 is the instantaneous response on compression

δ_1 is the instantaneous response after release of the load

and z_1 is the thickness at equilibrium before release of the load.

Combining these equations gives

$$\frac{\delta_0}{\delta_1} = \frac{\delta_x}{z_1} + 1$$

where δ_x is the creep deflection

Thus the ratio $\left(\delta_0/\delta_1\right)$ can never be less than 1. This expression seems to fit the experimental values fairly well for calculating the instantaneous response after release of load.

The variation in radial permeability will also be affected in some fashion by this lateral displacement. Because the lateral displacement is increasing, the cross-sectional area will increase throughout and, when the axial strain is equal to the initial porosity, the radial permeability will not be zero.

Under an oscillating load, the a.c. strain initially is larger than in the confined test, giving an elastic modulus of $0.04 - 0.1 \times 10^9 N/m^2$, and the strains reduce with time, so that at equilibrium the elastic modulus

is in the range 0.11 - 0.38 x 10^9 N/m^2. It must be stressed that these values of moduli are calculated using the initial cross-sectional area, and it would seem reasonable to attribute most of the apparent increase in the modulus to an increase in the cross-sectional area as the d.c. strain increases due to a large value of Poisson's ratio. This latter conclusion is borne out by the fact that the ratios of the elastic moduli at the start and at the end (i.e. the inverse ratios of the cross-sectional areas at the start and end) appear to be related to the final d.c. strain. The stress-strain characteristic for one cycle shown in Figure 55 again shows a hysteresis loop which is derived from a phase lag of about 16^o, but as has been shown in the confined case for rubber, this lag may well be typical of the phase lag of a non-metallic material which is within its "elastic" range.

It may be interesting to note quantitatively the effect of performing an unconfined test on a specimen of articular cartilage and holding the deformation constant. Having compressed the material initially to a certain axial strain and hence using a force to apply this strain, the instantaneous reaction of the cartilage is to expand laterally. The fluid in the mesh of fibres is then under pressure, and over a time seeps out to the atmosphere, and as this happens the force exerted by the cartilage decreases as would be expected. Because of the loss of fluid the diameter of the specimen, which initially had increased, returns slowly to its initial diameter. Eventually, the fluid pressures and fluid force are zero and the slight load exerted by the cartilage is that required to compress the solid matrix to the predetermined strain. Thus the instantaneous radial strain has disappeared due to the volume change of fluid flow out, and the specimen has finished almost as if it were in a confined test.

5.6 Results from Axial and Radial flow simultaneously

In referring to real joints, this combination is probably the most realistic, in the sense that, although the displacement may be predominantly uniaxial, flow will still take place in all directions, the distribution depending on fluid pressures in the lubricating film.

Unfortunately, this is also the most difficult to compute, not from the sense of the method of computation, which is the same as in a one-dimensional axial flow case, but because so many more nodal points have to be used when iteration is taking place, and the computing time is therefore much longer.

However, some results have been computed, and these results are shown in non-dimensional form in Figures 56 and 57. Figure 56 shows that a variation in $\left(k_r/R^2\right)$ only makes a slight difference to the deformations, even on the scale of a variation of two orders of magnitude. Figure 57 shows the effect of variation in $\left(k_z/z_0^2\right)$ on the deformation, and it therefore can be seen that it is the magnitude of this factor which governs the axial deformation rate. Comparing Figure 57 with Figure 34 shows the deformations are greater than with axial flow only. Although across a layer the fluid pressures are almost constant, except very near the boundary where they decrease to zero, these pressures are correspondingly lower than in the axial flow case, creating larger strains and larger deformations in the cartilage.

5.7 Discussion

To sum up, the experimental results seem to show that, both in confined and unconfined cases, the response to an oscillating and constant load together can be represented by the addition of a response due to the constant load and a response due to the oscillating load. The constant load response is due, in the confined case, almost solely to fluid flow out of the cartilage, and the oscillating response to an elastic distortion of the cartilage as a whole, the displacements being smaller in the confined case than in the unconfined case as would be expected for any material.

The modelling of articular cartilage as a deformable porous material, the matrix of which has a reversible, recoverable but non-linear, stress-strain characteristic, has shown that an approach of this kind will produce constant load deformations to a fair degree of accuracy at normal physiological loads, although because there is thought to be very little fluid flow due to a sinusoidal force alone, under an oscillating load an elastic modulus has to be added to account for the elastic deformations which take place. It is thought, however, that the variation of permeability with strain for cartilage, especially at strains nearing the initial porosity, is slightly more severe than the one used and this would give more accurate predictions of deformation with time at high loads.

In the actual working of an articulating joint, it would seem very rarely that articular cartilage undergoes deformation due only to constant loads for any length of time (perhaps sentries on duty, or spectators in a crowd) and even then there is probably a constant shifting of muscles creating varying loads in the joint. In any modelling of an actual joint undergoing normal motion, it would therefore appear that deformations of the cartilage layers will probably be elastic ones due to the varying

pressures during a walking cycle but the thickness of the layers will be changing due to the fluid flow out under the average load throughout the cycle.

However, in making observations of this sort, one must not lose sight of the object of this investigation. The aim has been to produce a model of articular cartilage which will predict the characteristics shown in a laboratory rig. Only when this has been done can the model be used with some confidence in the real situation of an articulating joint where the behaviour will be governed by the conditions existing in the joint. These conditions will involve the fact that the pressures are exerted on the cartilage by a fluid instead of a solid, and thus pressures on the cartilage may vary with, for instance, distance from the centre of the joint, which may affect the deformation.

6. Summary and Conclusions

With the eventual aim of looking at the special case of articular cartilage, this thesis has reported work performed on porous materials, and, because articular cartilage appears so dependent on its interstitial fluid for some of its mechanical properties, the main area of interest has been in the flow of fluids through porous materials.

The law governing the flow due to fluid pressure, Darcy's law, was investigated and a literature review revealed that the limit of its validity was thought to range from Reynolds' numbers of 0.1 up to 75, and an experimental investigation showed that in the case of 1 mm glass beads, the limit was of the order of 1. It was also shown that Darcy's law could be used in predicting the flowrates to some degree of accuracy when flow was taking place axially and radially simultaneously in a cylinder.

The variation of permeability with strain was investigated in directions parallel and perpendicular to the direction of applied strain in a porous polymeric material. It was found that variations were more pronounced in the perpendicular directions, as perhaps would be thought, although both permeabilities became zero only when the applied strain was approximately equal to the initial porosity and thus all the pores were closed.

The main conclusions from the work probably come from the section applying the work in other sections to the special case of articular cartilage. It appears that modelling articular cartilage as a deformable porous material whose matrix has a reversible, recoverable, but non-linear stress-strain characteristic, and assuming a simple variation in

permeability with strain predicts the time-dependent deformations to a good degree of accuracy, agreement being excellent at normal physiological loads. The experimental work, which will be reported in more depth later, has shown that under sinusoidal loads the oscillating deformations can be regarded as almost elastic, both in confined and unconfined cases, the modulus of which probably varies with position on the surface of the articulating joint.

References

1. McCutchen, C.W. — The frictional properties of animal joints. Wear 5 1 1962

2. Walker, P.S., Dowson D., Longfield M.D. and Wright V. — Boosted Lubrication in synovial joints by fluid entrapment and enrichment. Ann. rheum. Dis. 27 512 1968.

3. Dowson D., Unsworth A. and Wright V. — Analysis of 'boosted' lubrication in human joints. J.Mech. Eng. Sci. 12 364 1970

4. Higginson G.R. and Norman R. — The lubrication of porous elastic solids with reference to the functioning of human joints. J.Mech. Eng. Sci. To be published.

5. Higginson G.R. and Norman R. — A model investigation of squeeze-film lubrication in animal joints. Phys. Med. Biol. To be published.

6. Darcy, H.P.G. — Les Fontaines Publiques de la Ville de Dijon. Victor Dalmont. Paris 1856.

7. Scheidegger A.E. — Flow through porous media. Appl. Mech. Rev. 13 313 1960.

8. Hubbert M.K. — Darcy's law and the field equations of the flow of underground fluids. J. Petr. Tech. 8 222 1956

9. Whitaker S. — The equations of motion in porous media. Chem. Eng. Sci. 21 291 1966.

10. Poreh M and Elata C. — An analytical derivation of Darcy's law. Israel J. Tech. 4 214 1966.

11. Collins R.E. — Flow of fluids through porous materials. Reinhold Pub. Corp. 1961.

12. Scheidegger A.E. — The physics of flow through porous media. Univ. of Toronto Press. Toronto 1957.

13. Chambre P.L. and Selim M.A. — On unsteady flow of compressible liquid through porous medium. Appl. Sci. Res. 10A 363 1961.

14. Paria G. — Flow of fluids through porous deformable solids. Appl. Mech. Rev. 16 421 1963.

15. Polubarinova-Kochin P.Ya. — Theory of ground water movement. Princeton Univ. Princeton. 1960.

16. Hudson H.E.Jnr. and Roberts R.F. — Transfer from laminar to turbulent flow through granular media. Proc. 2nd Midwestern Conf. on Fluid Mech.1952.

17. Leva M., Weintraub M., Gemmer M., Pollchik M., and Storch H.H. — Fluid flow through packed and fluidized systems. U.S. Bureau Mines Bull. 504 1951

18. Nielsen R.F. — Permeability constancy range of porous medium World Oil 132 188 1951

19. Plain G.J. and Morrison H.L. — Critical Reynolds number and flow permeability Am. J. Phys. 22 143 1954

20. McKinley R.M., Jahns H.O., Harris W.W. and Greenkorn R.A. — Non-Newtonian flow in porous media A.I.Ch.E. 12 17 1966.

21. Fancher G.H., Lewis J.A. and Barnes K.B. — Some physical characteristics of oil sands The Pennsylvania State College Bulletin Bulletin 12 65 1933

22. Ohle E.L. — The influence of permeability on ore distribution in limestone and dolomite Economic Geology 46 667 1951.

23. Klinkenberg L.J. — The permeability of porous media to liquids and gases
Am. Petr. Inst. Drilling and Production Practice. 200 1941.

24. Noble B. — Numerical Analysis
Oliver and Boyd. Edinburgh. 1964.

25. Streeter V.L. — Fluid Mechanics
McGraw-Hill New York 1966.

26. Kozeny J. — Uber kapillare Leitung des Wassers im Boden
Ber. Wien. Aked. 136A 271 1927

27. Fair G.M. and Hatch L.P. — Fundamental factors governing the streamline flow of water through sand.
J. Am. Water Works Assoc. 25 1551 1933.

28. Mitchell J.K., Hooper D.R. and Campanella R.G. — Permeability of compacted clay
Proc. A.S.C.E. 91 (SM4) 41 1965.

29. Grootenhuis P. and Leadbetter C.J. — Discussion in : Symposium on Powder Metallurgy, Iron and Steel Inst. Special Report 58 361 1954

30. Morgan V.T. — Porous metal bearings
In : Principles of Lubrication
A. Cameron. Longmans London 1966.

31. Taylor D.W. — Fundamentals of Soil Mechanics
John Wiley and Sons. New York 1948.

32. Fraser H.J. — Experimental study of the porosity and permeability of elastic sediments
J. Geol. 43 966 1935

33. Schofield A.N. and Wroth C.P. — Critical State Soil Mechanics. McGraw-Hill. New York. 1968

34. Biot M.A. — General theory of three-dimensional consolidation. J. Appl. Phys. 12 155 1941

35. Biot M.A. — Theory of elasticity and consolidation for a porous anisotropic solid. J. Appl. Phys. 26 182 1955

36. Biot M.A. — Theory of deformation of a porous viscoelastic anisotropic solid. J. Appl. Phys. 27 459 1956.

37. Biot M.A. — General solutions of the equations of elasticity and consolidation for a porous material. J. Appl. Mech. 23 91 1956.

38. Hunter W. — Of the structure and diseases of articulating cartilages. Phil. Trans. 42 514 1743.

39. Hassell A.H. — Microscopic anatomy of the human body. Vol. 1. Samuel Highley. London 1849.

40. Schäfer E.S. — The essentials of histology. Longmans, Green and Co. London 1920.

41. Hultzkranz J.W. — Uber die spaltrichtungen der gelenk-knorpel. Verh. Anat. Ges. Jena. 12 248 1898.

42. Ramon Y. and Cajal S. — Histology. Tindall and Cox. London 1933.

43. Benninghof A. — Experimentelle untersuchungen uber den einfluss verschiedenartiger mechanischer beanspruchung auf der Knorfel. Verh. Anat. Ges. Jera. 33 194 1924.

44. Benninghof A. Form und bau der gelenk-knorpel in ihren beziehungen Zu funktion II. teil : der aufbau des gelenk-knorpel in seinen bezeihungen zu funktion
Z Zellforsch 2 783 1925.

45. Benninghof A. Die modellierenden und former haltenden fakaoren des knorpelreliefs
Z. Anat. Entw. Gesch. 76 43 1925.

46. MacConaill M.A. The movements of bones and joints : 4 the mechanical structure of articulating cartilage
J. Bone Jt. Surg. 33B 251 1951.

47. Zarek J.H. and Edwards J. The stress-structure relationship in articulating cartilage.
Med. Electron and Biol. Eng. 1 497 1963.

48. Little K., Pimm L.H. and Trueta J. Osteoarthritis of the hip.
J. Bone Jt. Surg. 40B 123. 1958

49. Davies D.V., Barnett C.H. Cochrane W. and Palfrey A.J. Electron microscopy of articular cartilage in the young adult rabbit.
Ann. Rheum. Dis. 21 11 1962.

50. McCall J. Load deformation response of the micro-structure of articular cartilage.
In : Lubrication and Wear in Joints.
Sector Pub. London 1969.

51. Davies D.V. Properties of synovial fluid
Proc. Instn. Mech. Engrs. 181 (3J) 25 1966-67.

52. King R.G. A rheological measurement of three synovial fluids
Rheological Acta. 5 41 1966.

53. Bär E. Elastizitätsprufungen der gelenk-knorpel
Arch. f. Entw. d. Orgen. 108 739 1926

54. Göcke E. Elastizitätsstudien am jungen und alten gelenk-knorpel
Verh. d. dutsch Orthop. Ges. 130 1927.

55. Hirsch C. A contribution to the pathogenesis of chondromalacia of the patella
Acta Chir. Scand. 90 Suppl 83 9 1944.

56. Elmore S.M., Sokoloff L., Norris G. and Carmeci P. Nature of imperfect elasticity of articular cartilage.
J. Appl. Physiol. 18 393 1963.

57. Sokoloff L. Elasticity of aging cartilage
Fed. Proc. 25 1089 1966.

58. Kempson G.E., Freeman M.A.R. and Swanson S.A.V. The determination of a creep modulus for articular cartilage from indentation tests on the human femoral head.
J. Biomechanics 4 239 1971.

59. Kempson G.E., Spivey C.J., Swanson S.A.V. and Freeman M.A.R. Patterns of cartilage stiffness on normal and degenerate human femoral heads.
J. Biomechanics 4 597 1971

60. Kempson G.E., Spivey C.J., Freeman M.A.R. and Swanson S.A.V. Indentation stiffness in articular cartilage in normal and osteoarthosic femoral heads.
In : Lubrication and Wear in Joints.
Sector Pub. London 1969.

61. Edwards J. Physical characteristics of articular cartilage
Proc. Instn. Mech. Engrs. 181 (3J) 16 1966-67

62. Camosso M.E. and Marotti G. — The mechanical behaviour of articular cartilage under compressive stress. J. Bone Jt. Surg. 44A 699 1962.

63. Linn F.C. and Sokoloff L. — Movement and composition of interstitial fluid of cartilage. Arthr. Rheum. 8 481 1965

64. Hayes W.C. and Mockros L.F. — Viscoelastic properties of human articular cartilage. J. Appl. Physiol. 31 481 1971.

65. Swanson S.A.V., Kempson G.E. and Freeman M.A.R. — Tensile properties of articular cartilage In : Lubrication and Wear in Joints Sector Pub. London 1969.

66. Maroudas A. — Physicochemical properties of cartilage in the light of ion exchange theory. Biophys. J. 8 575 1968.

67. Maroudas A. and Bullough P.G. — The permeability of articular cartilage Nature 219 1260 1968.

68. Yannas I.V. — Involvement of articular cartilage in a linear relaxation process during walking. Nature 227 1358 1970.

69. Fantuzzo D.G. and Graziati G. — A mathematical model for articular cartilage. Digest of 7th Int. Conf. on Med. and Biol. Eng. 1967.

70. Waters N.E. — The indentation of thin rubber sheets by spherical indenters. Br. J. Appl. Phys. 16 557 1965.

71. Waters N.E. — The indentation of thin rubber sheets by cylindrical indenters. Br. J. Appl. Phys. 16 1387 1965.

72. Hayes W.C., Keer L.M., Herrmann G. and Mockros L.F. — A mathematical analysis for indentation tests of articular cartilage. J. Biomech. 5 541 1972.

73. Freeman M.A.R. (ed) — Adult Articular Cartilage Pitmans London 1973.

74. Snaith J.E. — M.Sc. Thesis. Durham University. To be published.

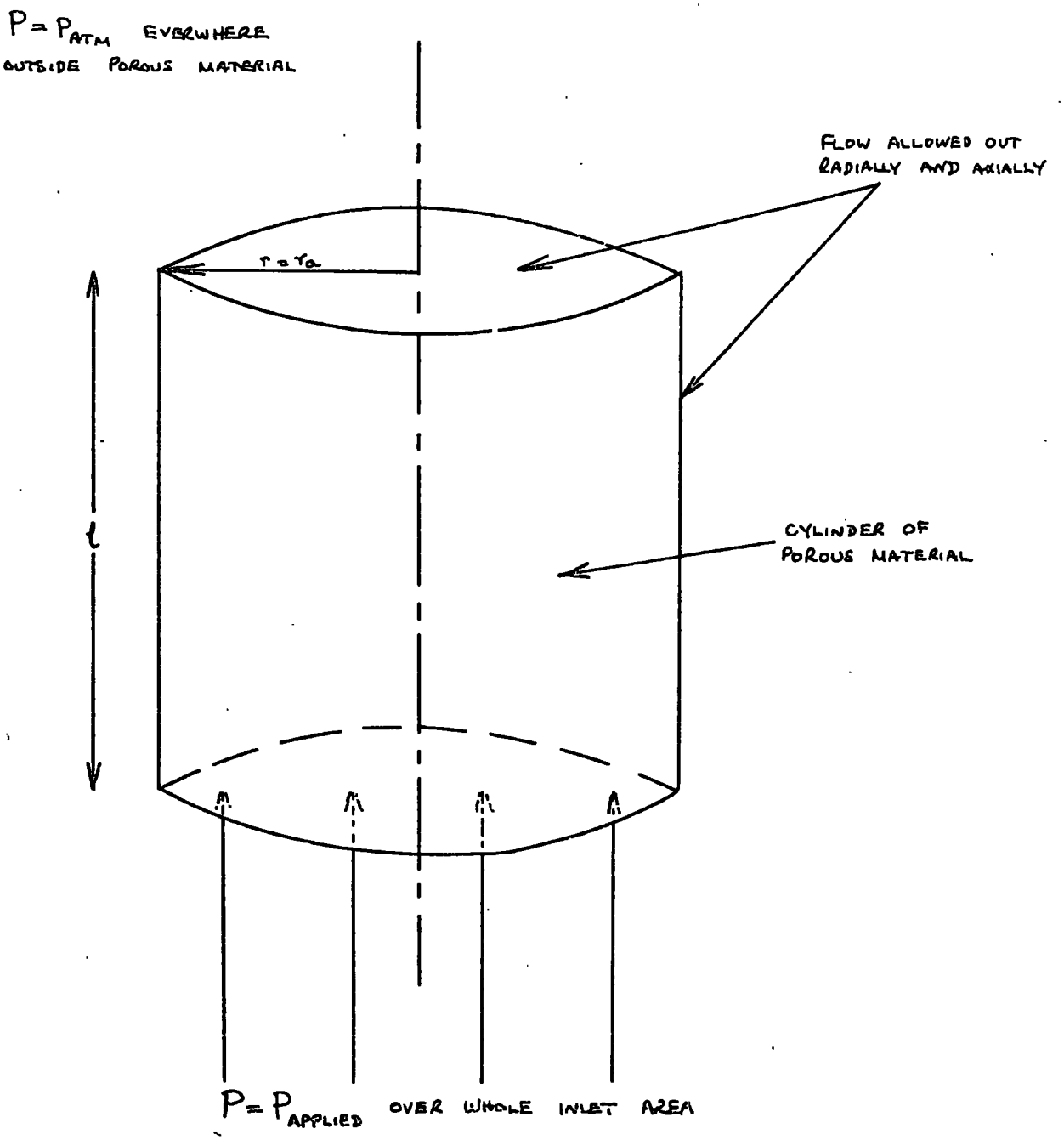

FIGURE 1 : GENERAL SCHEME OF FLOW IN POROUS MATERIAL

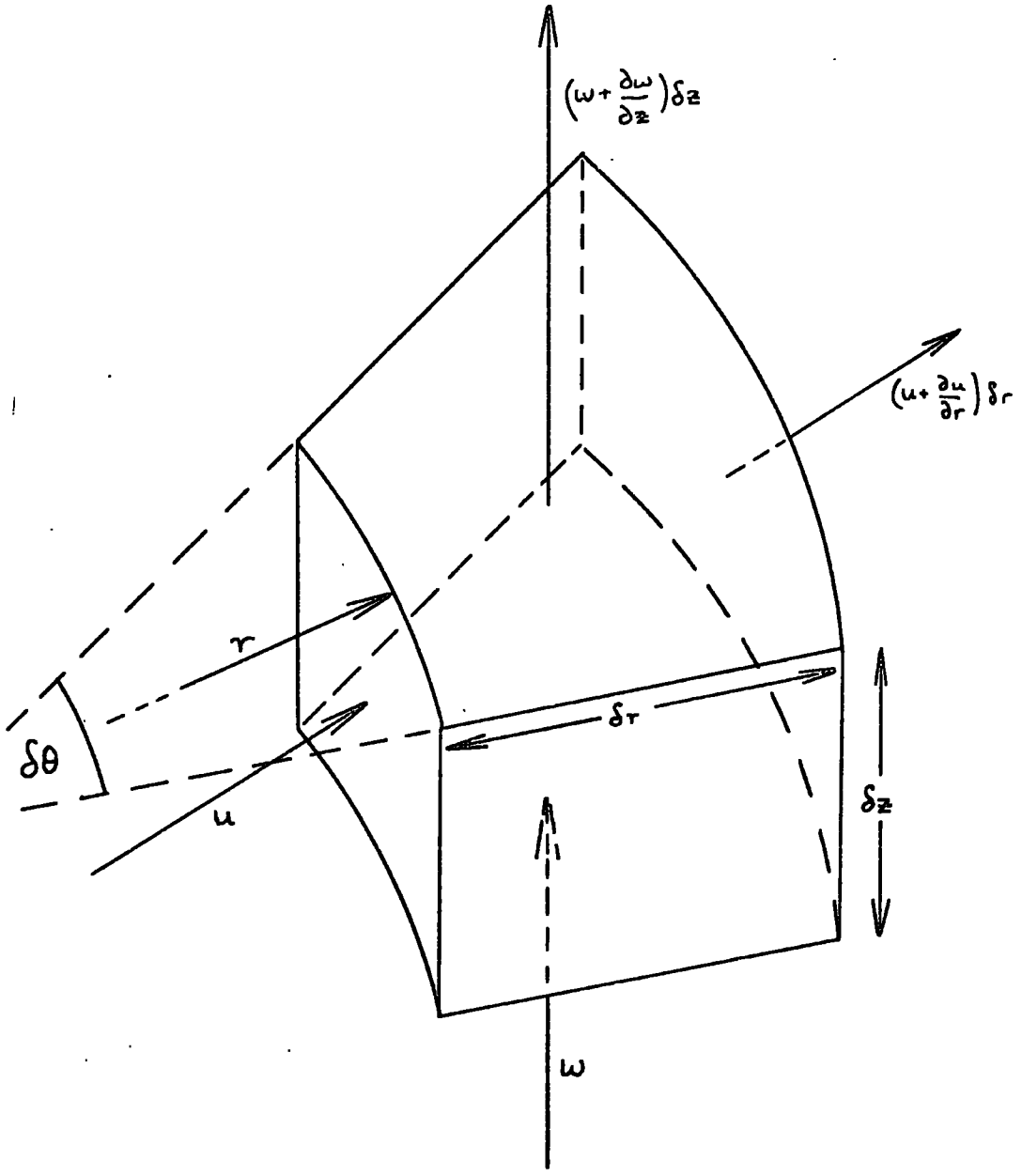

FIGURE 2 : FLOWS IN AN ELEMENT OF A MATERIAL WITH AXIAL SYMMETRY.

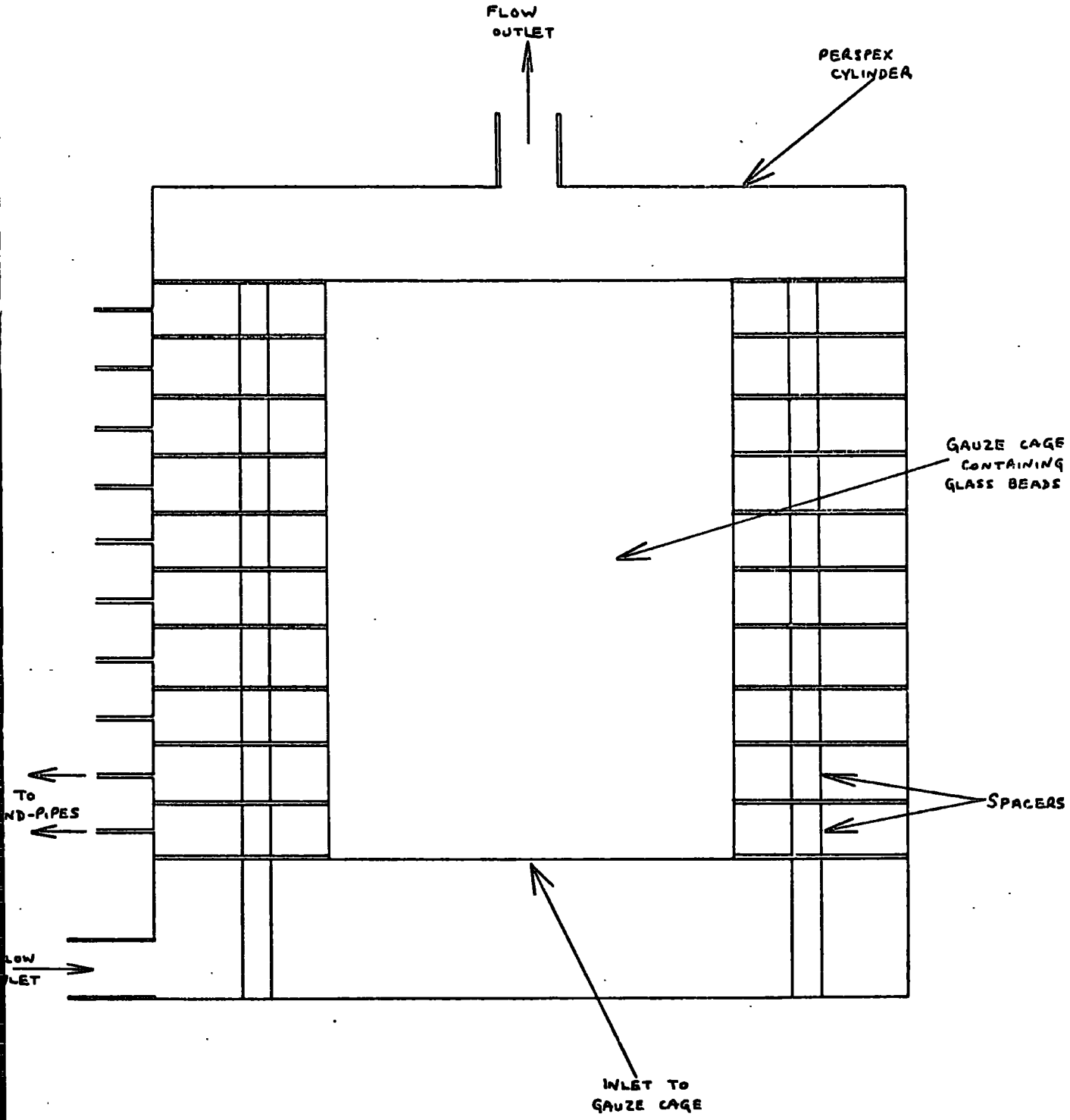

FIGURE 3 : APPARATUS FOR ONE-DIMENSIONAL FLOW

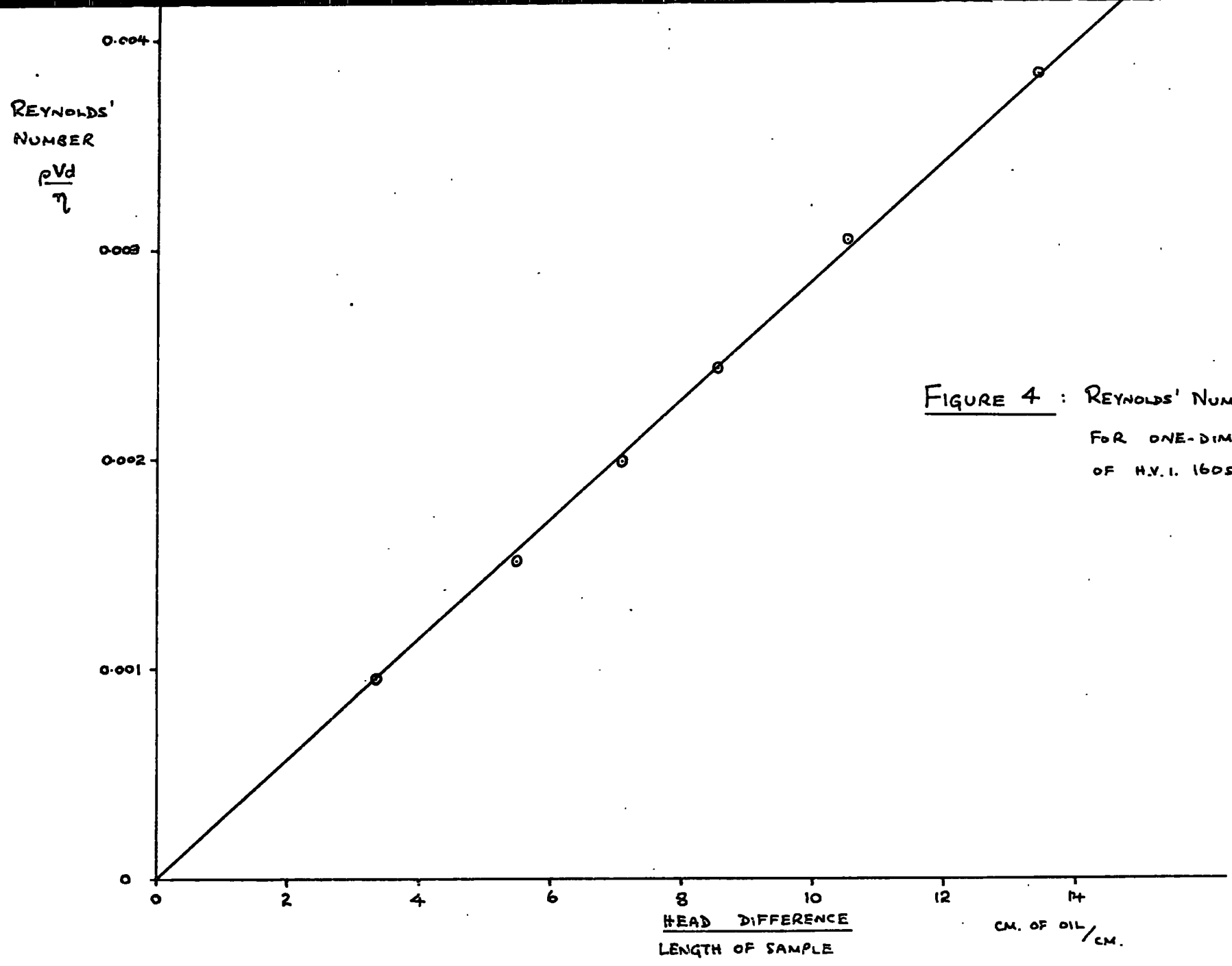

FIGURE 4 : REYNOLDS' NUMBER VS. $\frac{\text{HEAD DIFFERENCE}}{\text{LENGTH OF SAMPLE}}$
FOR ONE-DIMENSIONAL FLOW
OF H.V.I. 160S MINERAL OIL

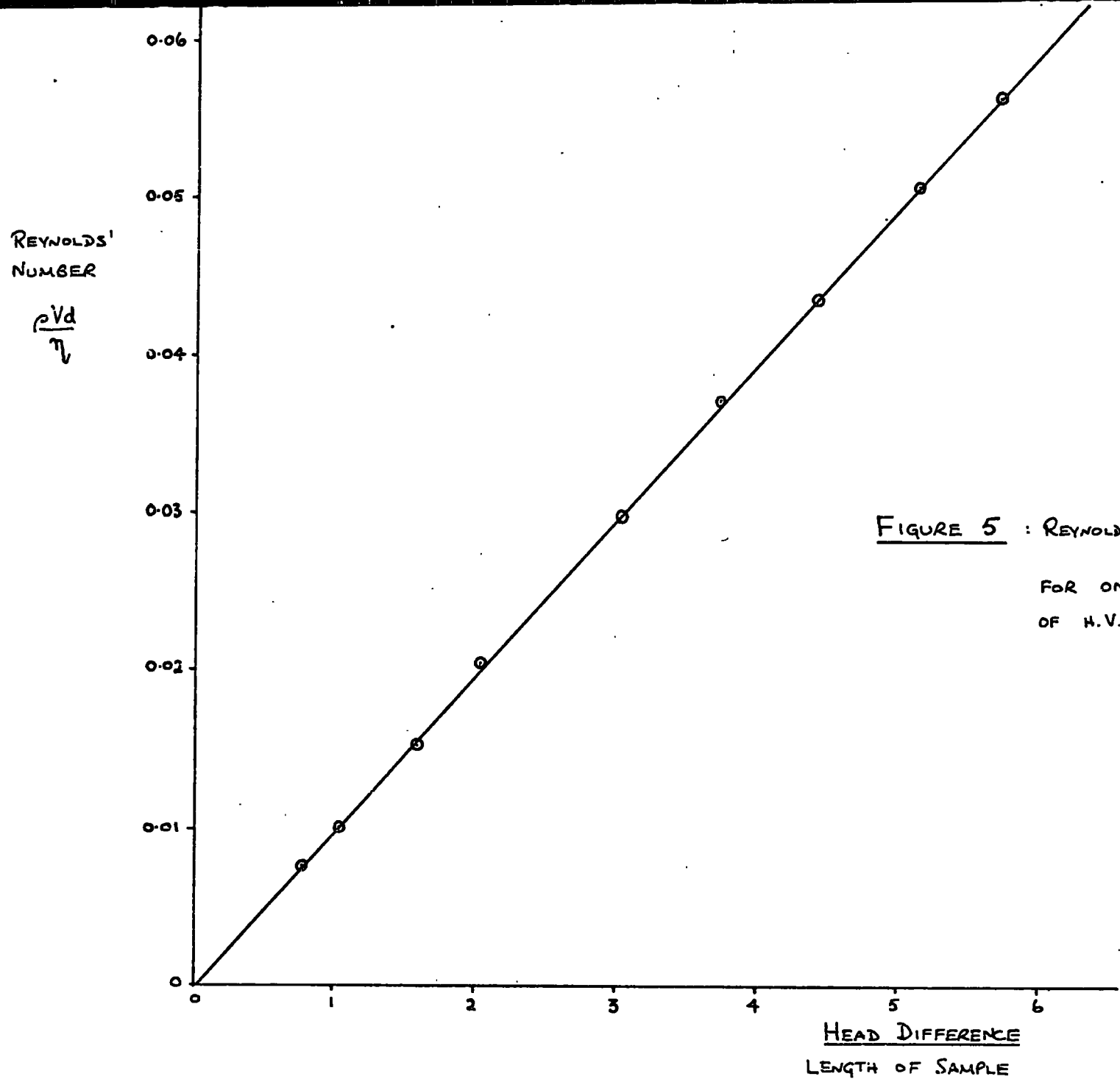

FIGURE 5 : REYNOLDS' NUMBER VS. HEAD DIFFERENCE / LENGTH OF SAMPLE

FOR ONE-DIMENSIONAL FLOW OF H.V.I. 55 MINERAL OIL.

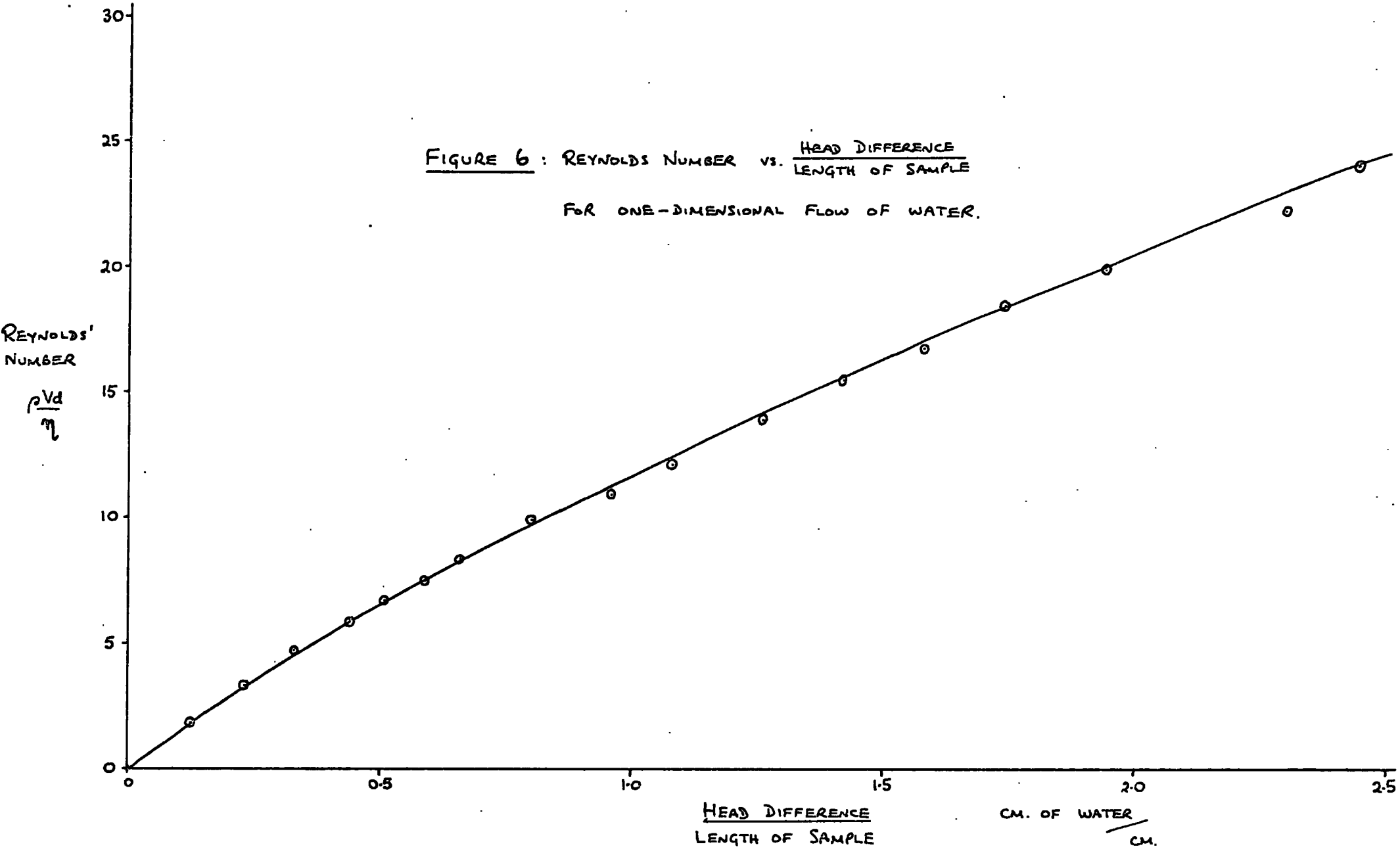
FIGURE 6 : REYNOLDS NUMBER vs. HEAD DIFFERENCE / LENGTH OF SAMPLE
FOR ONE-DIMENSIONAL FLOW OF WATER.
REYNOLDS' NUMBER
ρVd/η
30
25
20
15
10
5
0
0
0·5
1·0
1·5
2·0
2·5
HEAD DIFFERENCE / LENGTH OF SAMPLE
CM. OF WATER / CM.

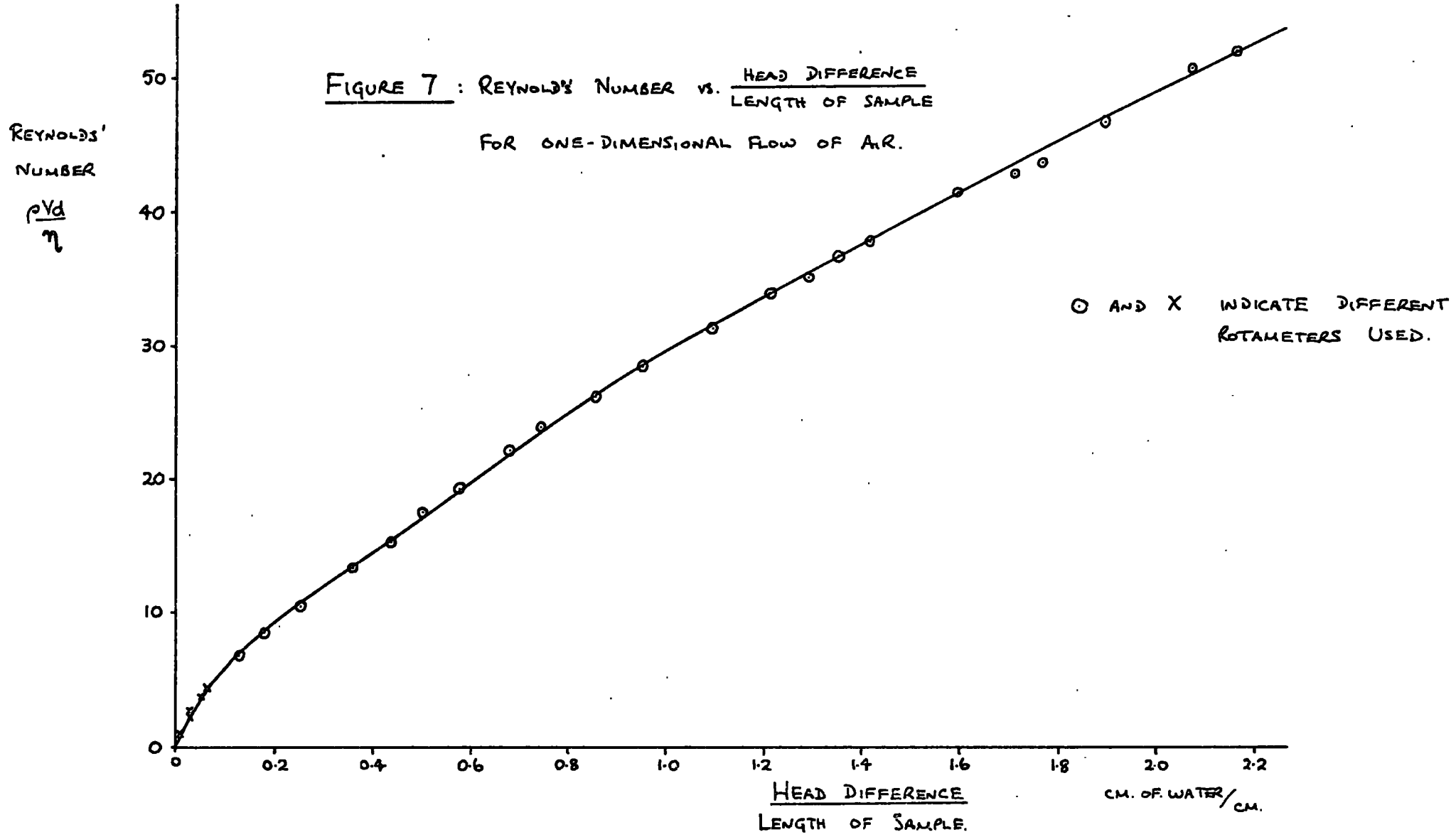
FIGURE 7 : REYNOLD'S NUMBER vs. HEAD DIFFERENCE / LENGTH OF SAMPLE
FOR ONE-DIMENSIONAL FLOW OF AIR.
REYNOLDS' NUMBER ρVd/η
50
40
30
20
10
0
0
0·2
0·4
0·6
0·8
1·0
1·2
1·4
1·6
1·8
2·0
2·2
HEAD DIFFERENCE / LENGTH OF SAMPLE.
CM. OF WATER/CM.
⊙ AND X INDICATE DIFFERENT ROTAMETERS USED.

FIGURE 8 : COMPARISON OF THEORY AND EXPERIMENT FOR THE FLOW OF WATER FROM THE SIDES OF A CYLINDER.

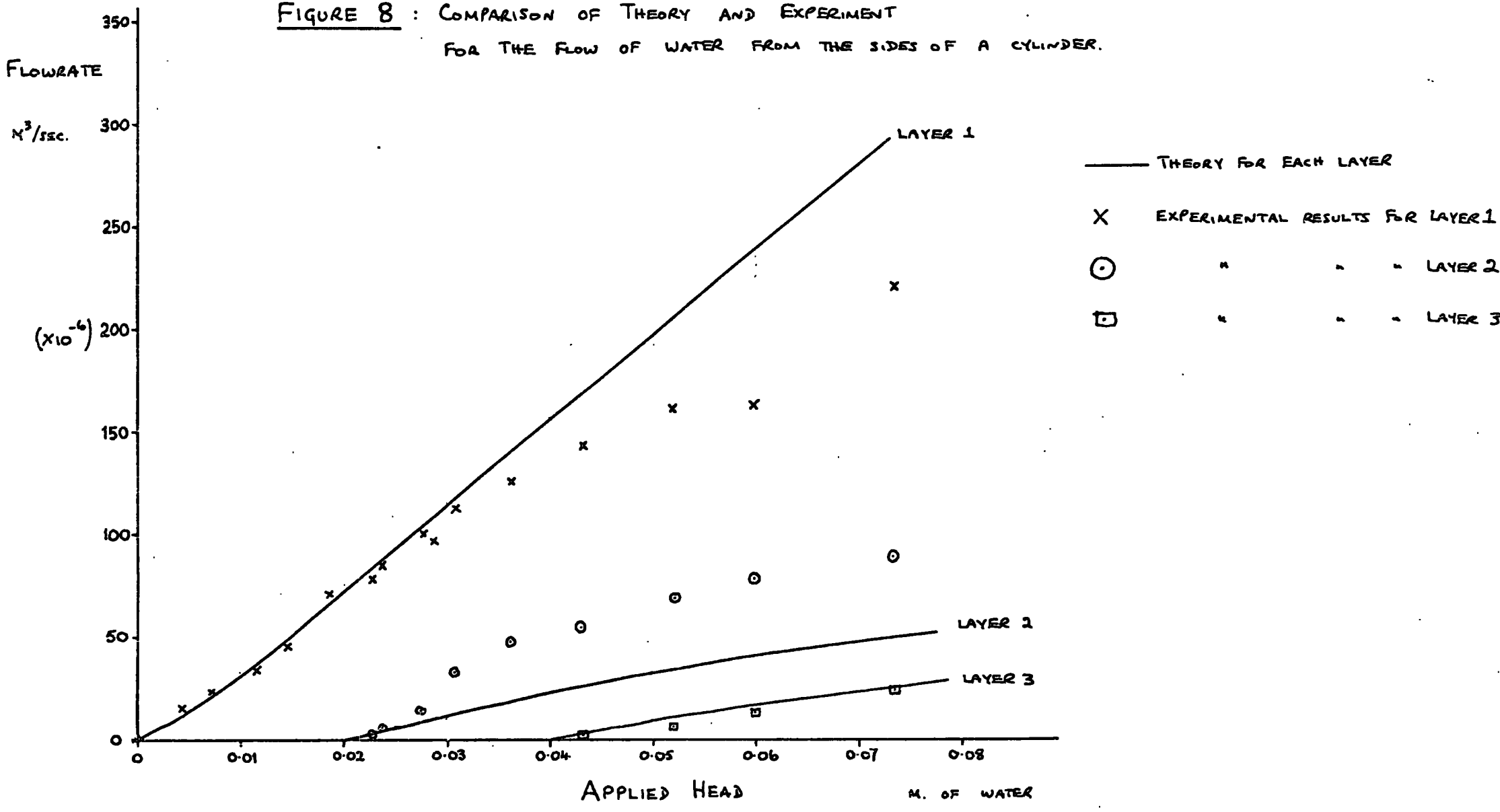

FIGURE 9 : COMPARISON OF THEORY AND EXPERIMENT
FOR THE TOTAL FLOWRATE OF WATER FROM THE SIDES OF A CYLINDER

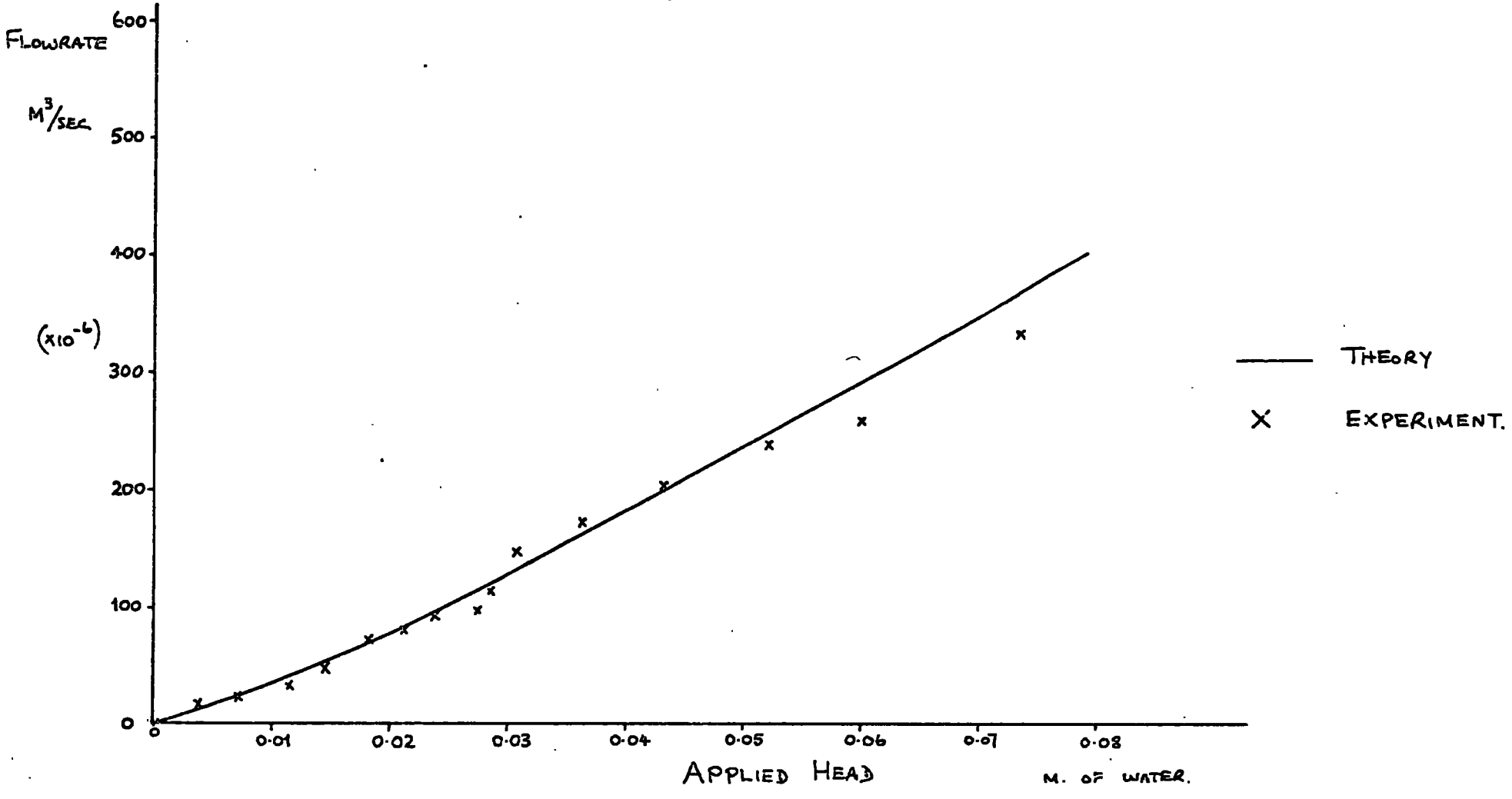

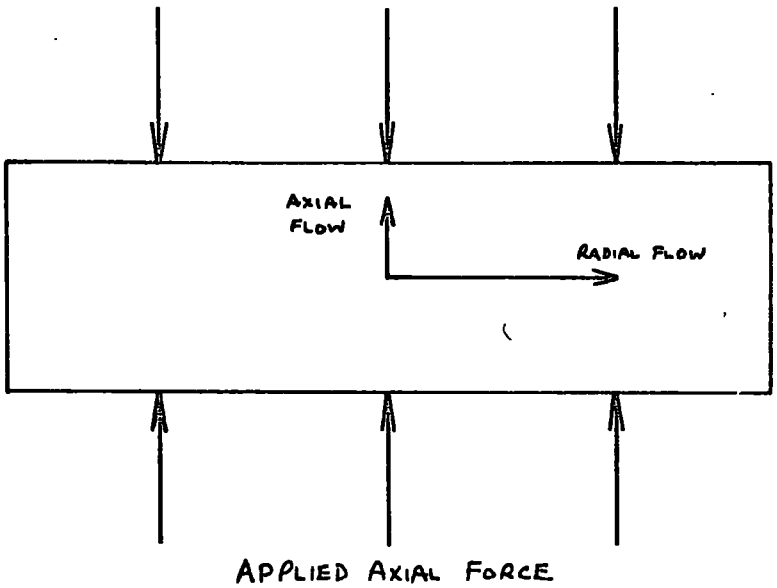

FIGURE 10: DIRECTIONS OF AXIAL AND RADIAL FLOW WITH APPLIED STRAIN

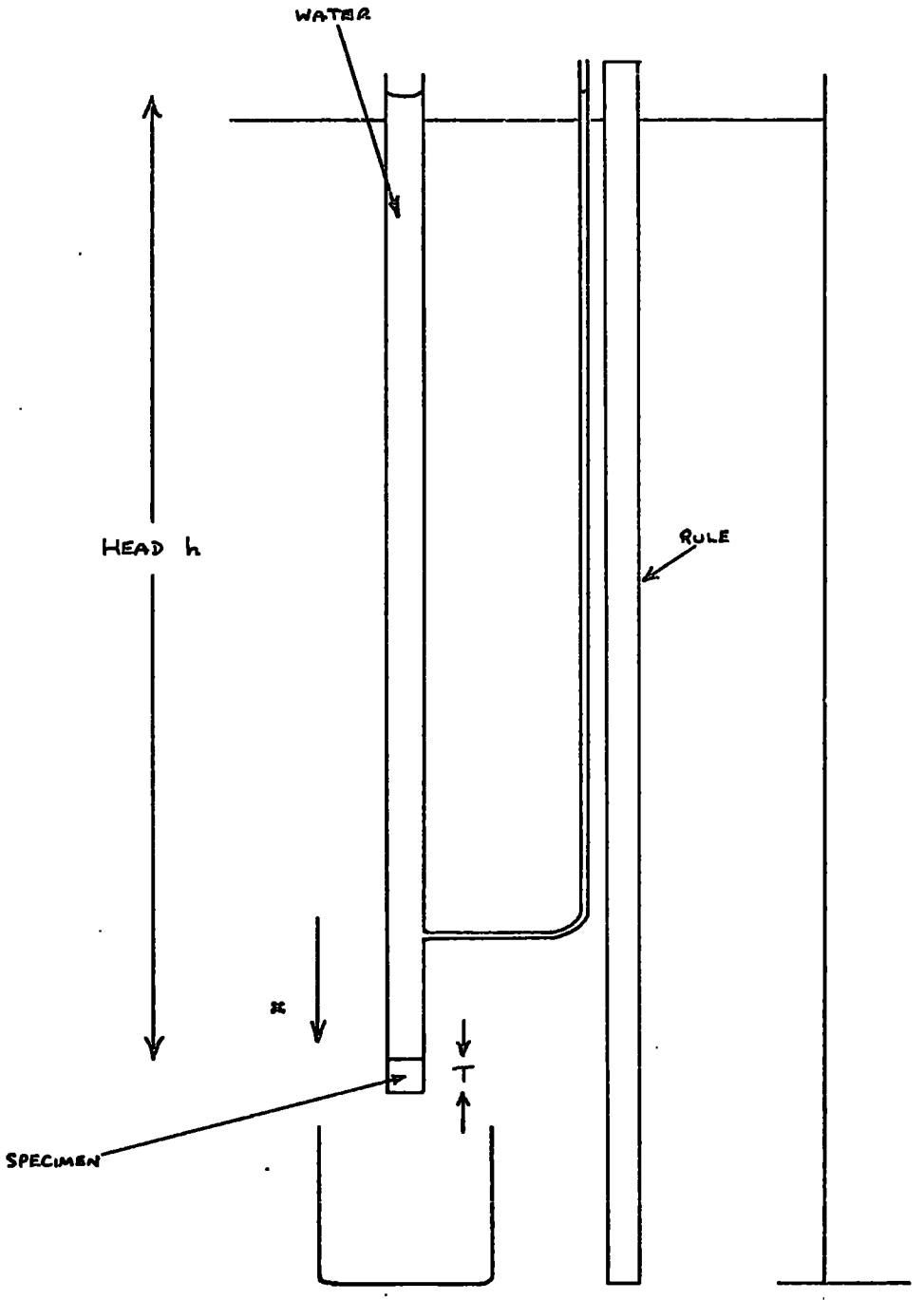

FIGURE 11: FALLING HEAD PERMEAMETER

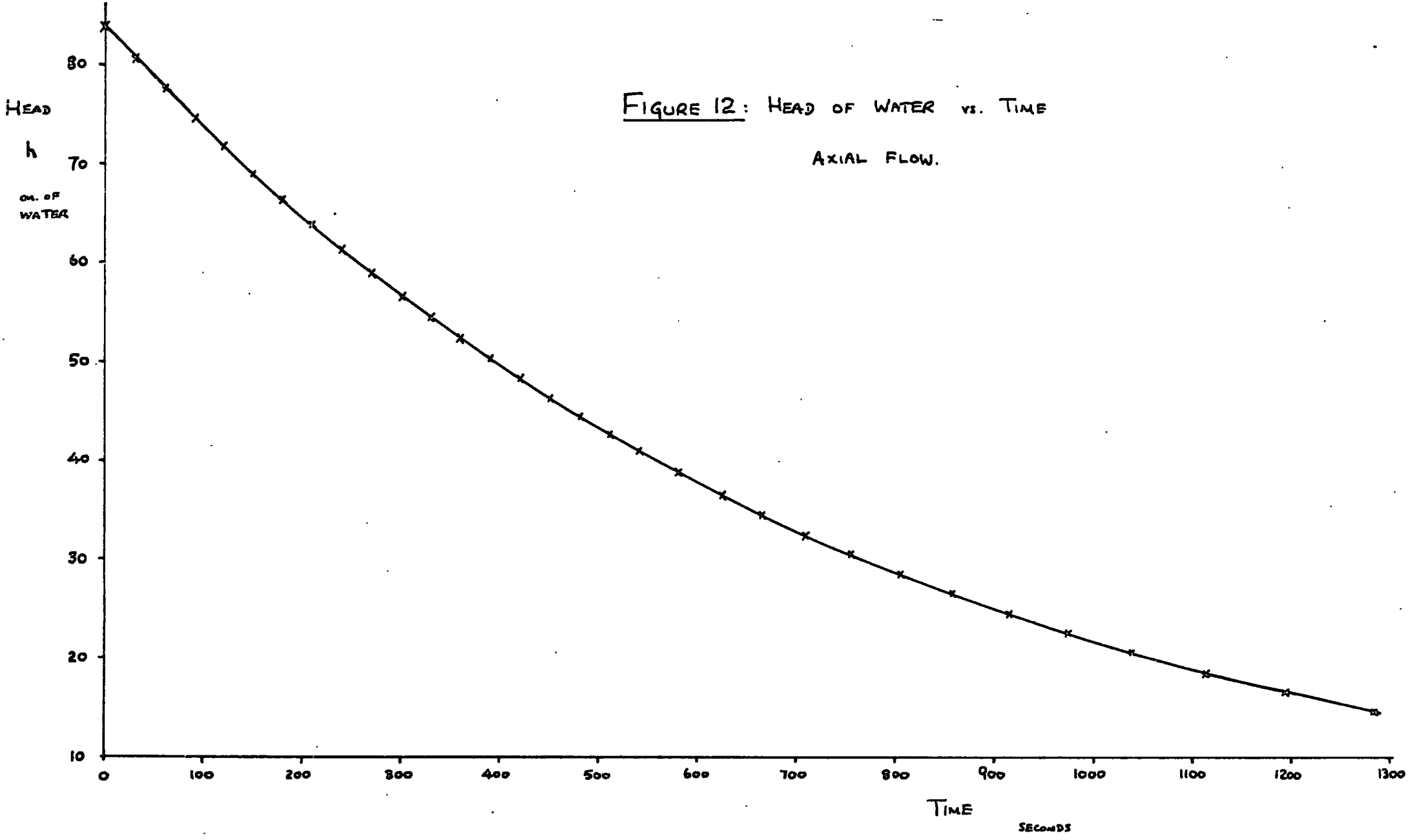

FIGURE 12: HEAD OF WATER vs. TIME

AXIAL FLOW.

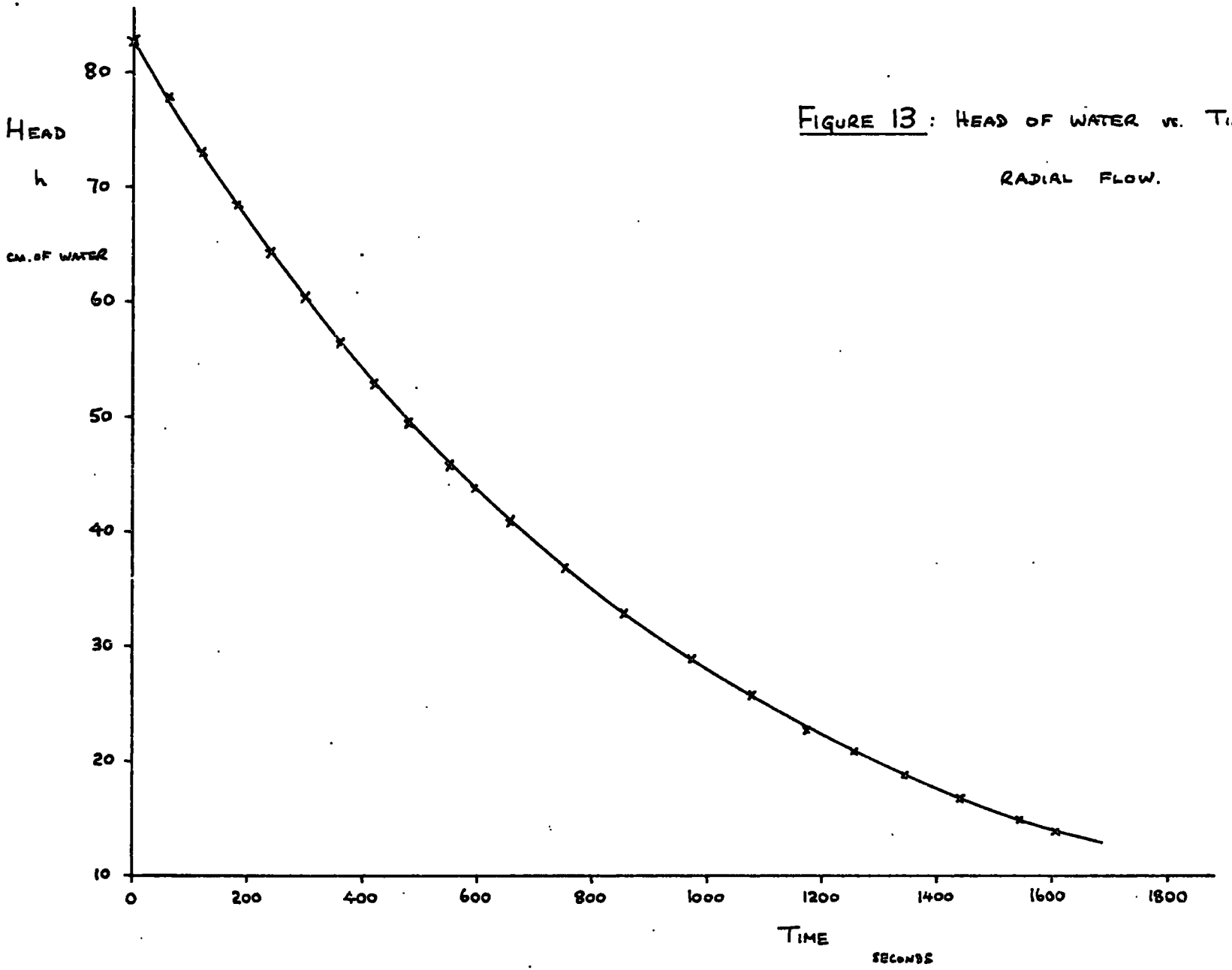

FIGURE 13 : HEAD OF WATER VS. TIME

RADIAL FLOW.

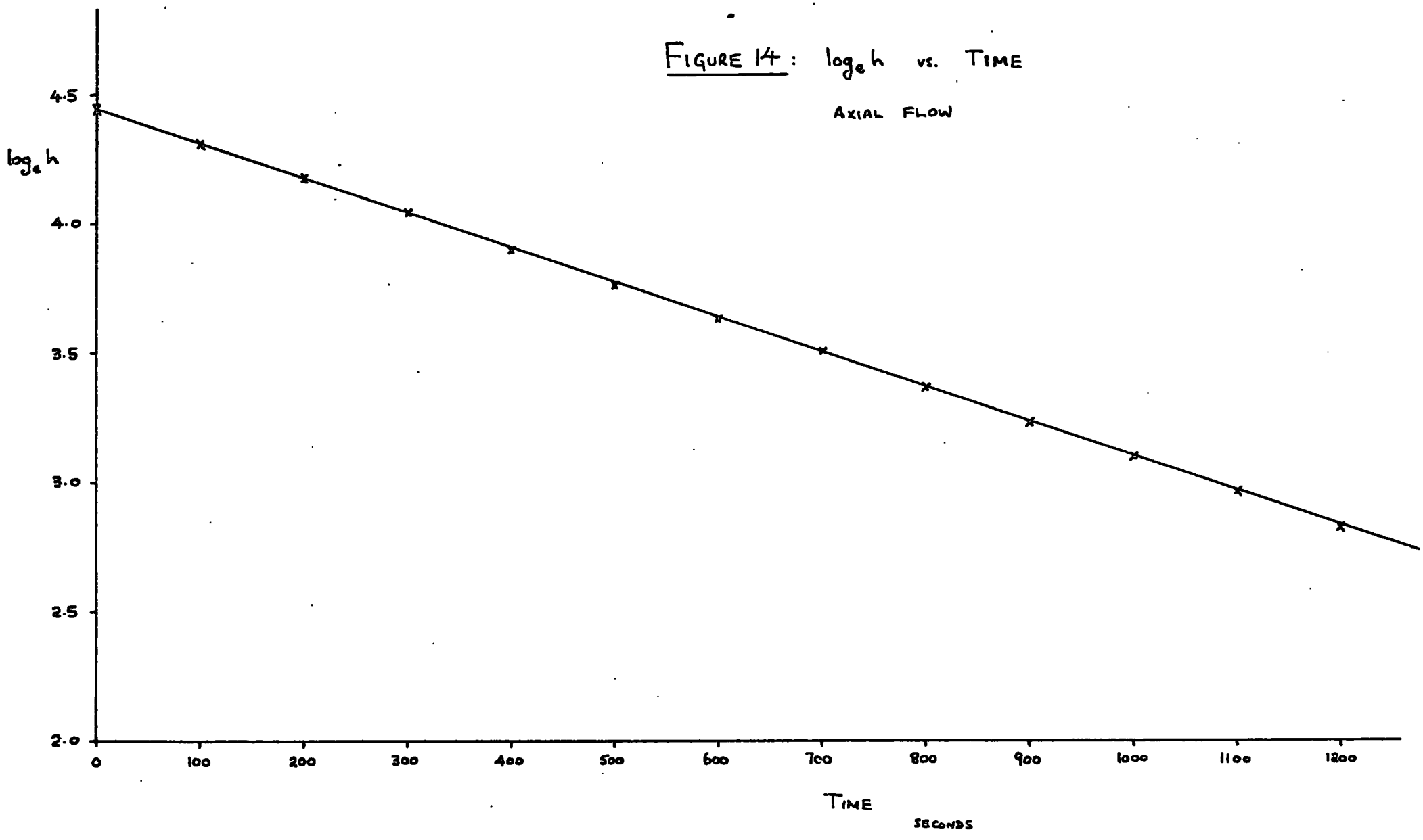
FIGURE 14: $\log_e h$ vs. TIME
AXIAL FLOW
$\log_e h$
4.5
4.0
3.5
3.0
2.5
2.0
0
100
200
300
400
500
600
700
800
900
1000
1100
1200
TIME
SECONDS

FIGURE 15: $\log_e h$ vs. TIME

RADIAL FLOW

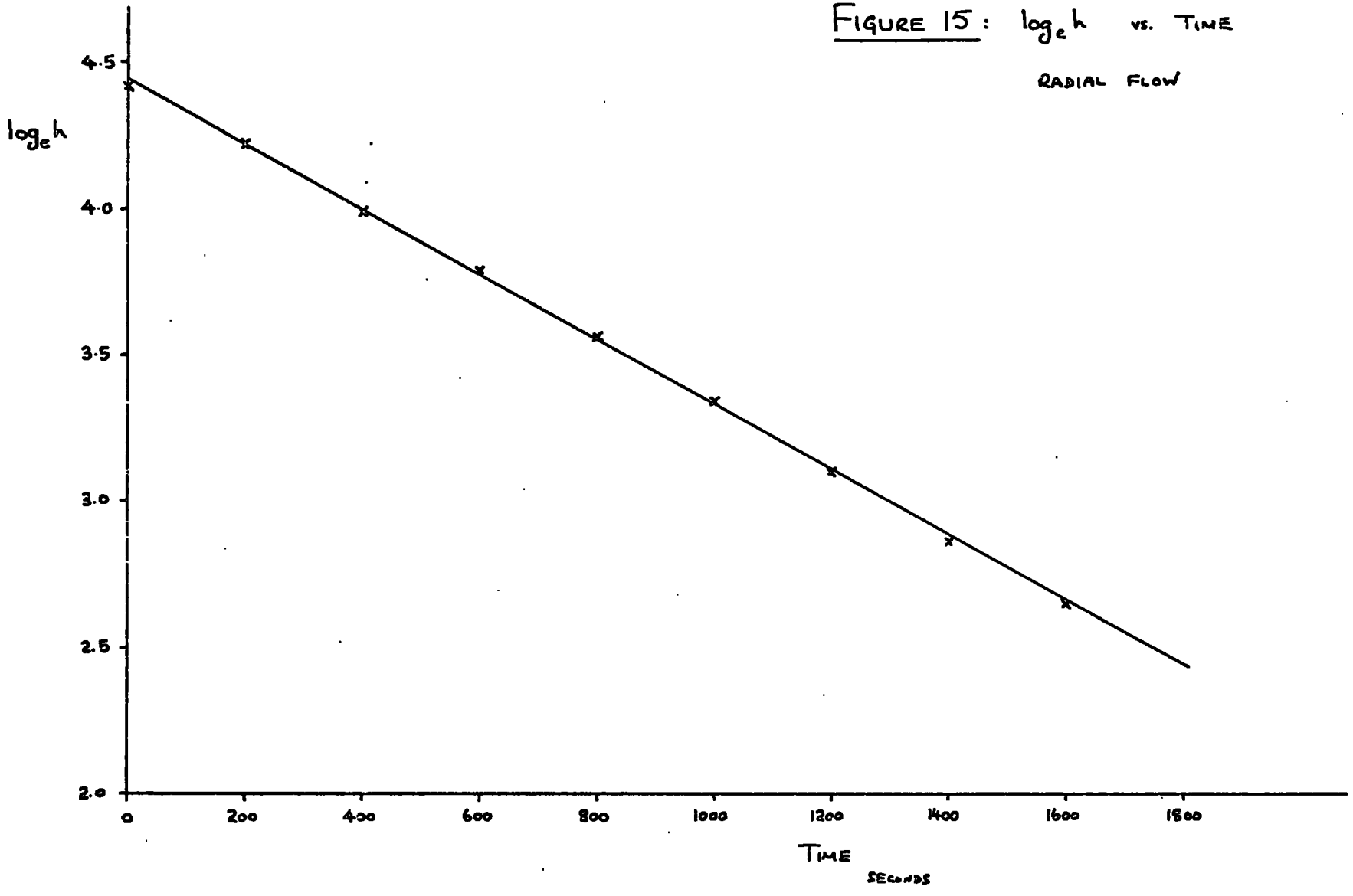

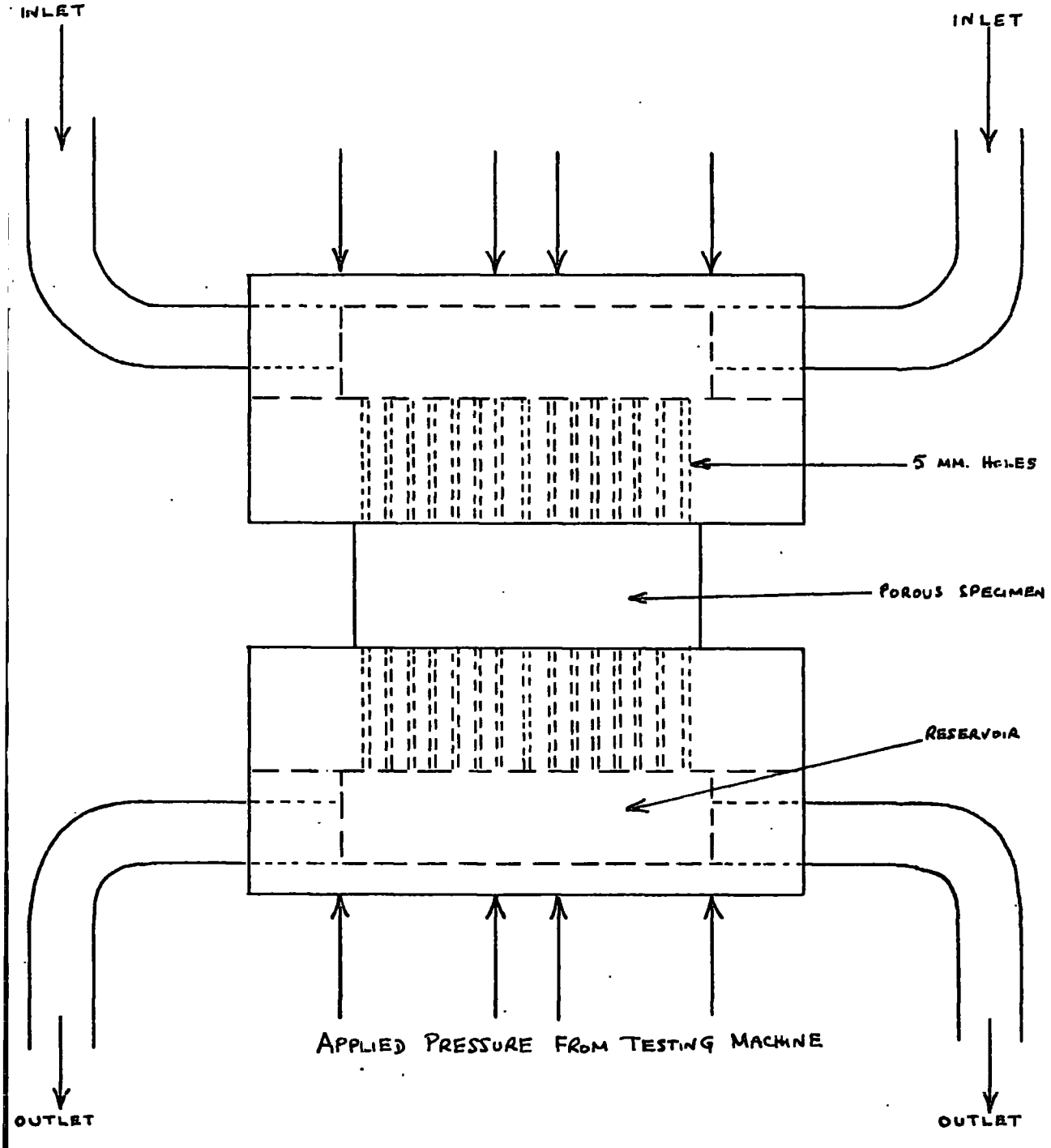

FIGURE 16: APPARATUS FOR MEASURING PERMEABILITY OF A MATERIAL UNDER STRAIN

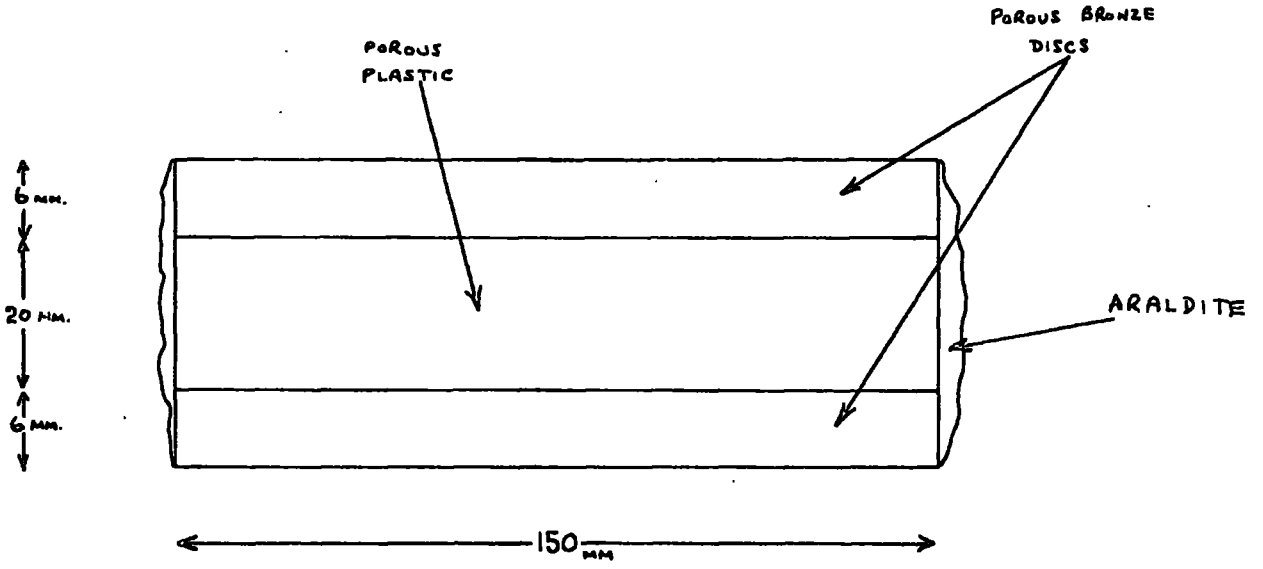

(a) AXIAL FLOW

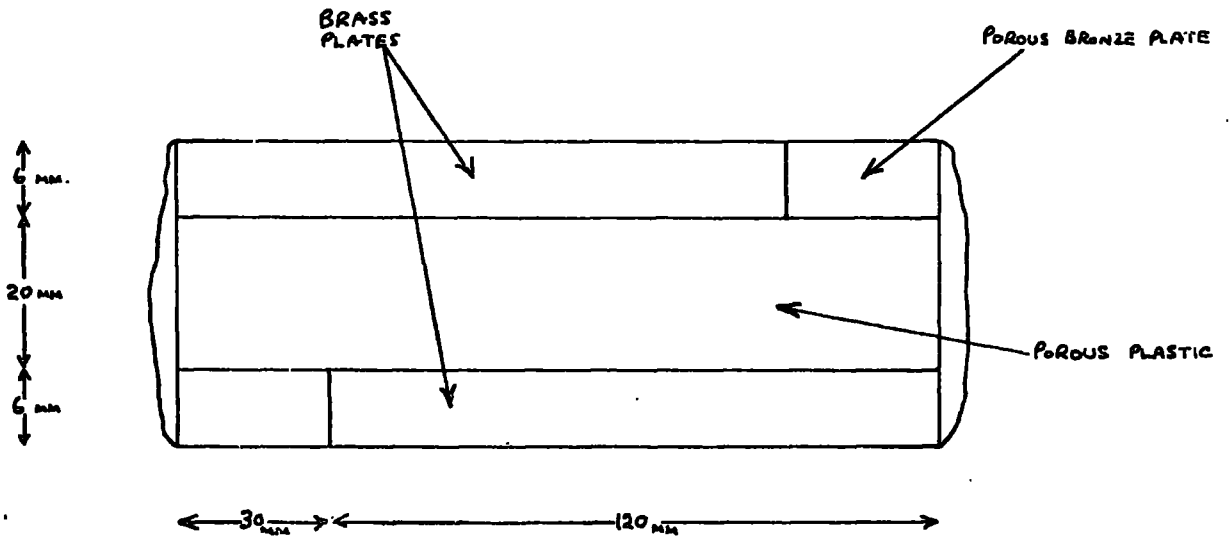

(b) RADIAL FLOW

FIGURE 17 : POROUS SPECIMENS.

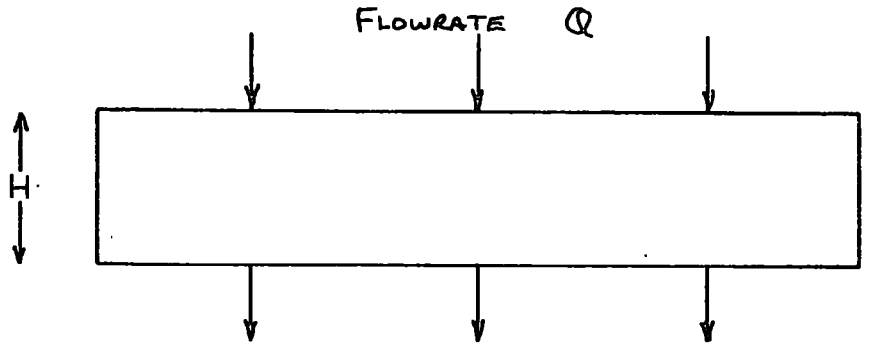

(a) AXIAL FLOW

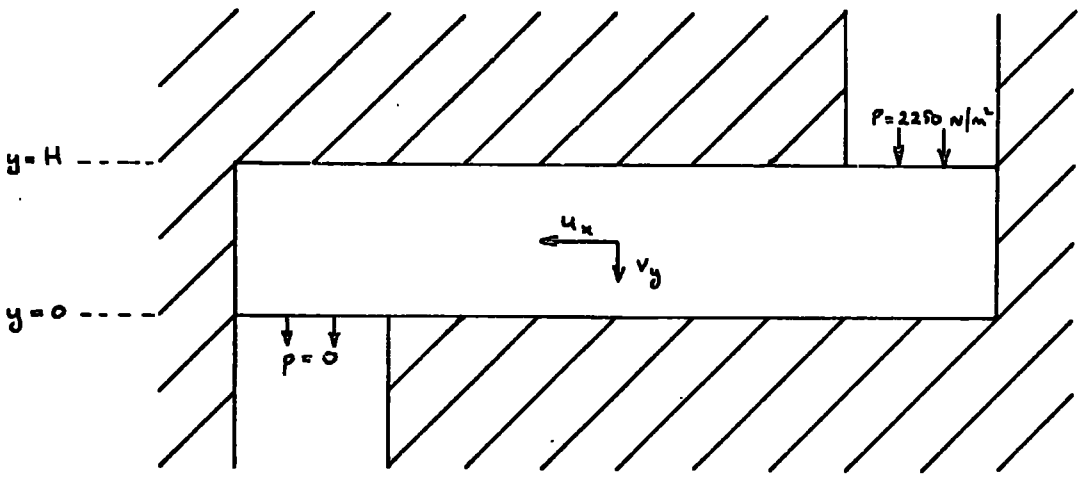

(b) "RADIAL" FLOW

FIGURE 18: DIRECTIONS OF FLOW IN POROUS SPECIMENS

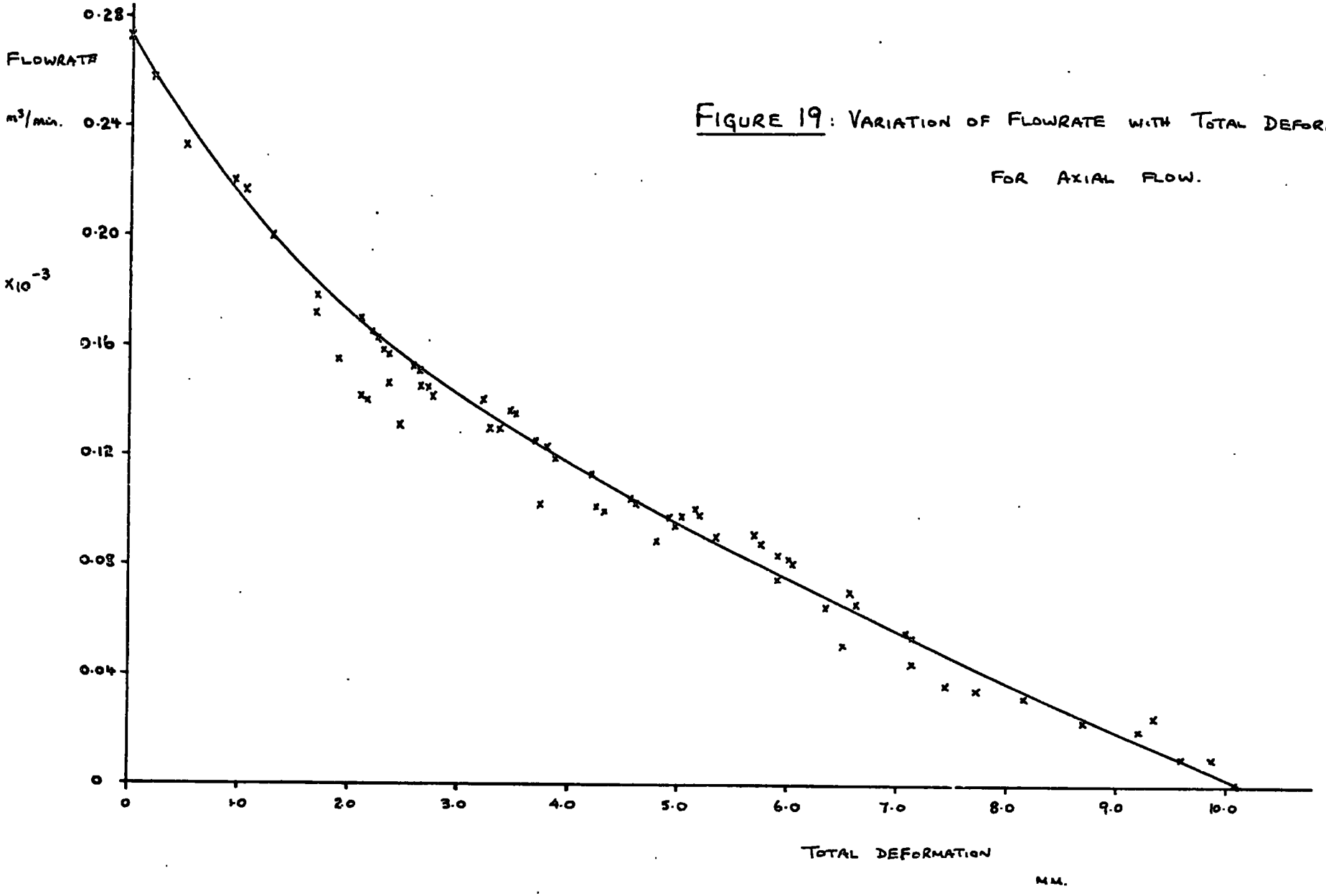

FIGURE 19: VARIATION OF FLOWRATE WITH TOTAL DEFORMATION FOR AXIAL FLOW.

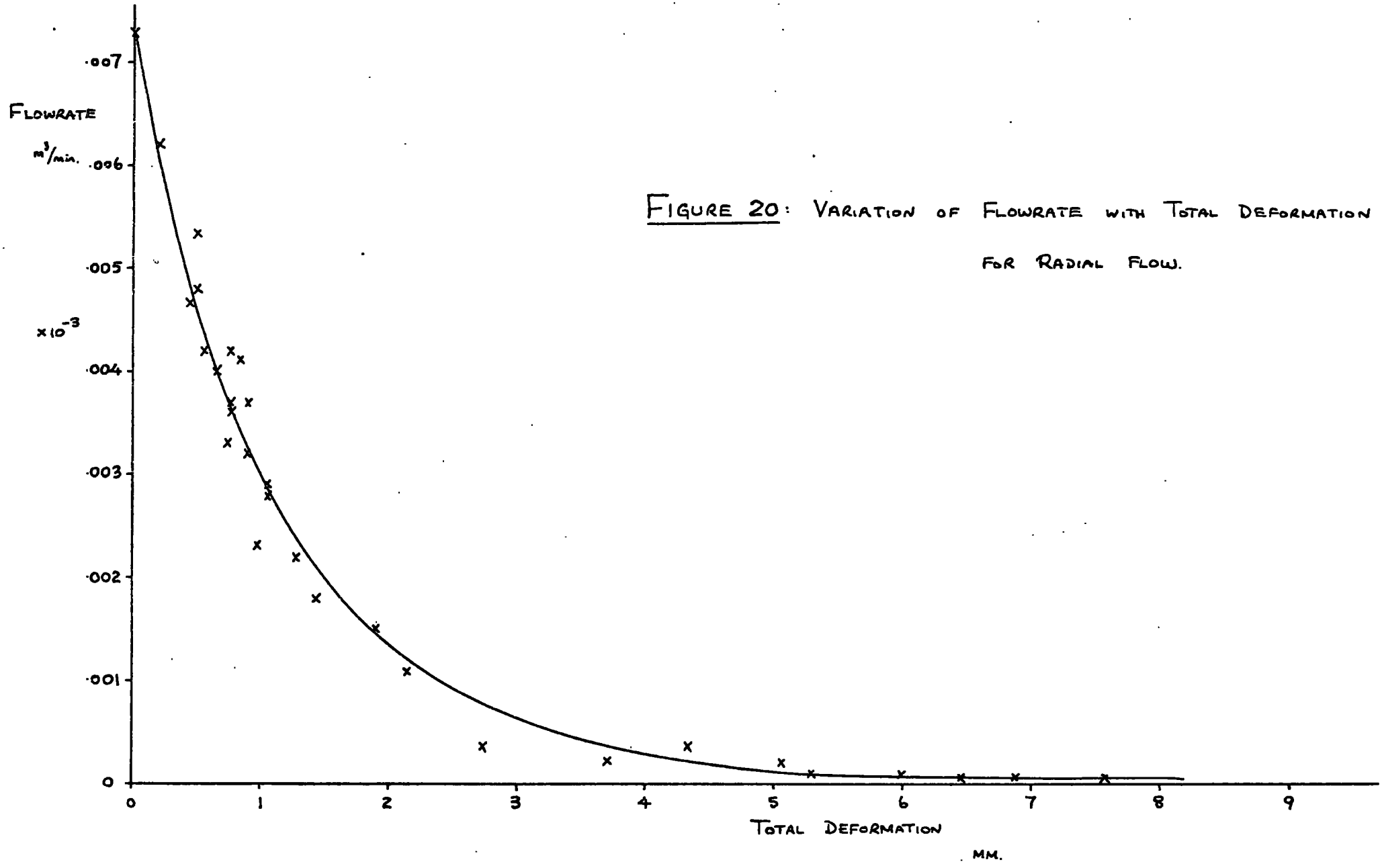

FIGURE 20: VARIATION OF FLOWRATE WITH TOTAL DEFORMATION FOR RADIAL FLOW.

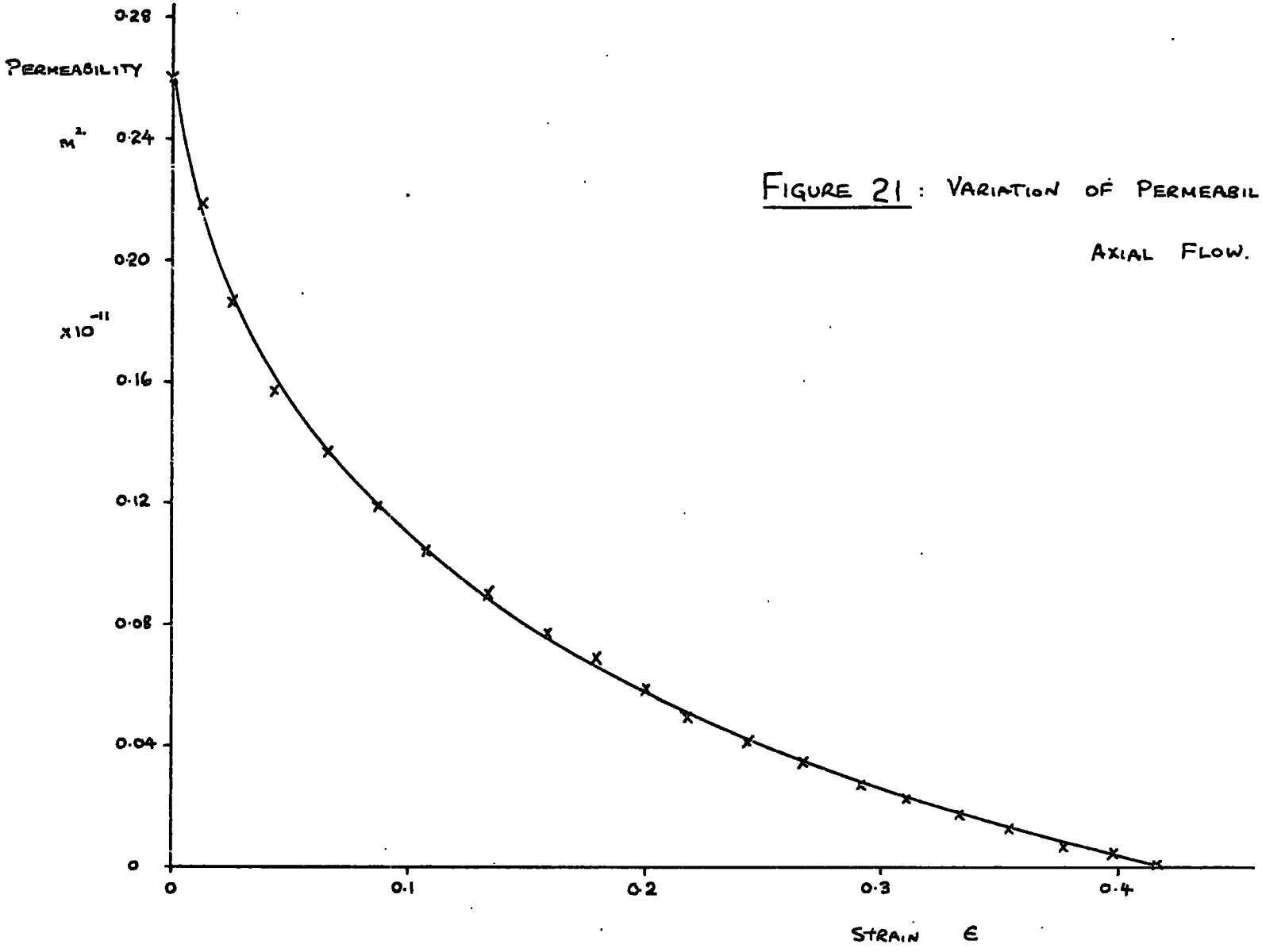

FIGURE 21 : VARIATION OF PERMEABILITY WITH STRAIN

AXIAL FLOW.

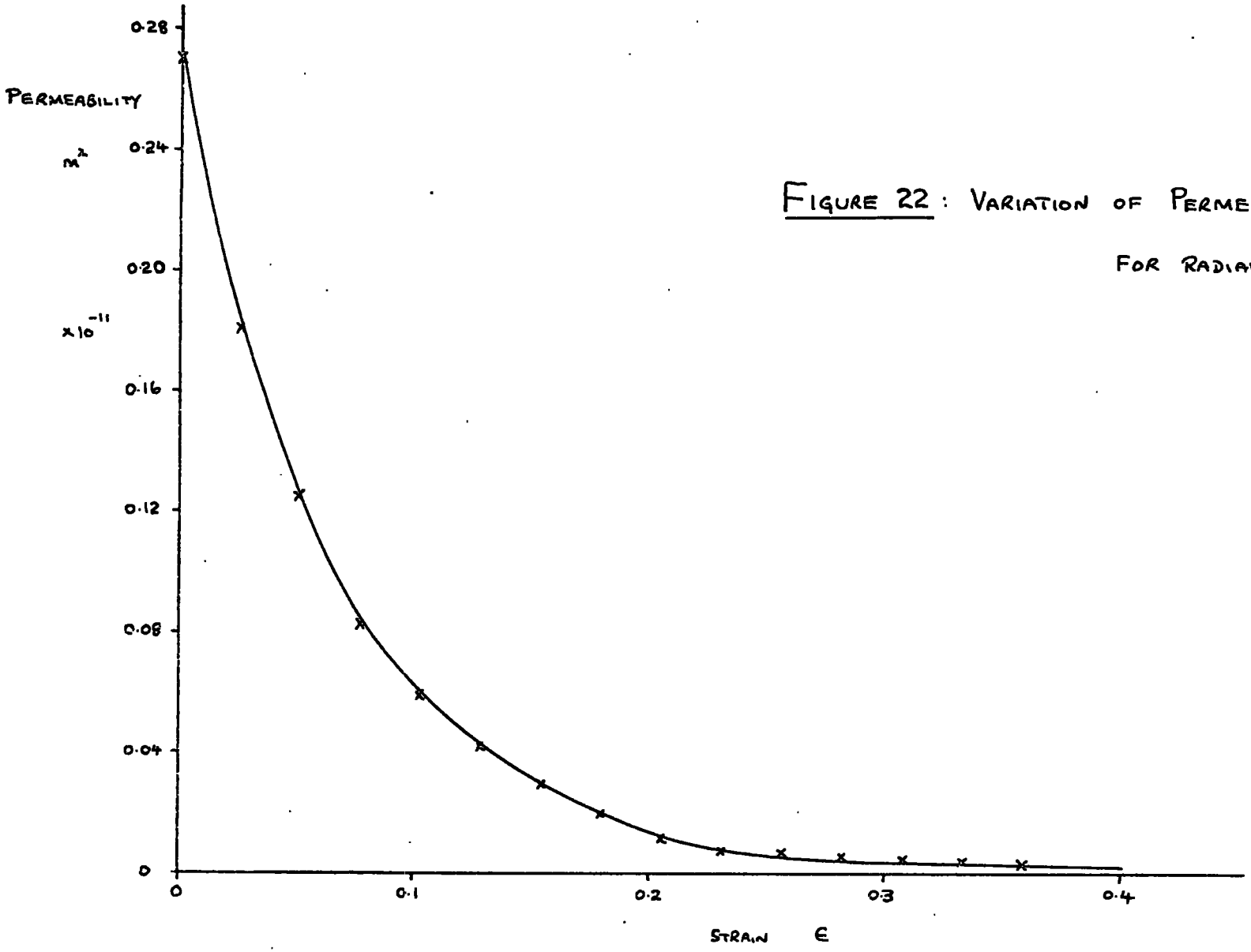

FIGURE 22 : VARIATION OF PERMEABILITY WITH STRAIN FOR RADIAL FLOW

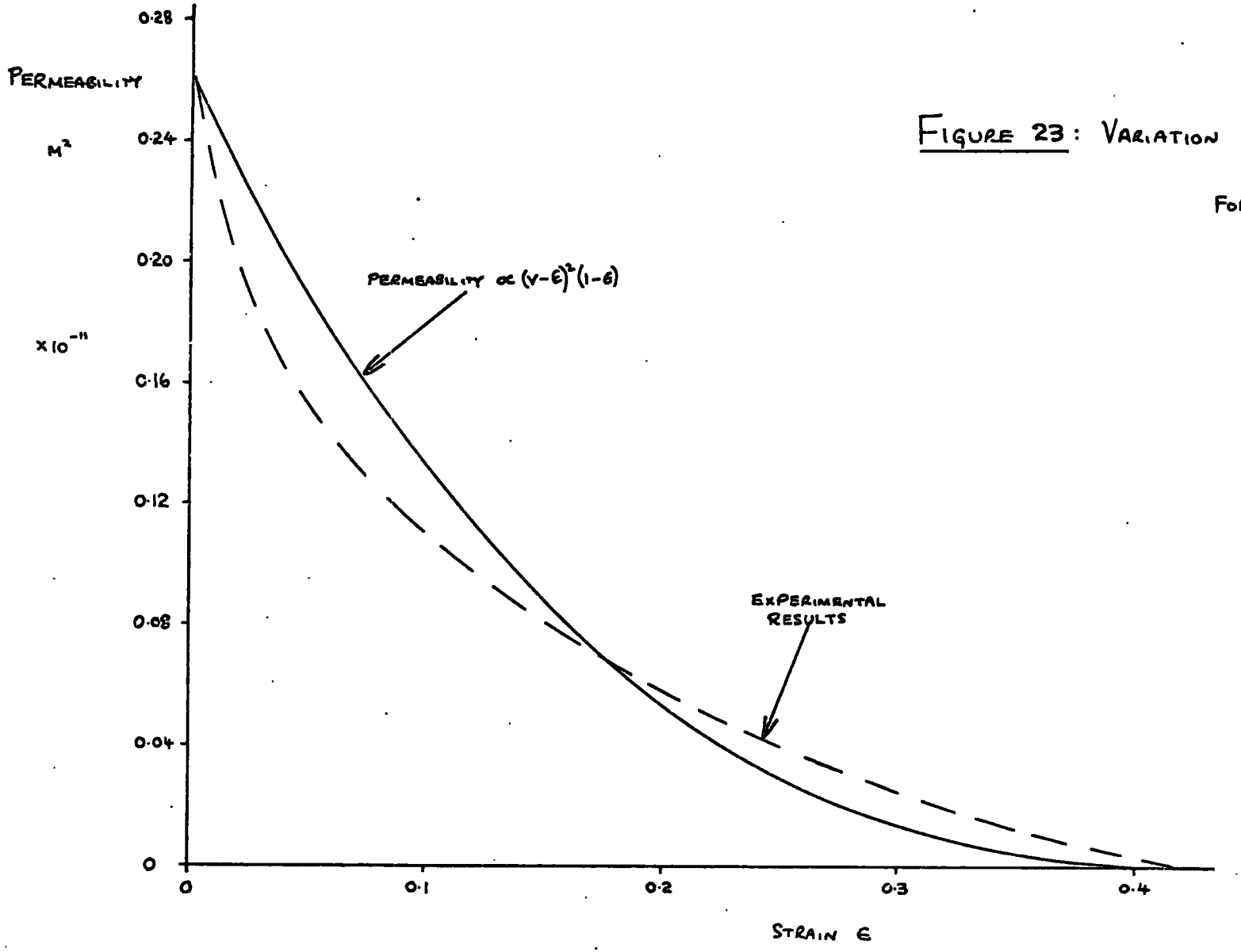

FIGURE 23: VARIATION OF $(V-\epsilon)^2(1-\epsilon)$ WITH ϵ FOR AXIAL FLOW.

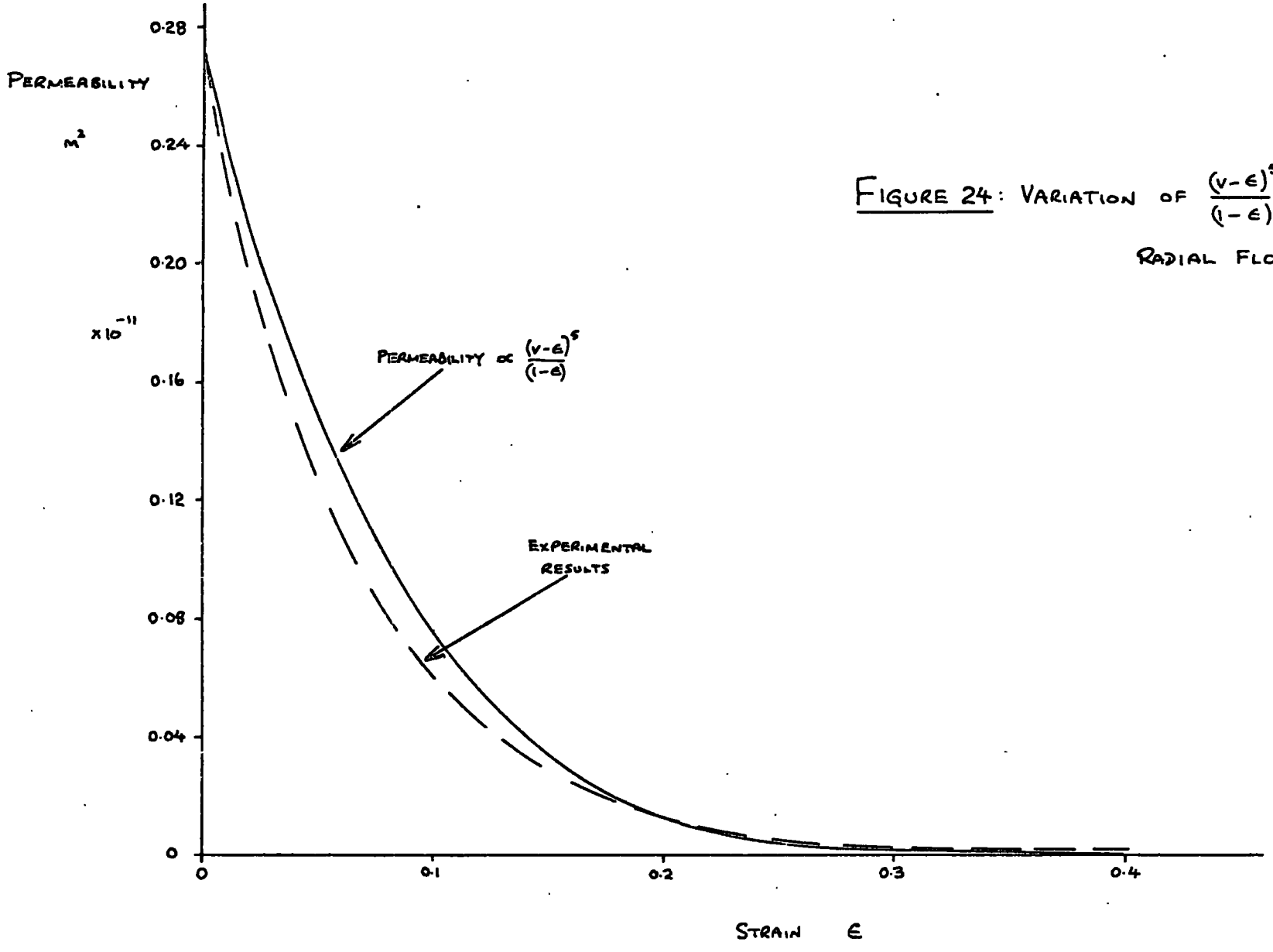

FIGURE 24: VARIATION OF $\frac{(v-\epsilon)^5}{(1-\epsilon)}$ WITH ϵ.

RADIAL FLOW.

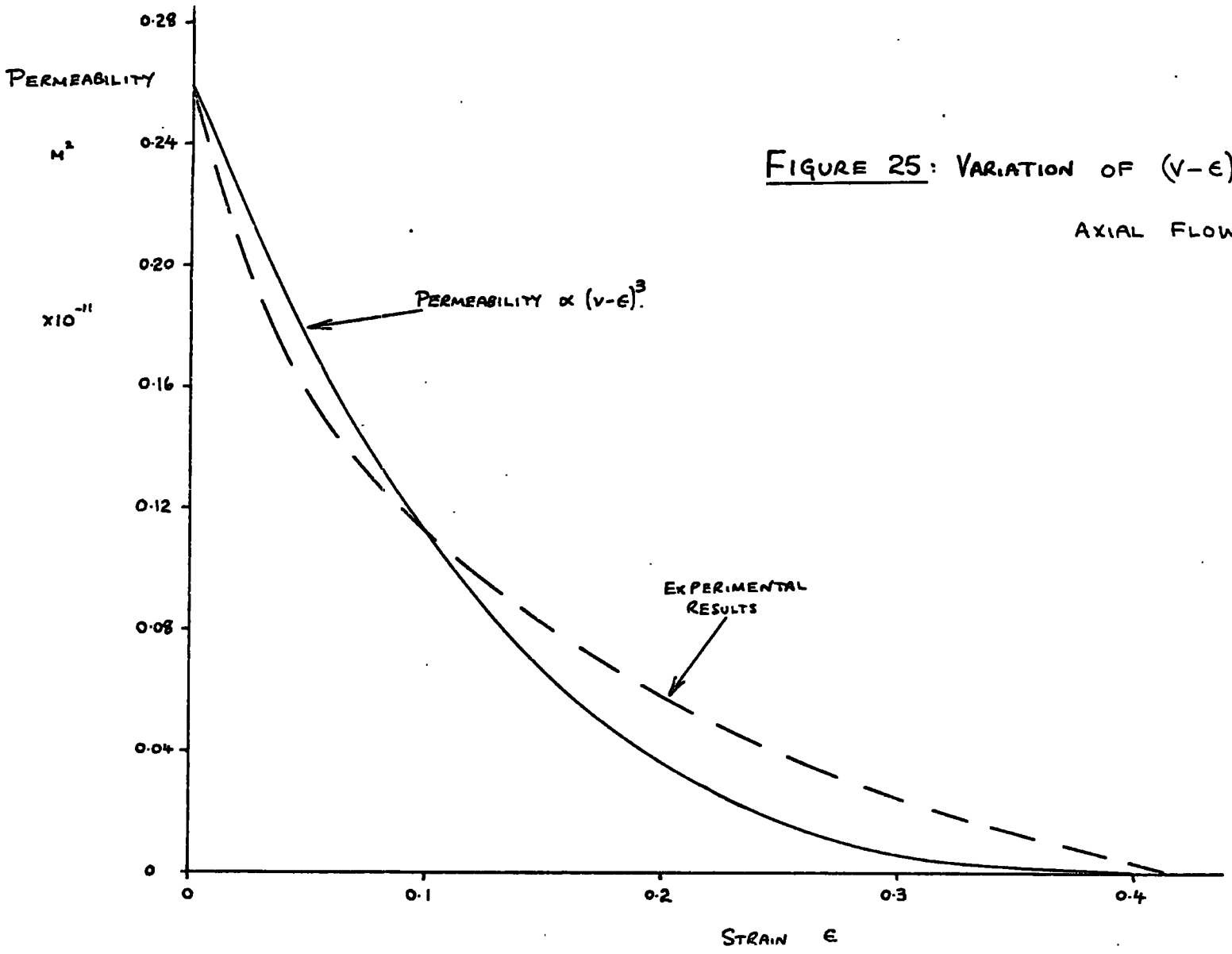

FIGURE 25: VARIATION OF $(V-\epsilon)^3$ WITH ϵ

AXIAL FLOW.

(a) RADIAL FLOW ONLY

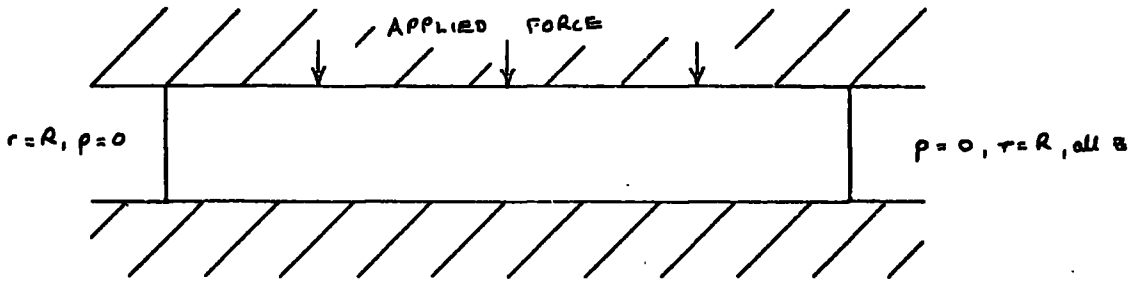

(b) AXIAL FLOW ONLY

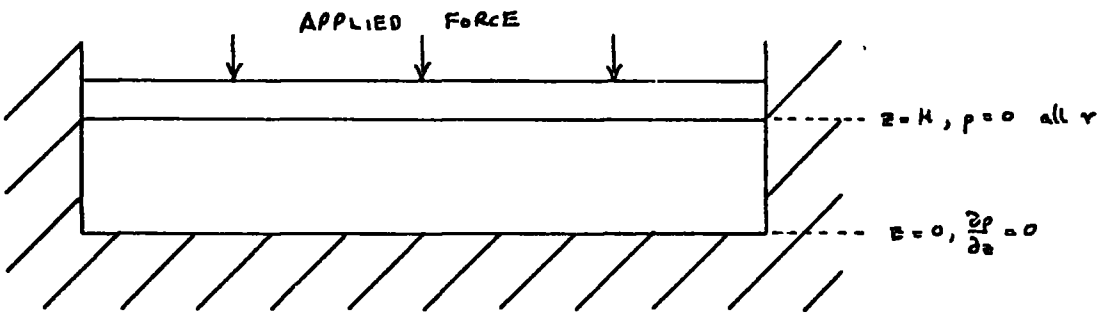

(c) AXIAL AND RADIAL FLOW

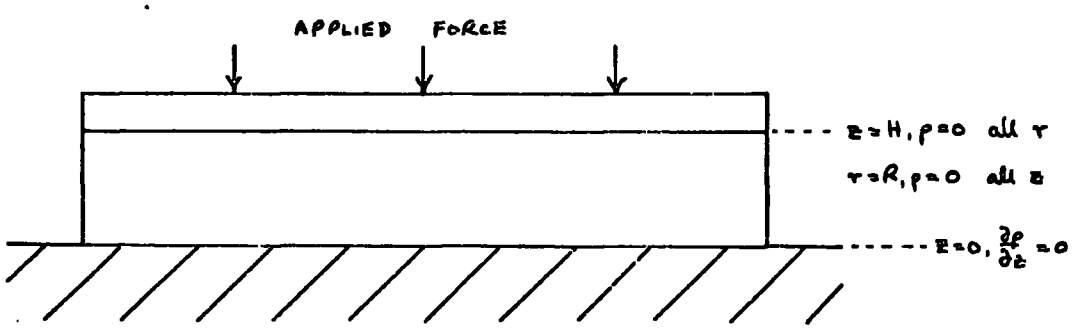

FIGURE 26 : CONFIGURATIONS AND BOUNDARY CONDITIONS FOR SPECIAL CASES

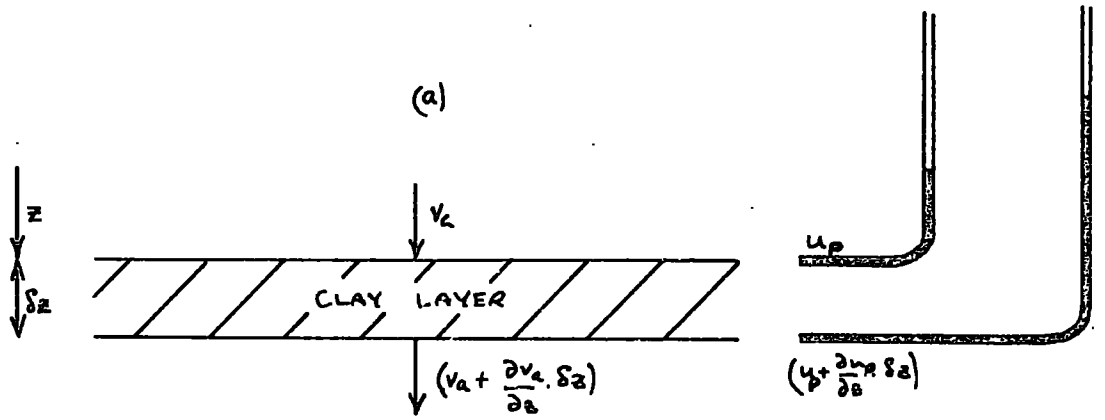

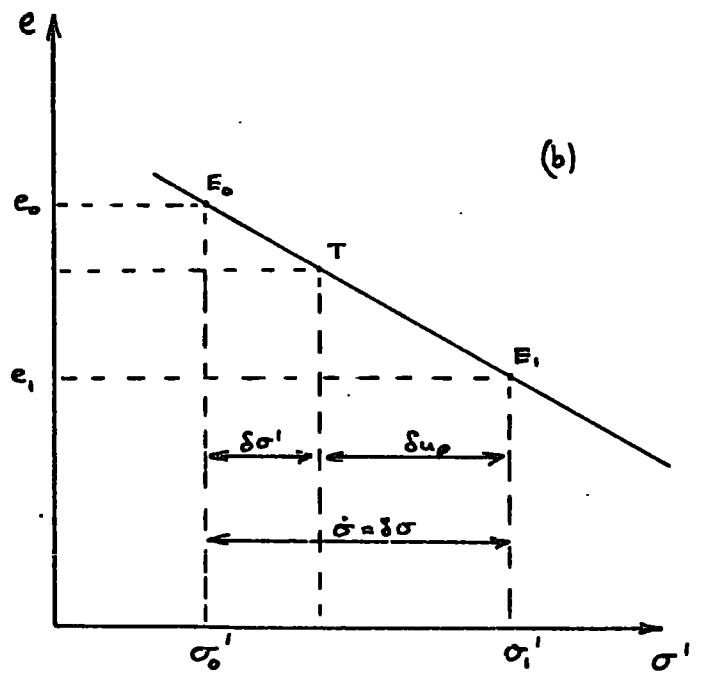

FIGURE 27: SOIL MECHANICS APPROACH

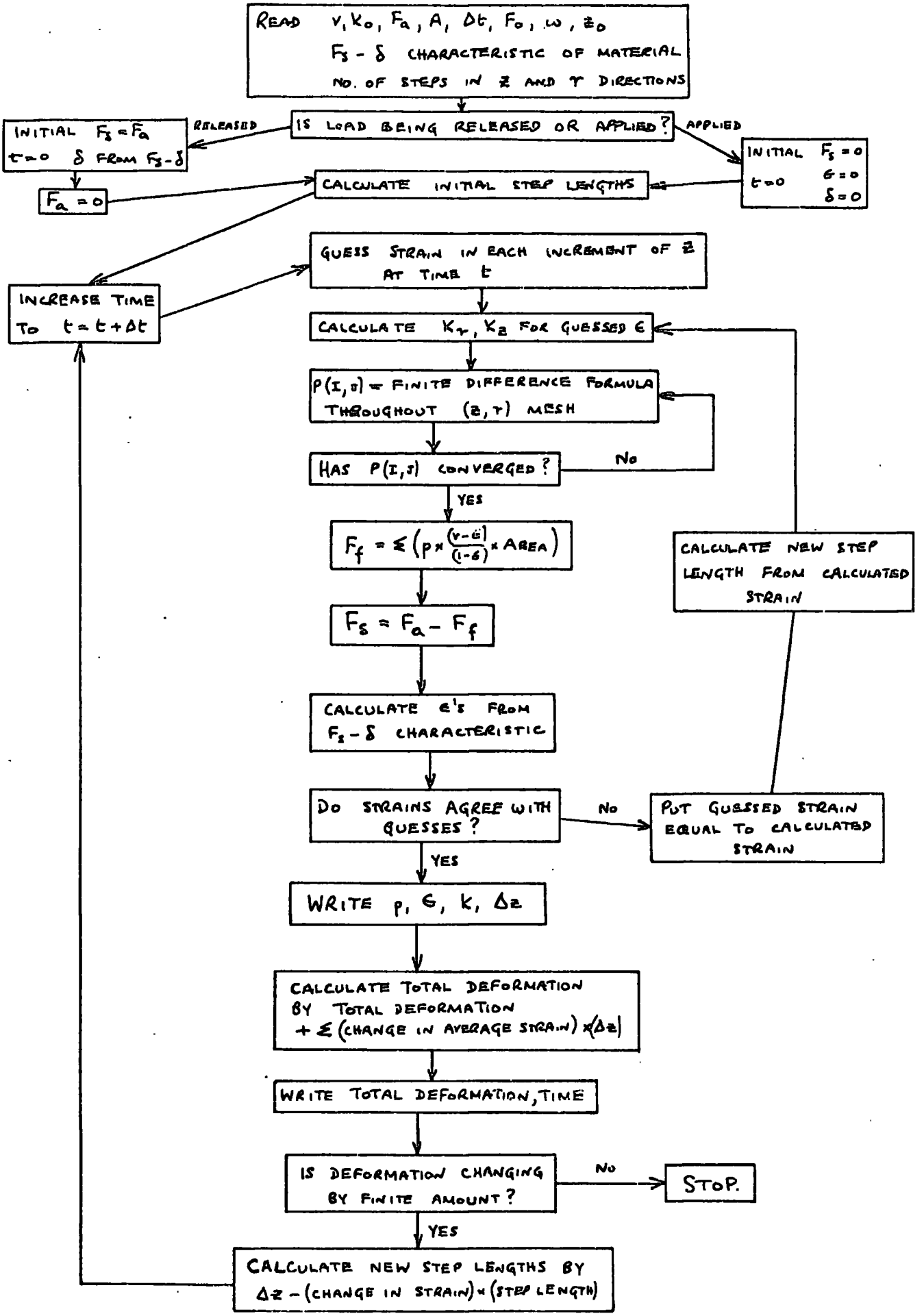

FIGURE 28: BLOCK DIAGRAM OF COMPUTER PROGRAM FOR AXIAL AND RADIAL FLOW.

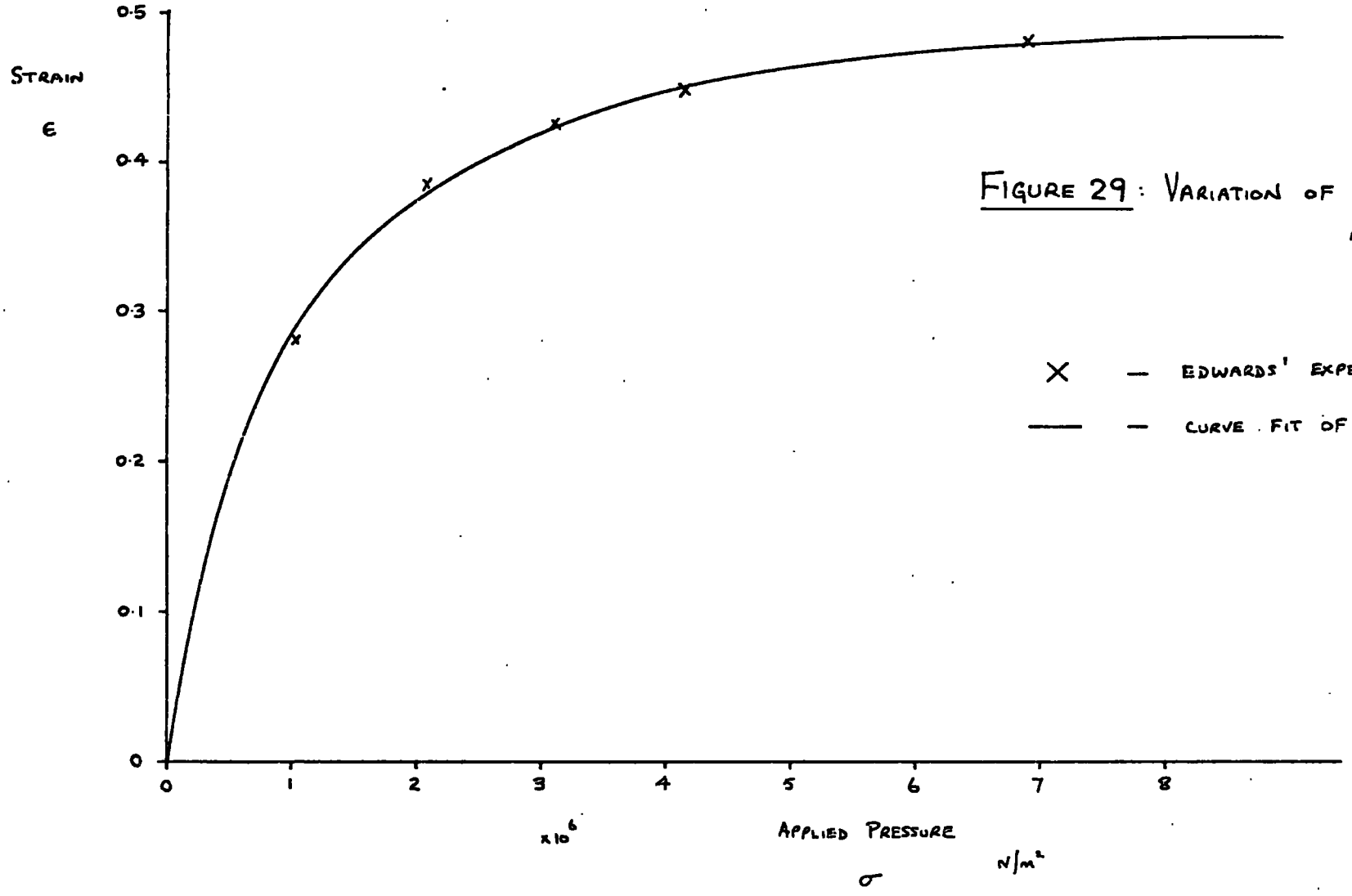

FIGURE 29 : VARIATION OF STRAIN WITH APPLIED PRESSURE AT EQUILIBRIUM.

× — EDWARDS' EXPERIMENTAL VALUES

—— — CURVE FIT OF $\sigma = \frac{1.655 \times 10^6 \epsilon}{1 - 1.825\epsilon}$

FIGURE 30: STRAIN vs. TIME FOR 1.02×10^6 N/m² (= 148 lbs/in²)
AXIAL FLOW ONLY.

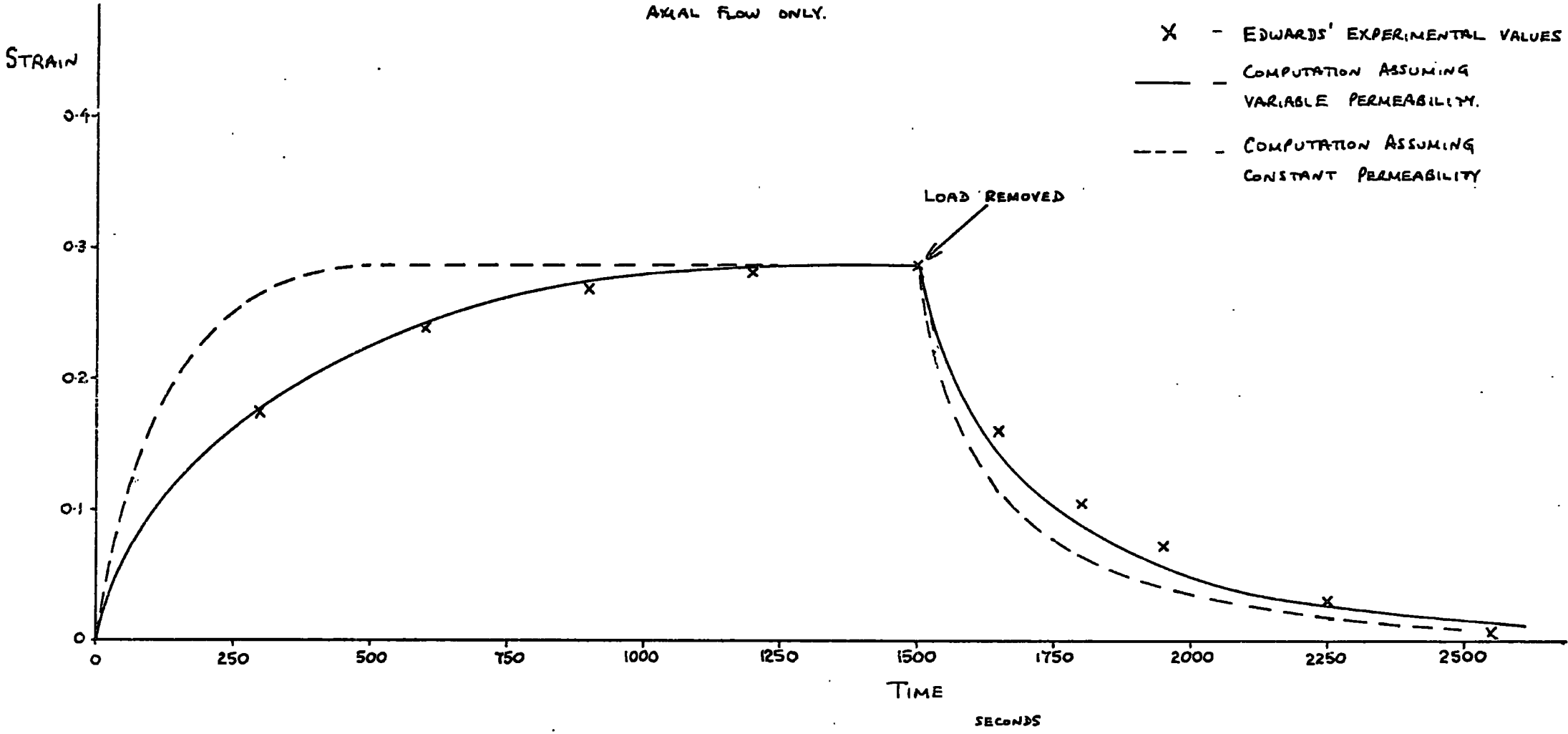

FIGURE 31 : STRAIN VS. TIME FOR 2.04×10^6 N/m² (=296 lbs/in²)

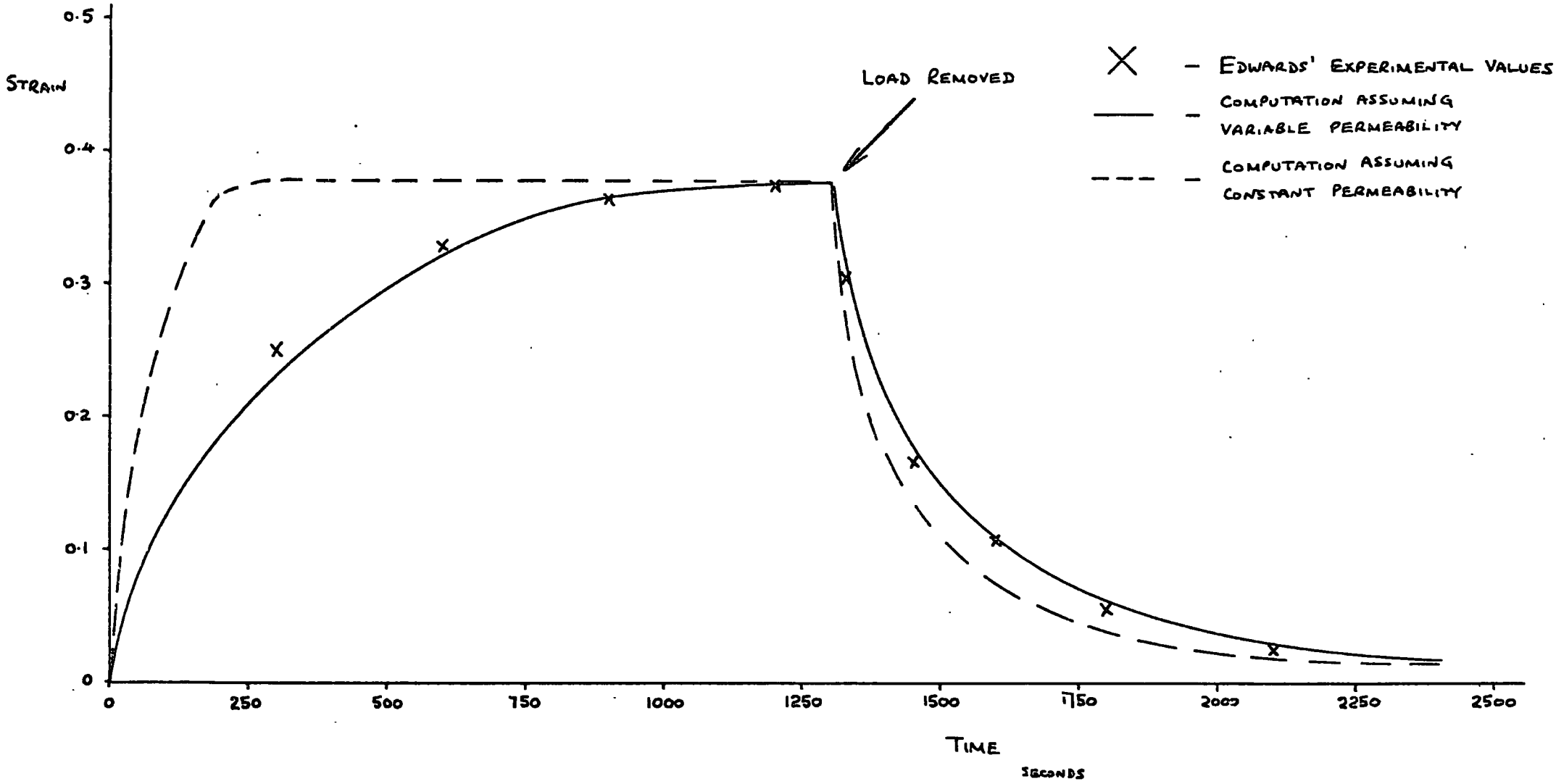

FIGURE 32 : STRAIN vs. TIME FOR $3{\cdot}10 \times 10^6$ N/m² (= 450 lbs/in²)

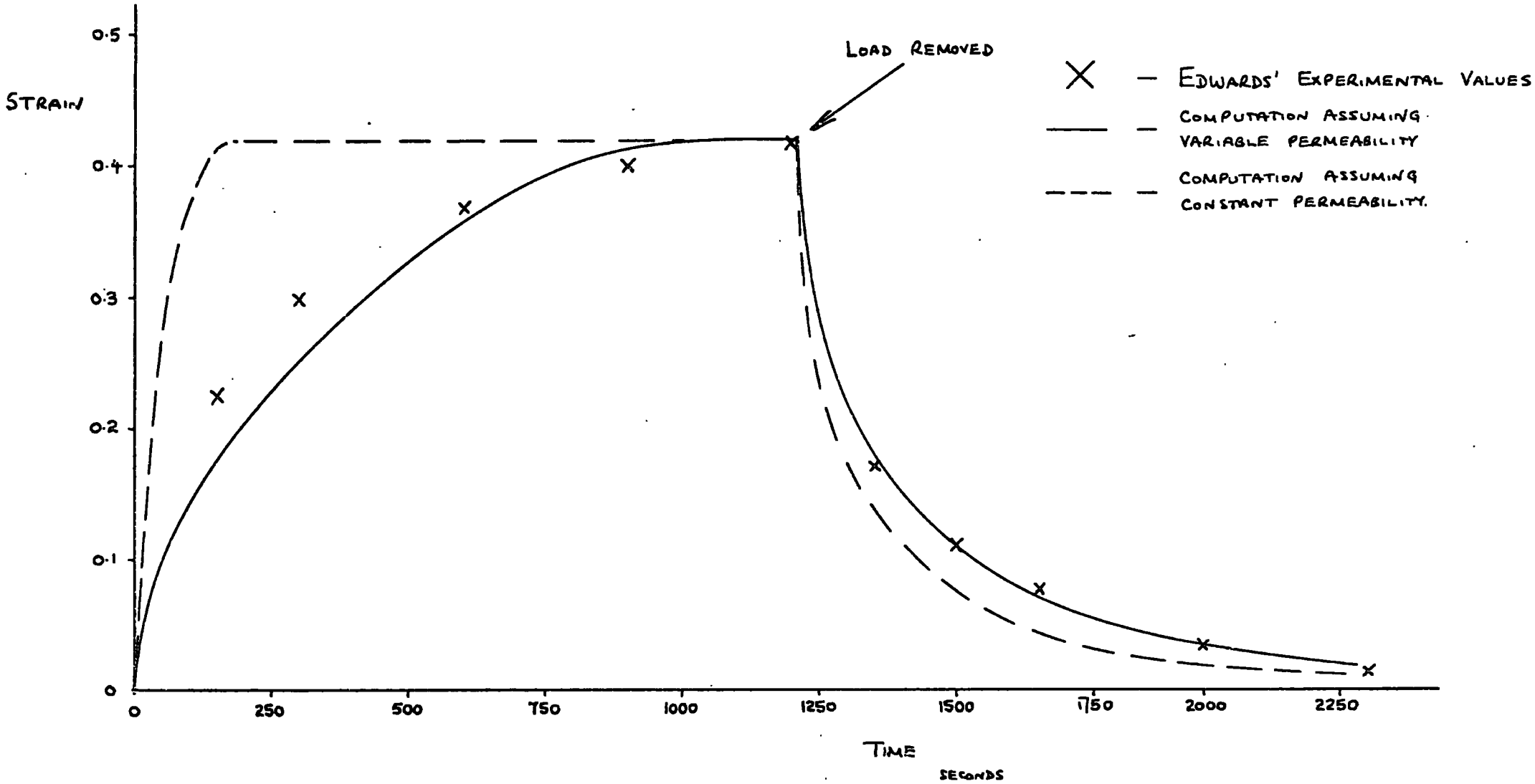

FIGURE 33: STRAIN vs. TIME FOR 6.895×10^6 N/m^2 (= 1000 lbs/in^2)

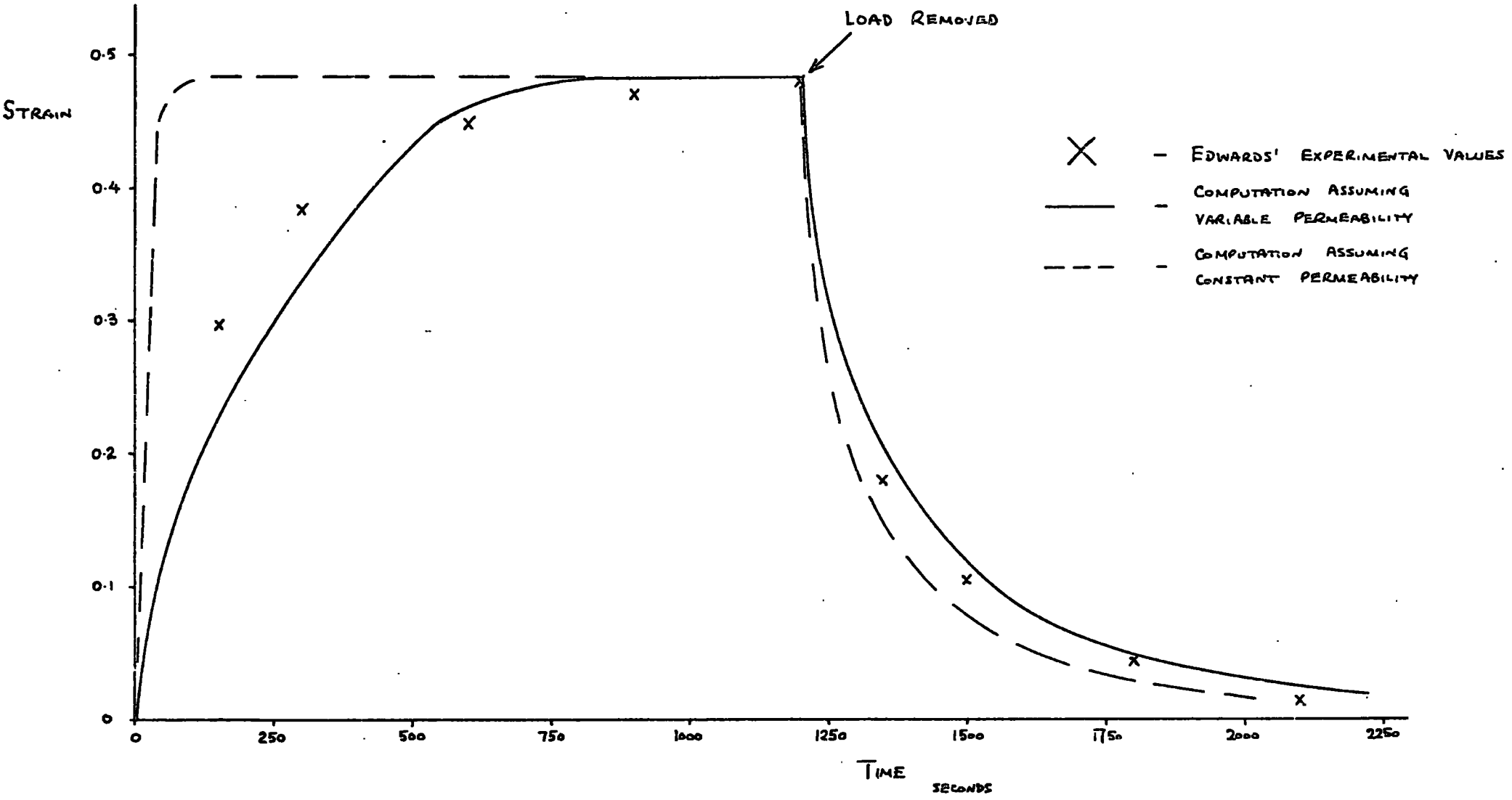

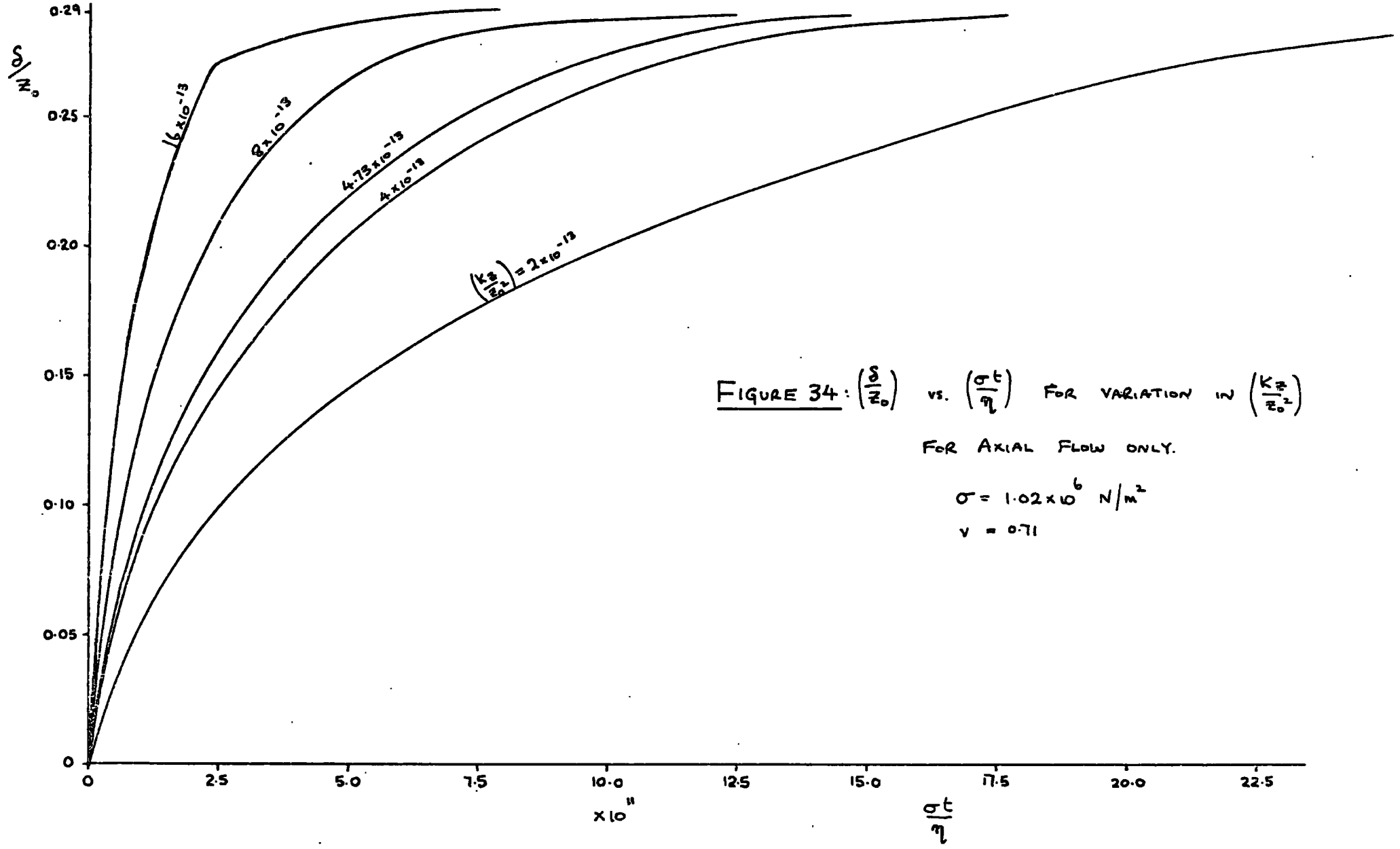

FIGURE 34: $\left(\frac{\delta}{z_0}\right)$ vs. $\left(\frac{\sigma t}{\eta}\right)$ FOR VARIATION IN $\left(\frac{K_\phi}{z_0^2}\right)$

FOR AXIAL FLOW ONLY.

$\sigma = 1.02 \times 10^6$ N/m²

$\nu = 0.71$

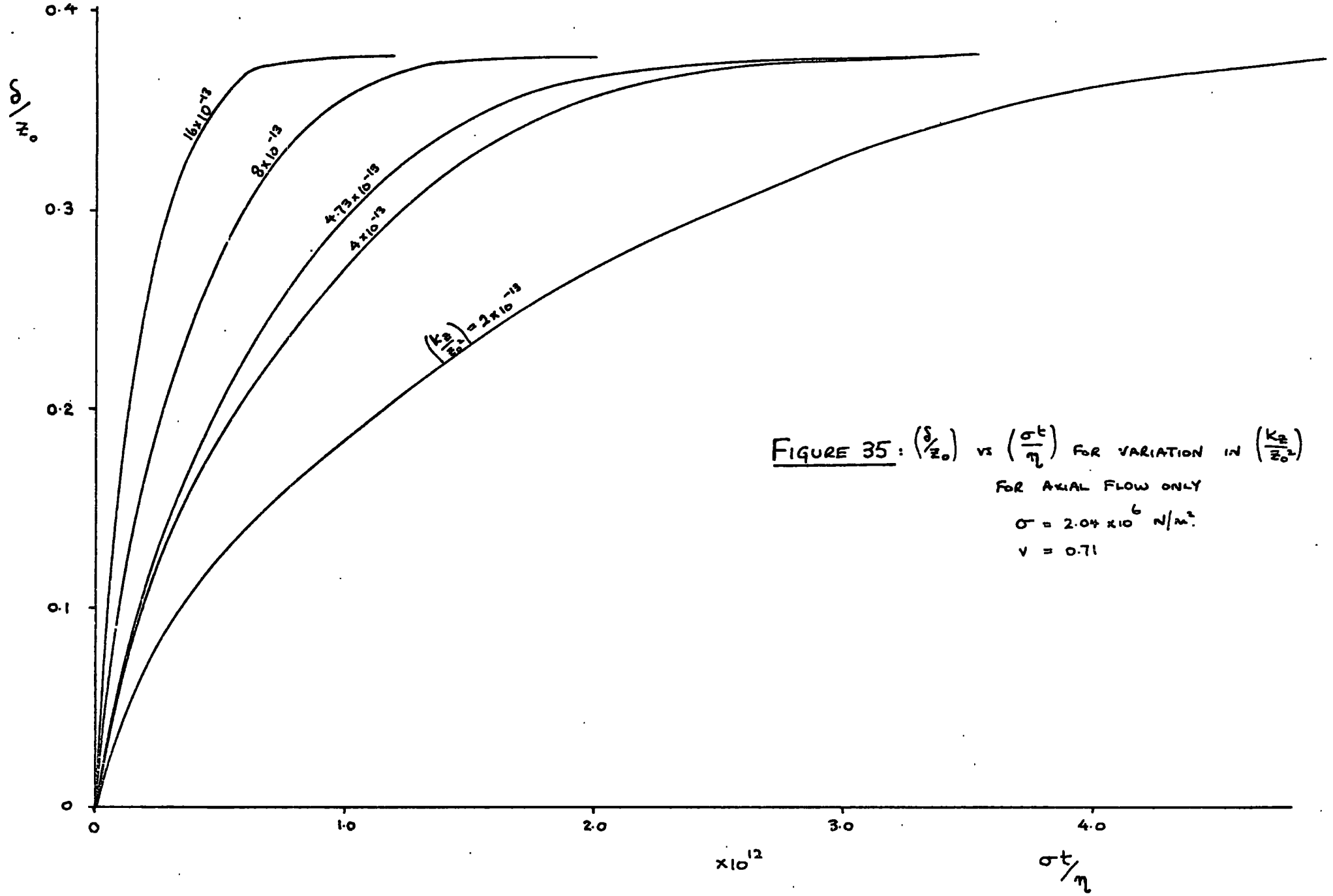

FIGURE 35: (δ/z_0) vs $\left(\frac{\sigma t}{\eta}\right)$ FOR VARIATION IN $\left(\frac{k_2}{z_0^2}\right)$

FOR AXIAL FLOW ONLY

$\sigma = 2.04 \times 10^6$ N/m²

$\nu = 0.71$

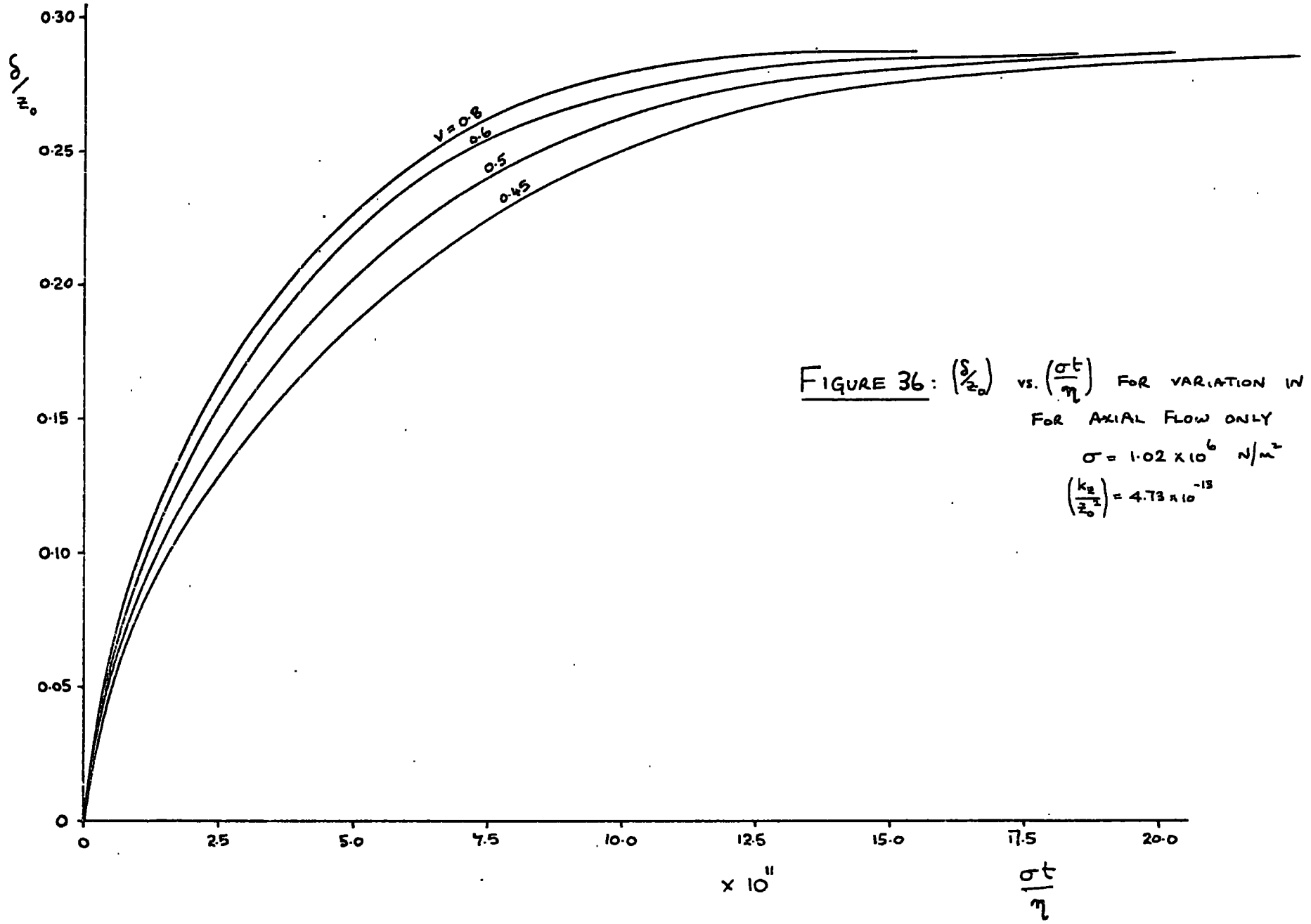

FIGURE 36: $\left(\frac{\delta}{z_0}\right)$ vs. $\left(\frac{\sigma t}{\eta}\right)$ FOR VARIATION IN (V)
FOR AXIAL FLOW ONLY
$\sigma = 1.02 \times 10^{6}$ N/m²
$\left(\frac{k_2}{z_0^2}\right) = 4.73 \times 10^{-13}$

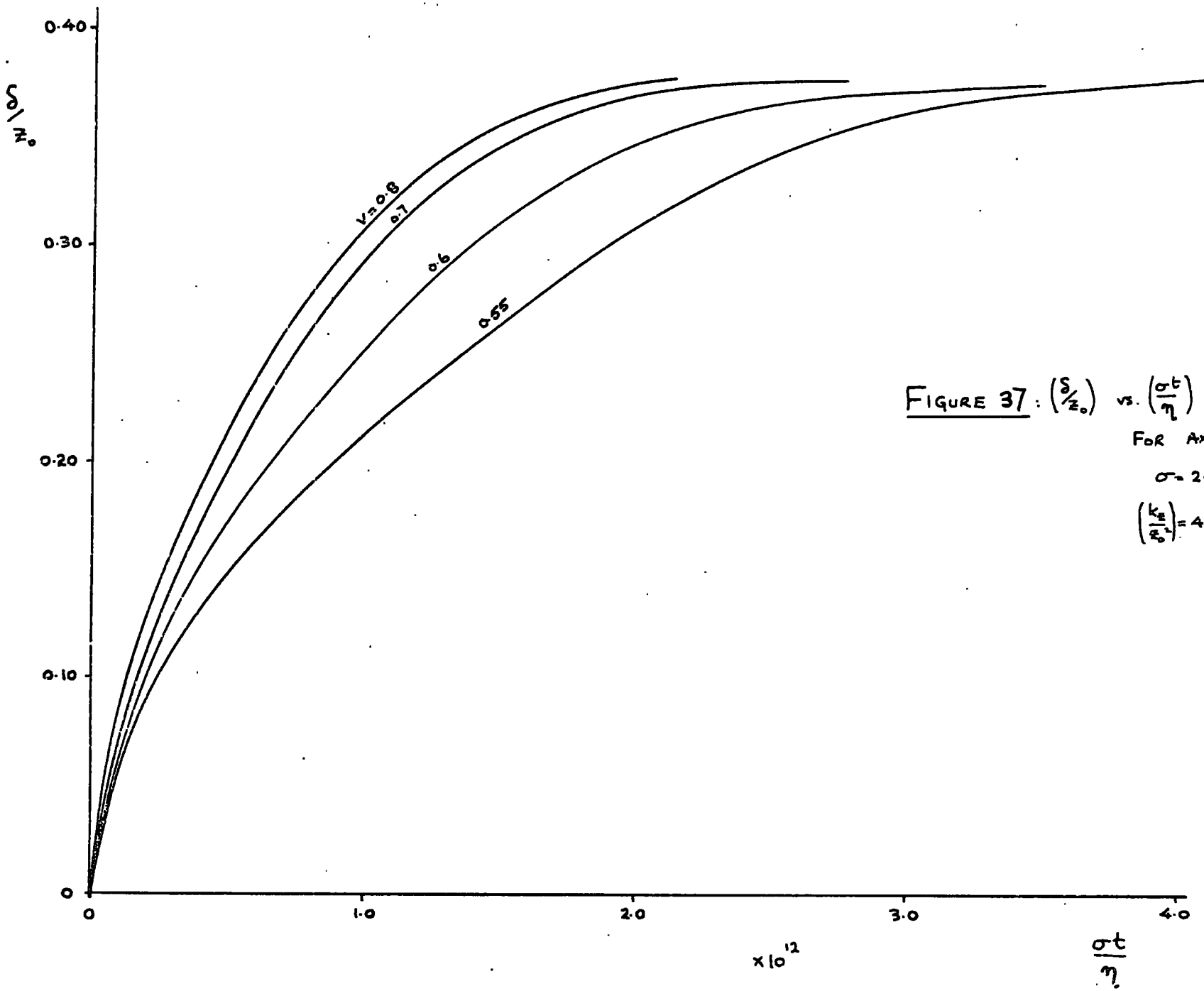

FIGURE 37 : $\left(\frac{\delta}{z_0}\right)$ vs. $\left(\frac{\sigma t}{\eta}\right)$ FOR VARIATION IN (v) FOR AXIAL FLOW ONLY.

$\sigma = 2.04 \times 10^6$ N/m²

$\left(\frac{k_2}{z_0^2}\right) = 4.73 \times 10^{-13}$

FIGURE 38: VARIATION OF STRAIN THROUGH THE DEPTH WITH TIME. (UNDER LOAD)

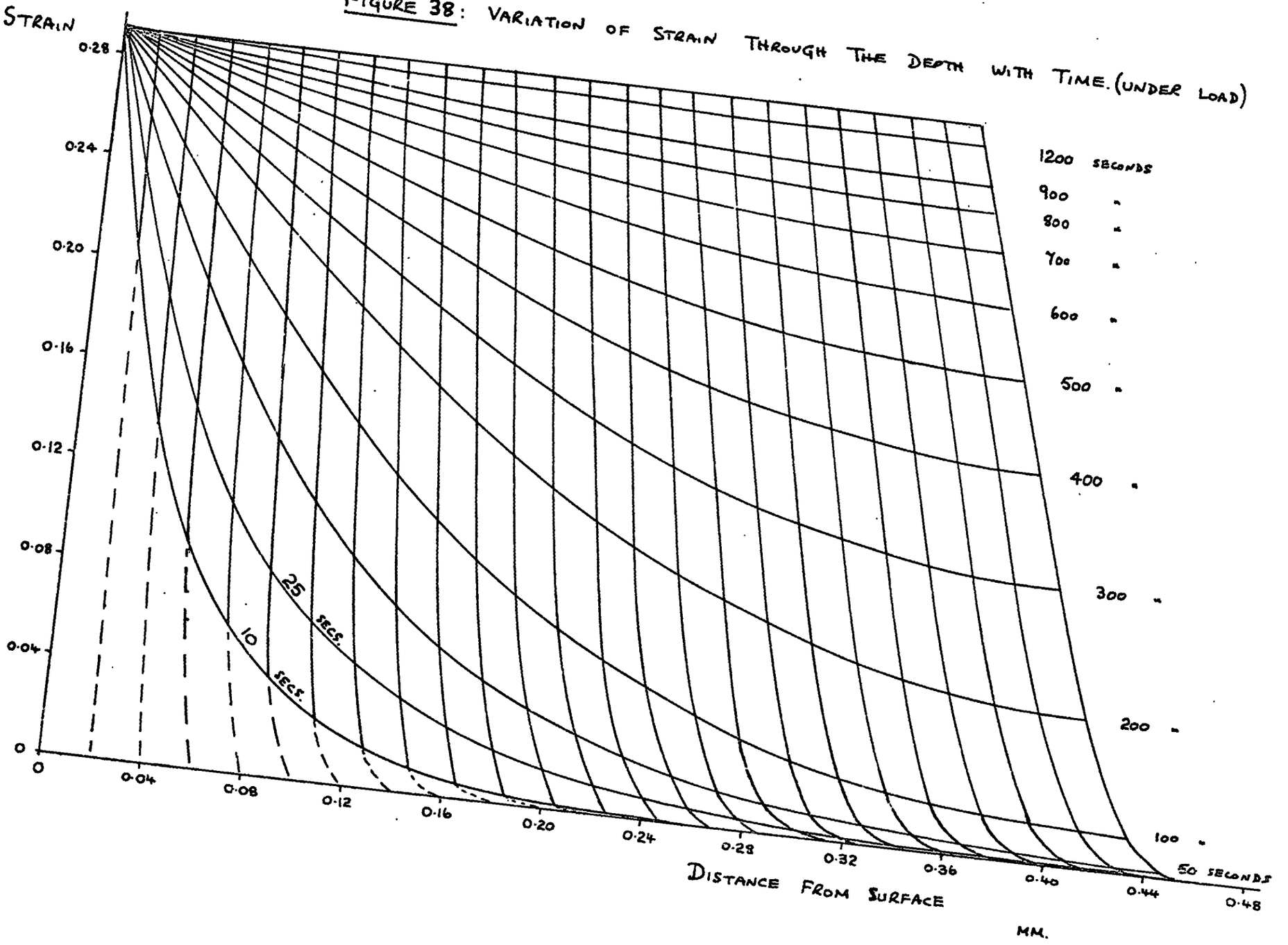

FIGURE 39 : FLUID PRESSURE vs. DISTANCE FROM SURFACE FOR INCREASING TIME UNDER LOAD.

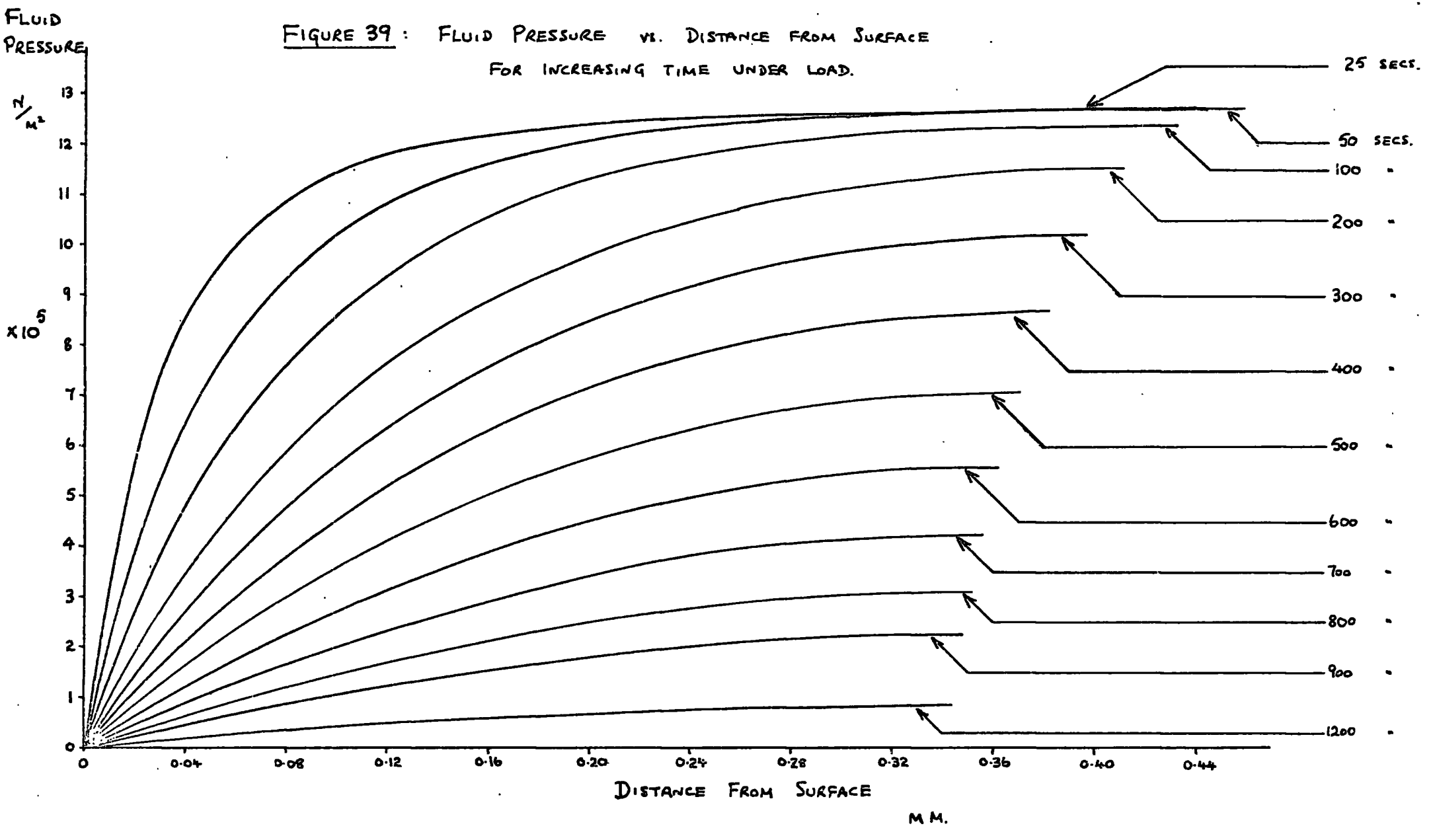

FIGURE 40: VARIATION OF STRAIN THROUGH THE DEPTH WITH TIME (UNDER RELEASE OF LOAD)

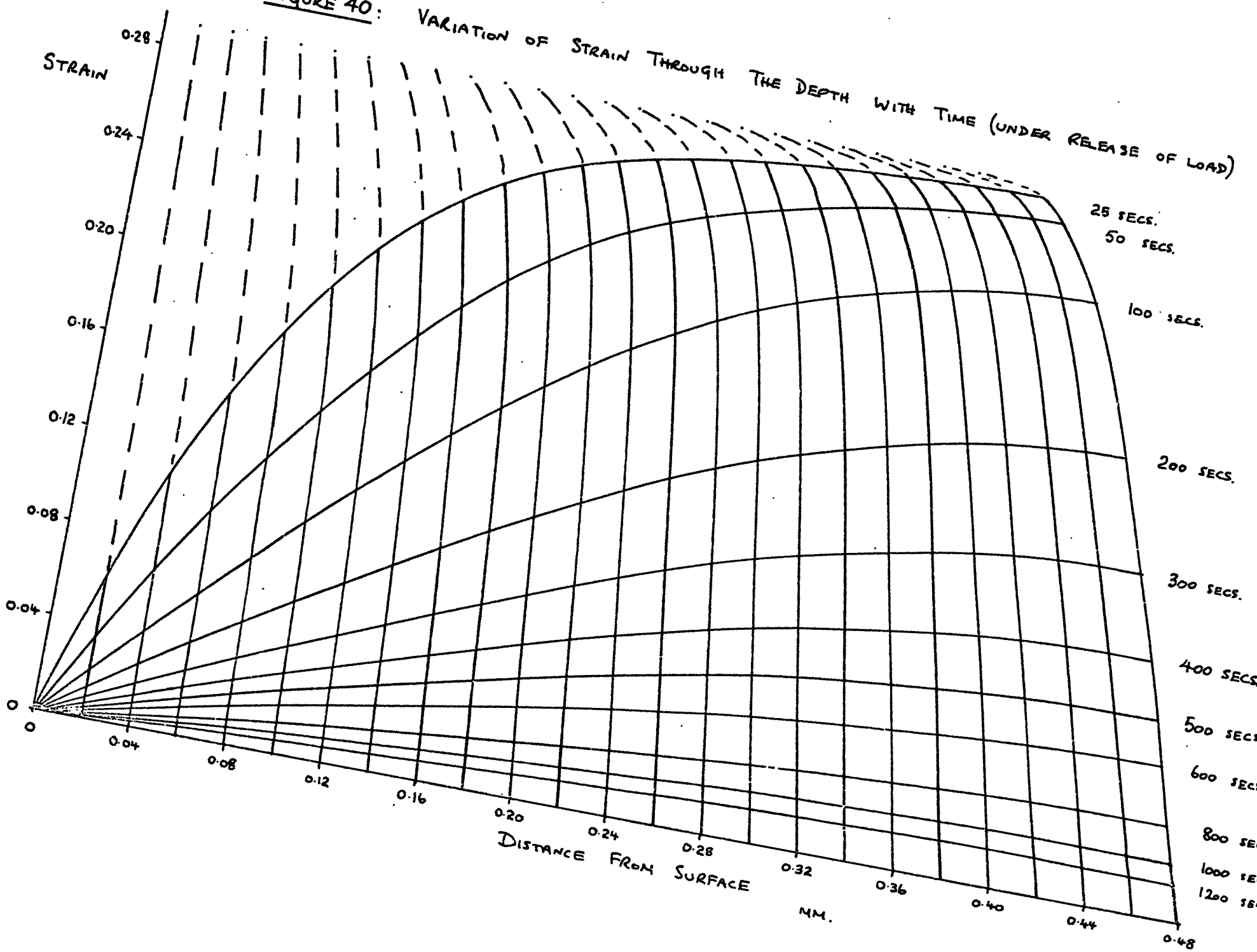

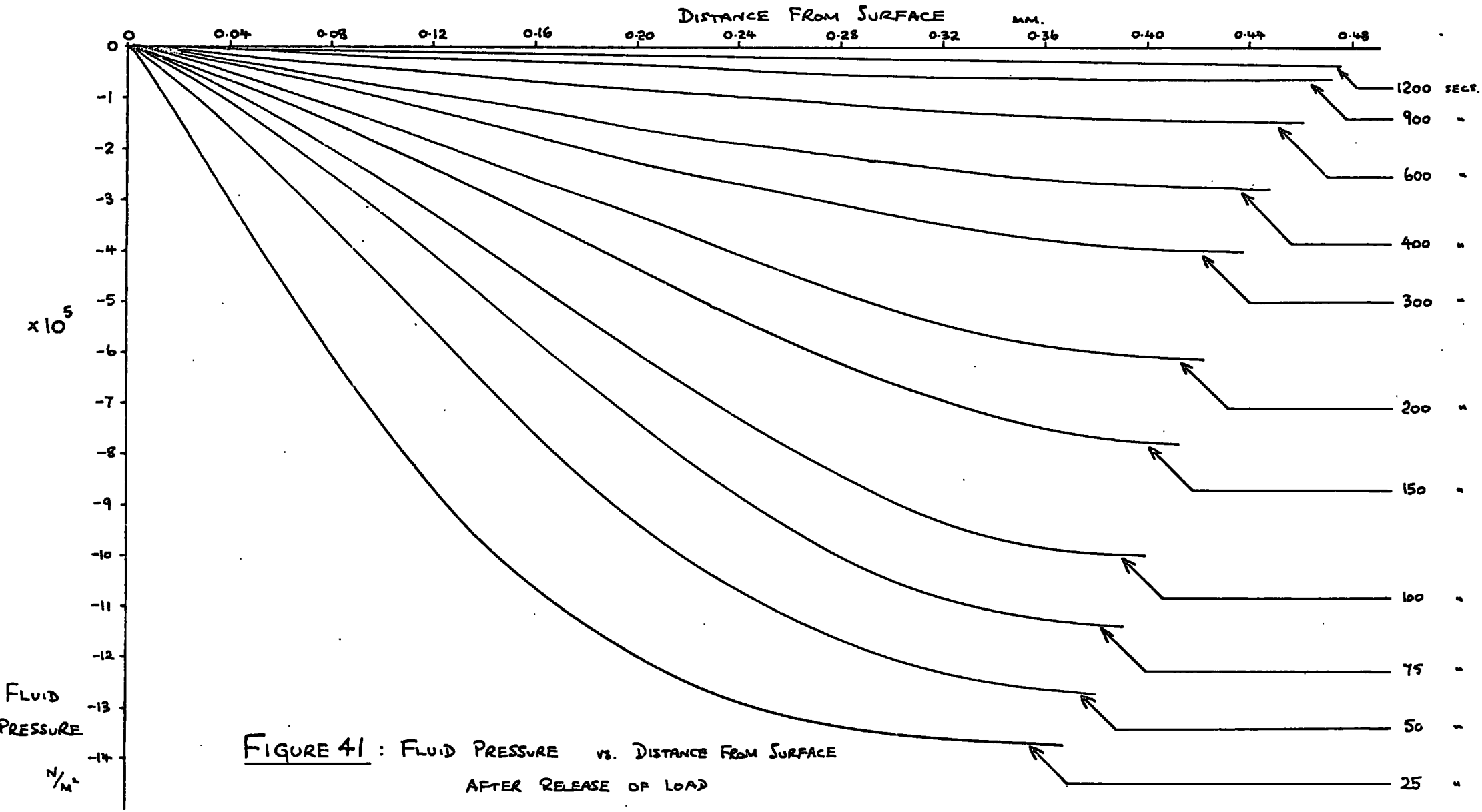

FIGURE 41 : FLUID PRESSURE vs. DISTANCE FROM SURFACE AFTER RELEASE OF LOAD

FIGURE 42: VARIATION OF STRAIN WITH TIME
FOR CONFINED CARTILAGE
APPLIED PRESSURE = 1.02×10^6 N/m^2

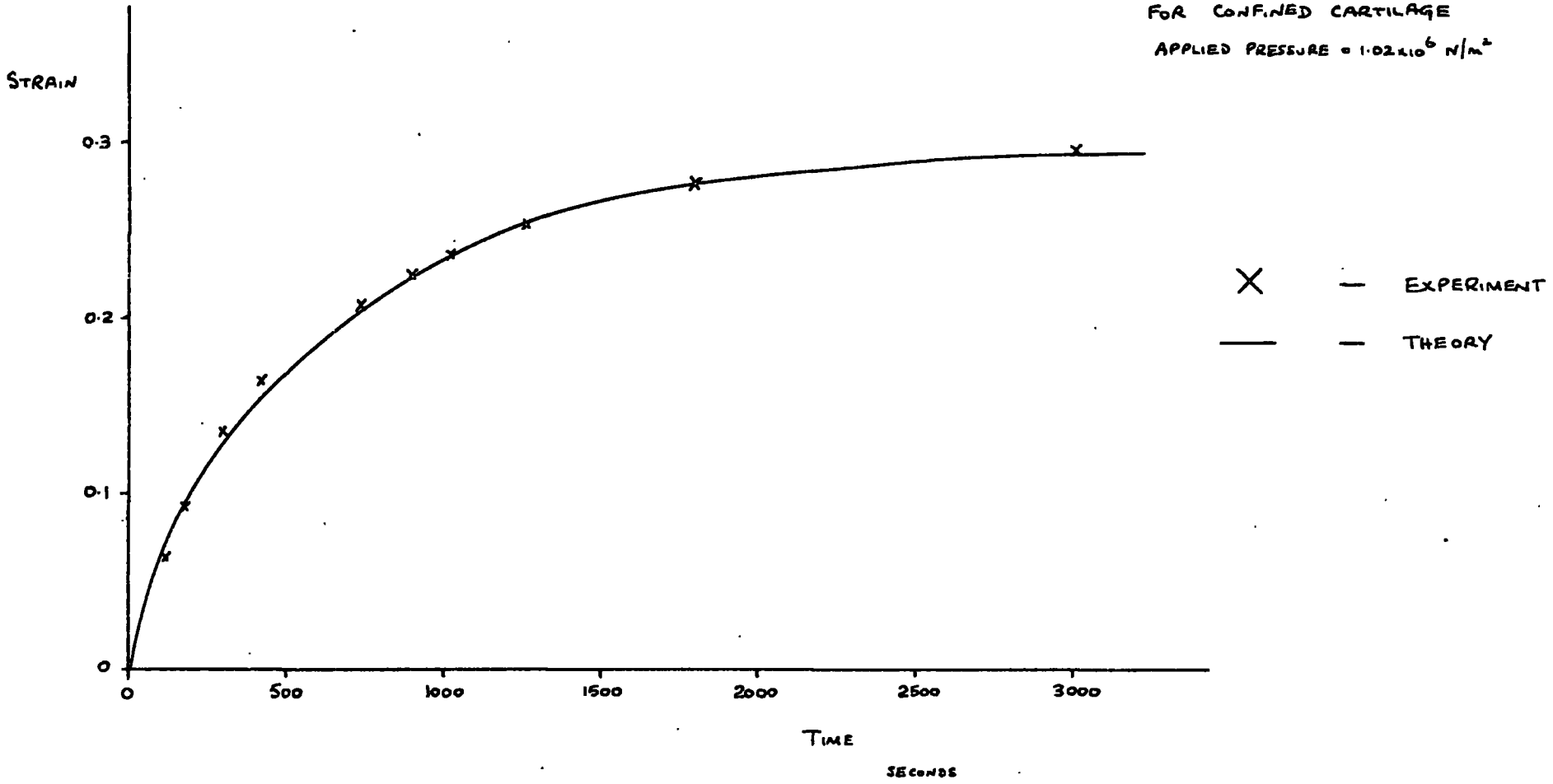

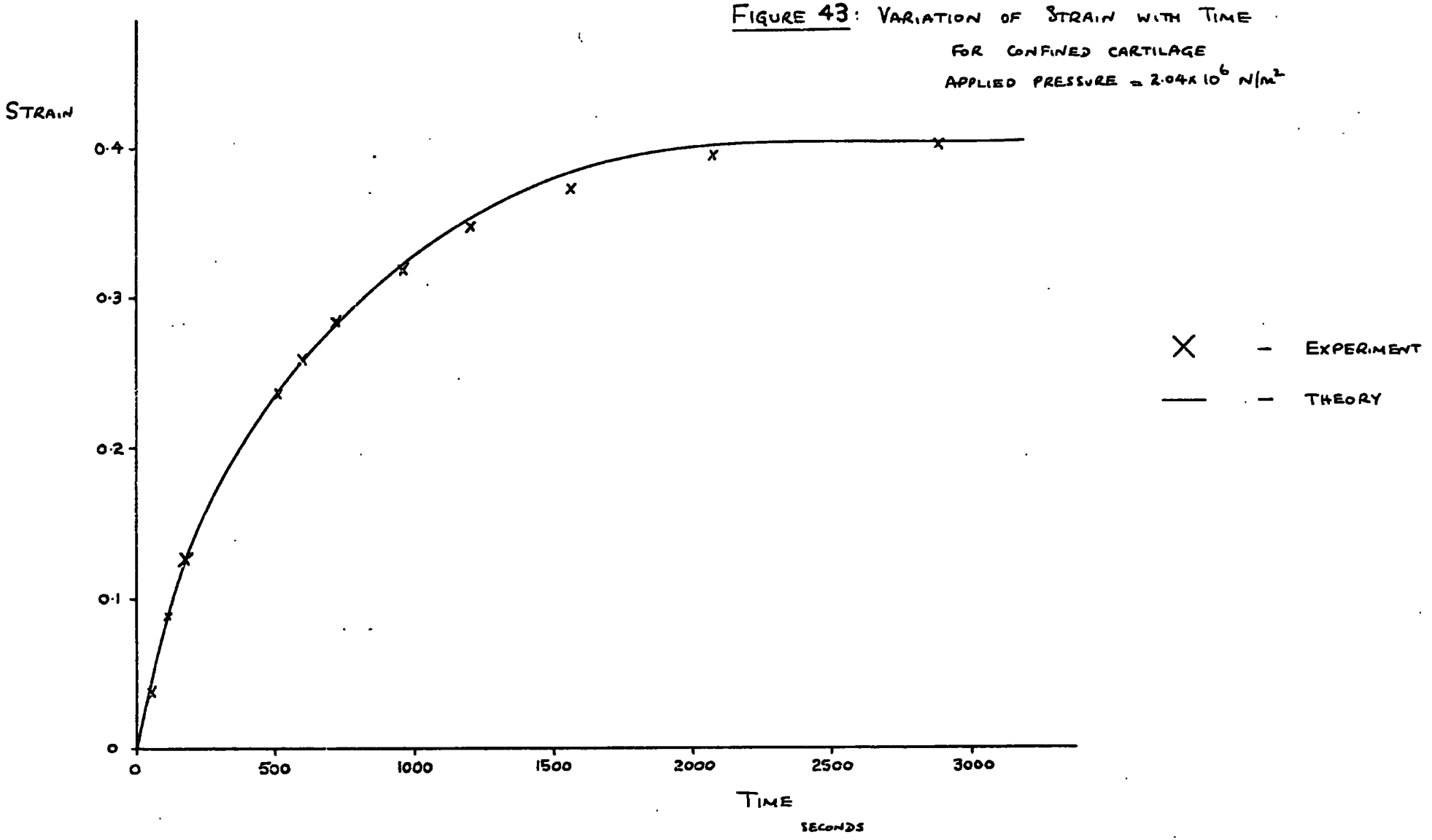

FIGURE 43: VARIATION OF STRAIN WITH TIME FOR CONFINED CARTILAGE APPLIED PRESSURE = 2.04×10^6 N/m^2

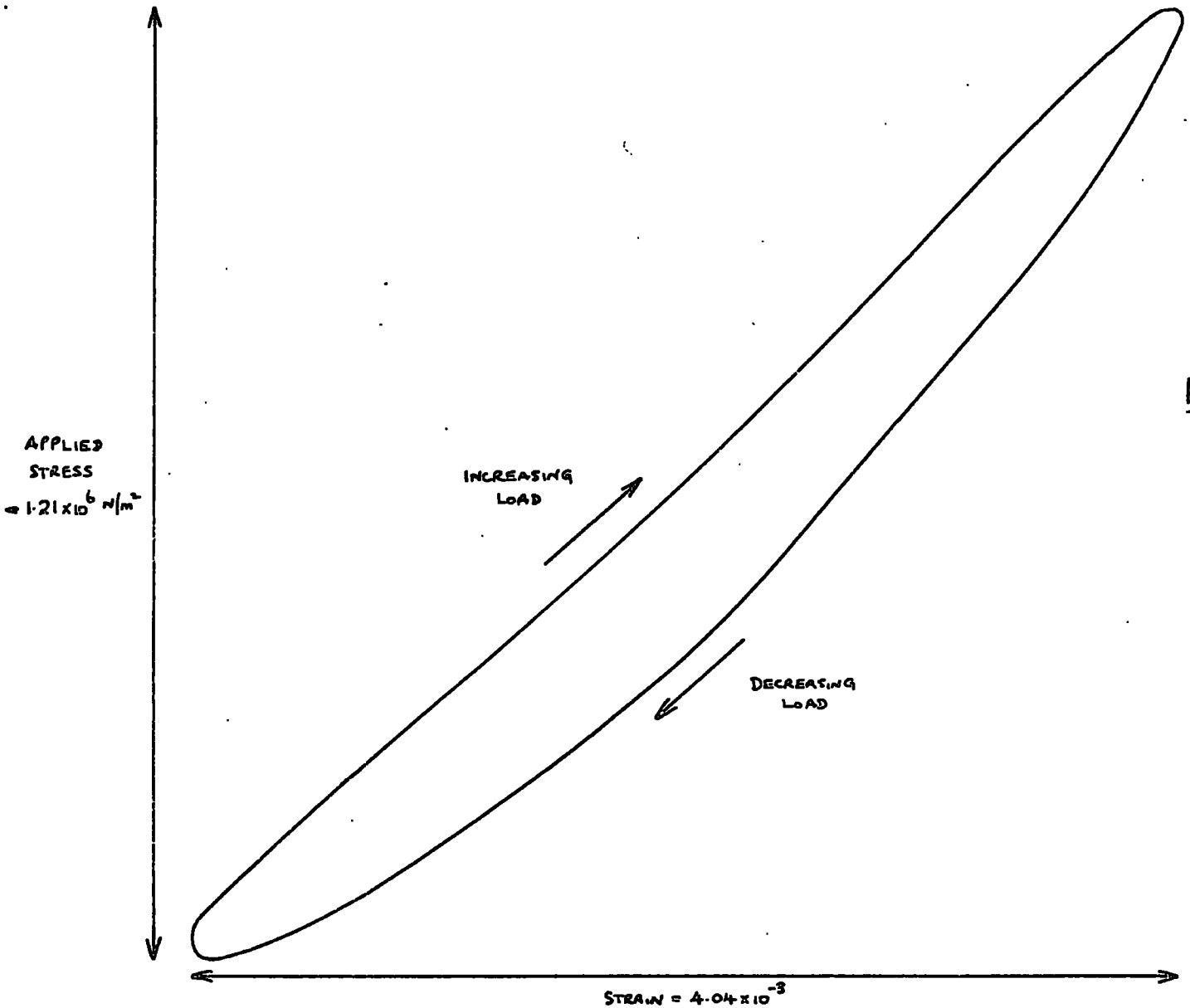

FIGURE 44: HYSTERESIS LOOP FOR SINUSOIDAL OSCILLATION OF CONFINED ARTICULAR CARTILAGE

FIGURE 45: HYSTERESIS LOOP FOR SINUSOIDAL OSCILLATION OF CONFINED RUBBER.

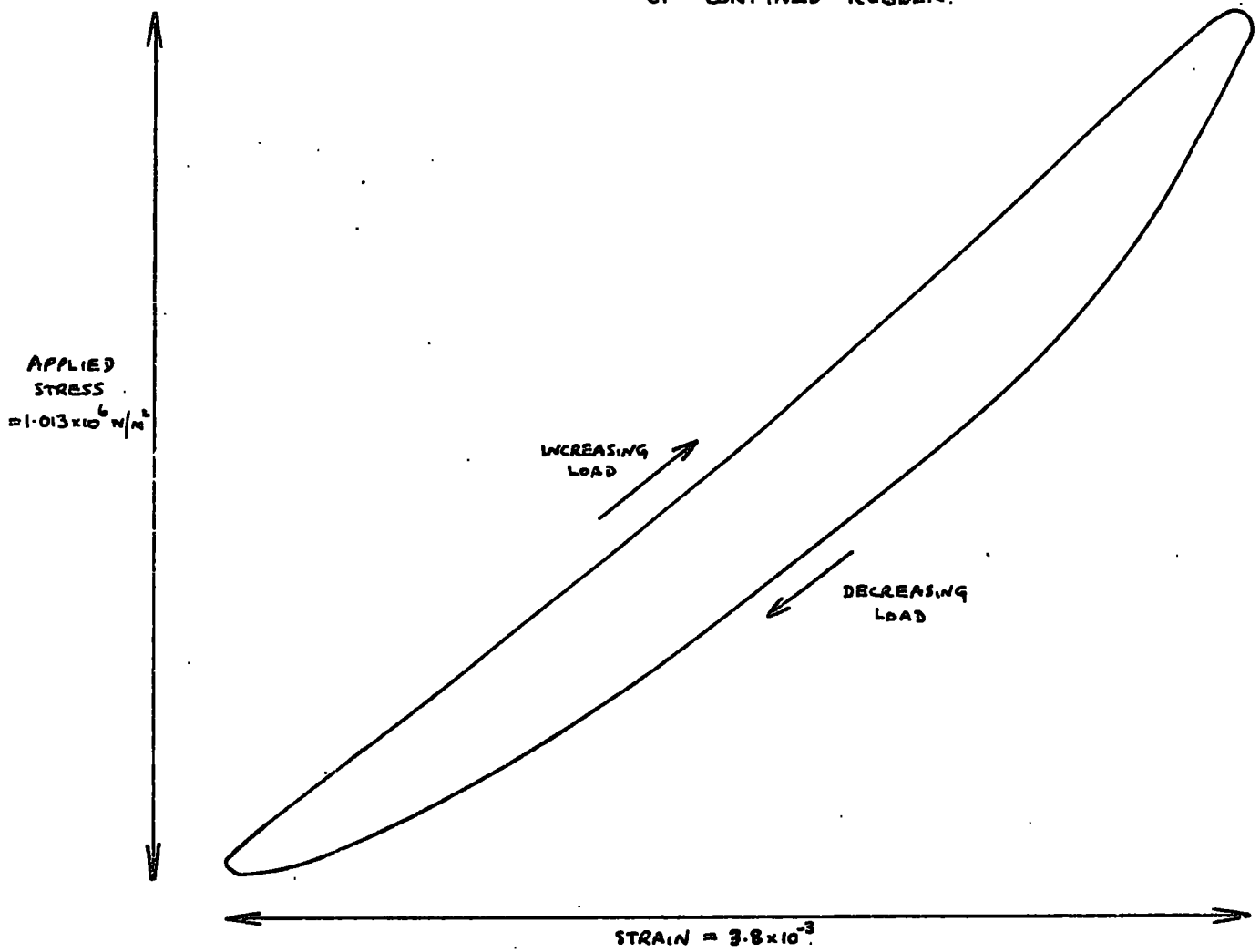

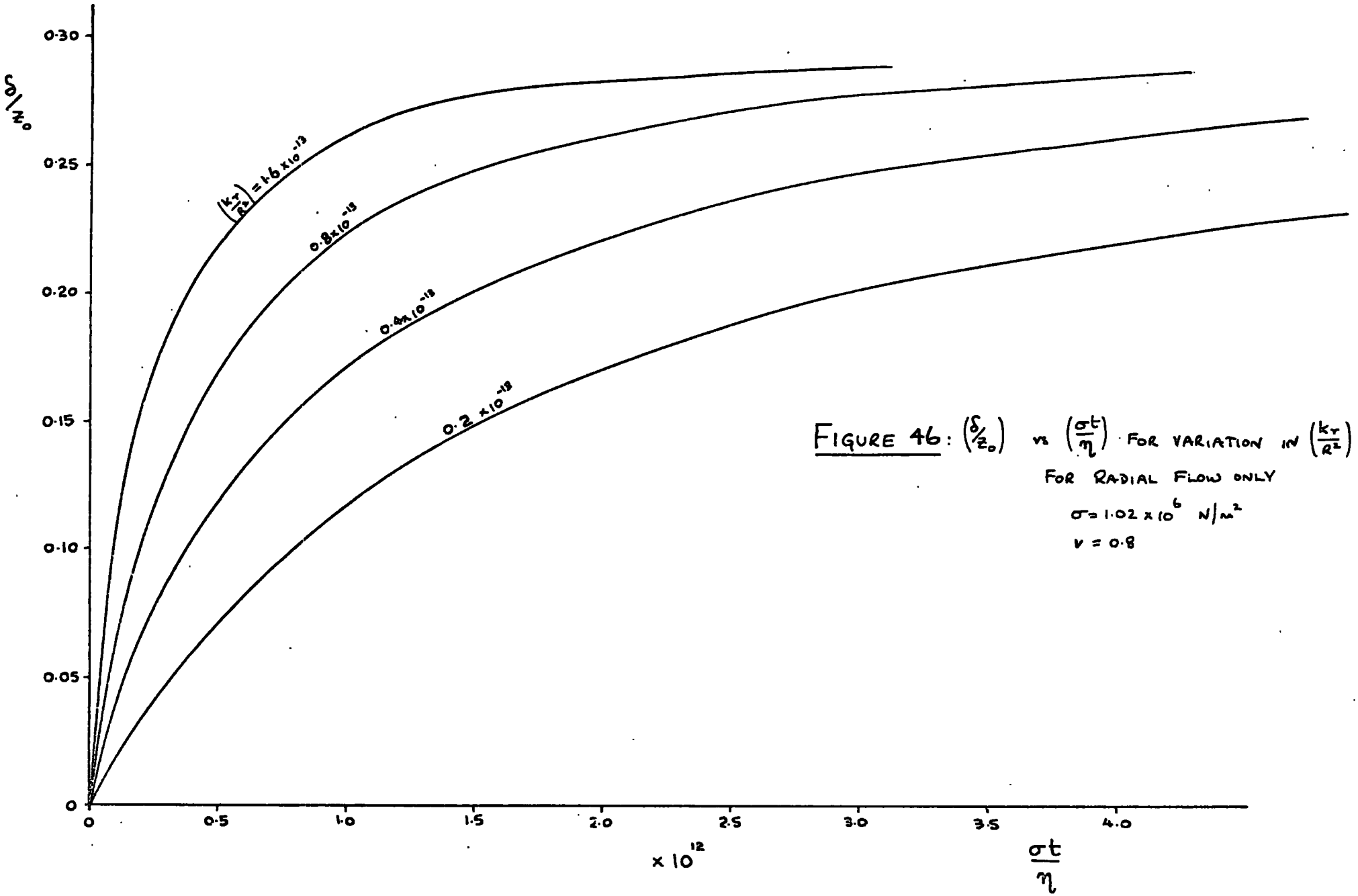

FIGURE 46: $\left(\frac{\delta}{z_0}\right)$ vs $\left(\frac{\sigma t}{\eta}\right)$ FOR VARIATION IN $\left(\frac{k_T}{R^2}\right)$

FOR RADIAL FLOW ONLY

$\sigma = 1.02 \times 10^6$ N/m²

$\nu = 0.8$

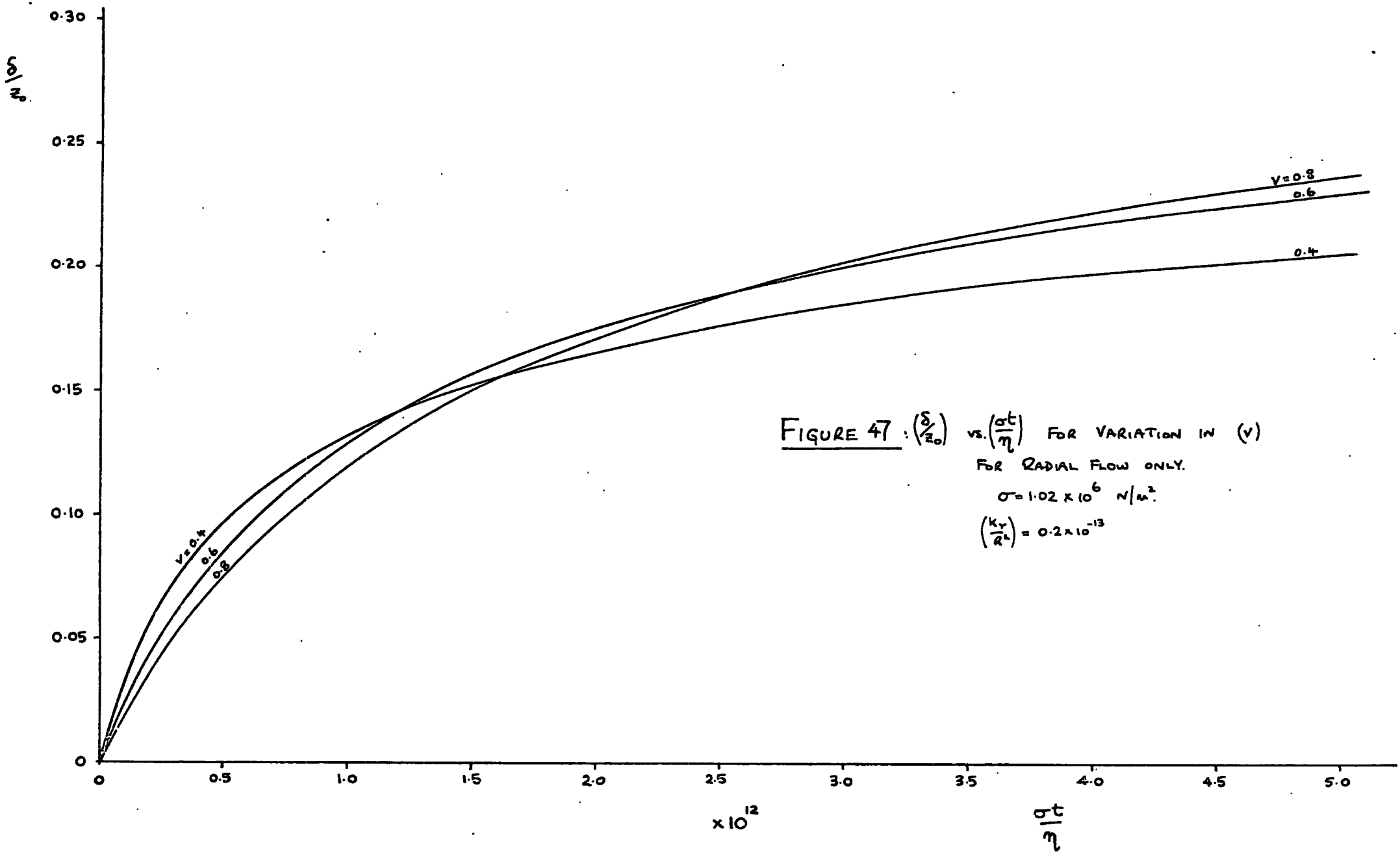

FIGURE 47 : $\left(\frac{\delta}{z_0}\right)$ vs. $\left(\frac{\sigma t}{\eta}\right)$ FOR VARIATION IN (V)
FOR RADIAL FLOW ONLY.
$\sigma = 1.02 \times 10^{6}$ N/m².
$\left(\frac{k_r}{R^2}\right) = 0.2 \times 10^{-13}$

FIGURE 48: STRAIN VS. TIME FOR RADIAL FLOW ONLY, SHOWING RELEASE OF LOAD.

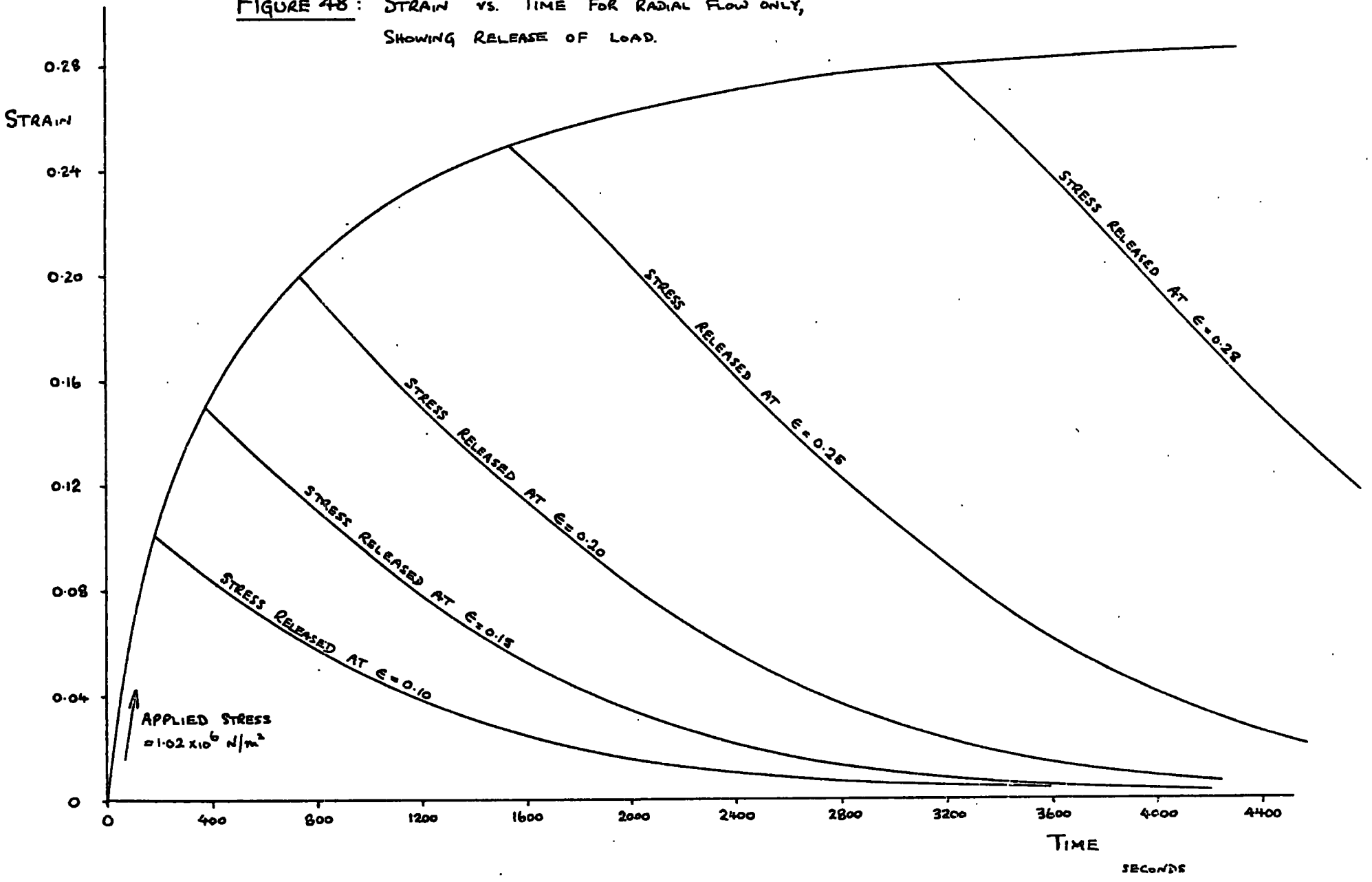

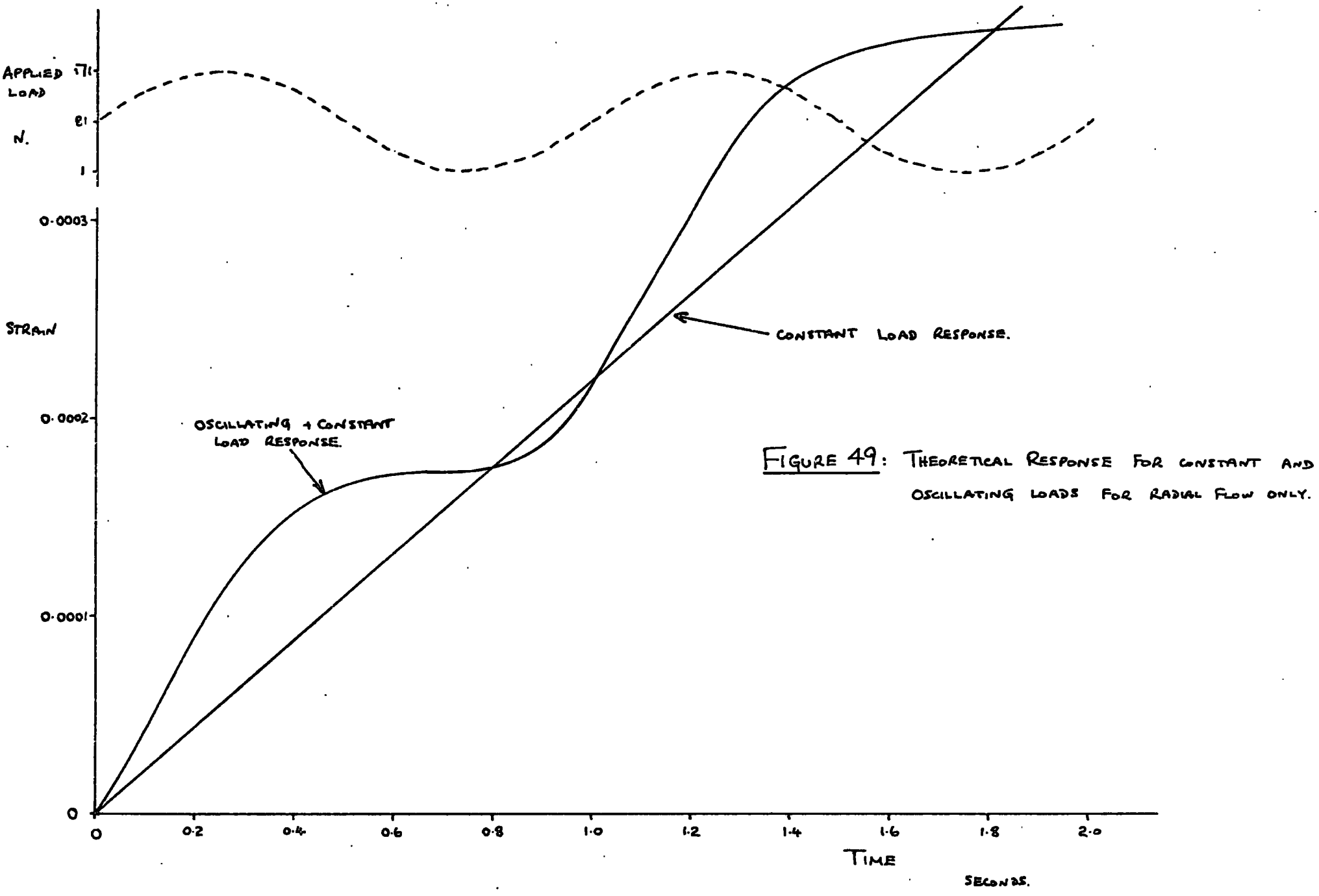

FIGURE 49: THEORETICAL RESPONSE FOR CONSTANT AND OSCILLATING LOADS FOR RADIAL FLOW ONLY.

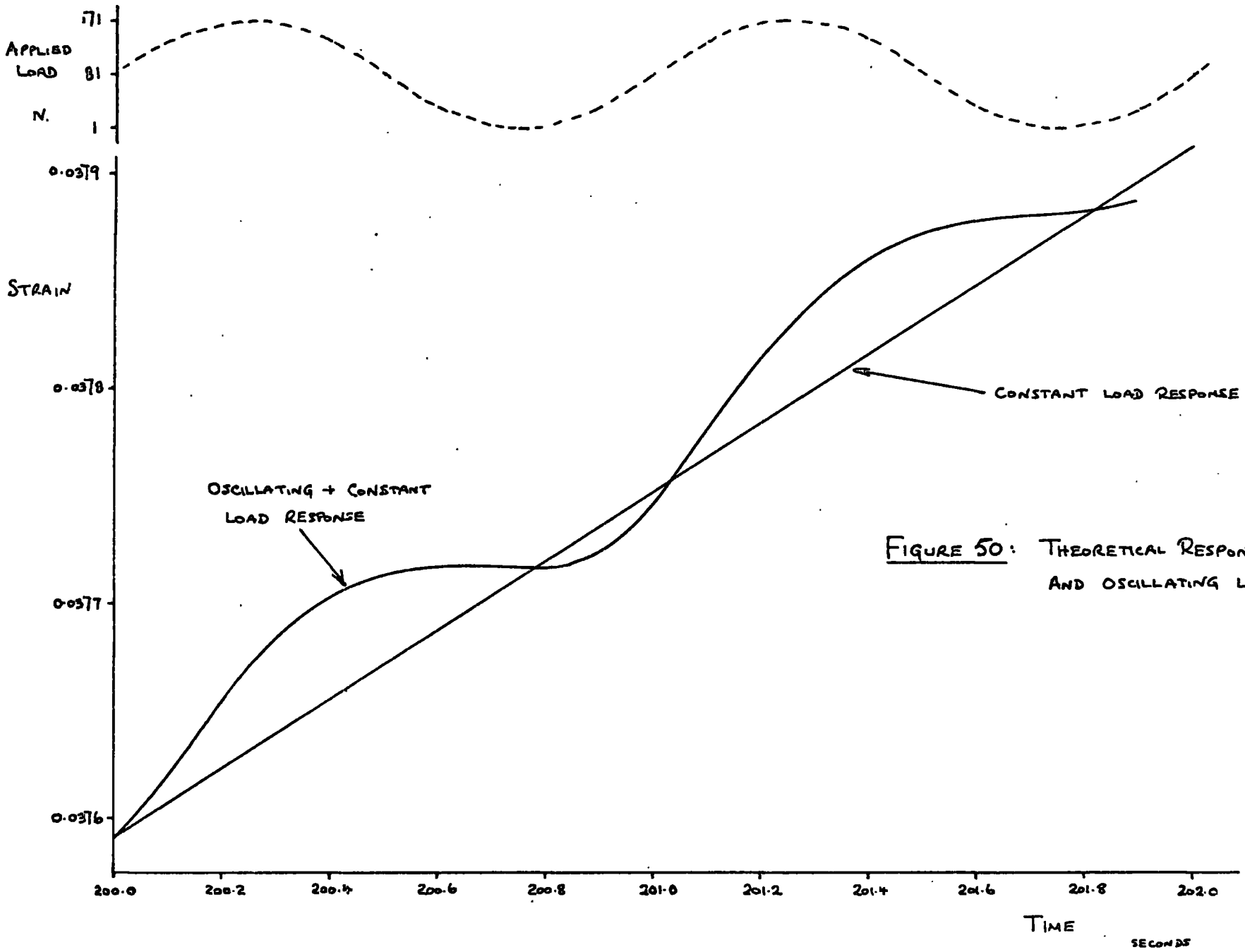

FIGURE 50: THEORETICAL RESPONSE FOR CONSTANT AND OSCILLATING LOADS FOR RADIAL FLOW ONLY.

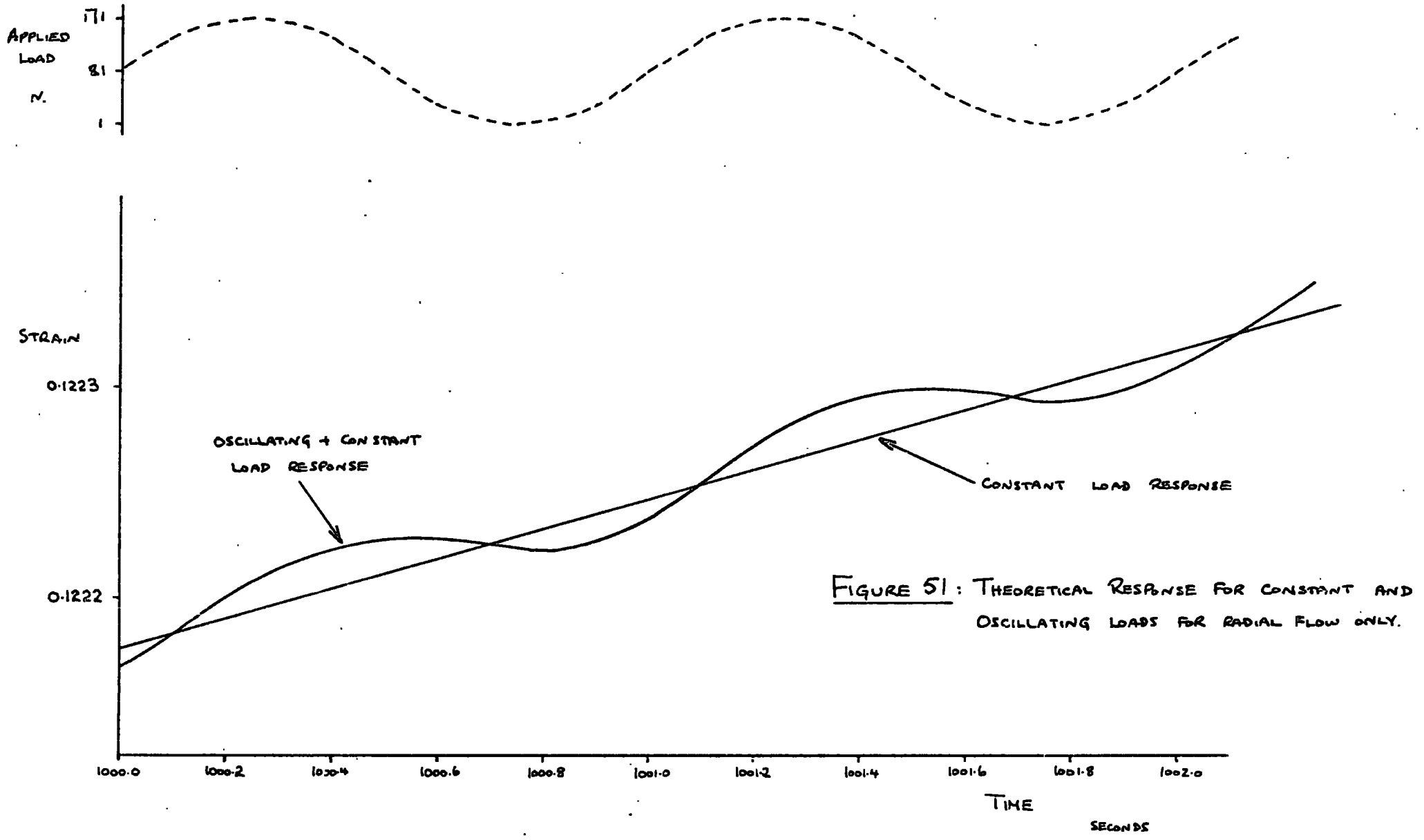

FIGURE 51: THEORETICAL RESPONSE FOR CONSTANT AND OSCILLATING LOADS FOR RADIAL FLOW ONLY.

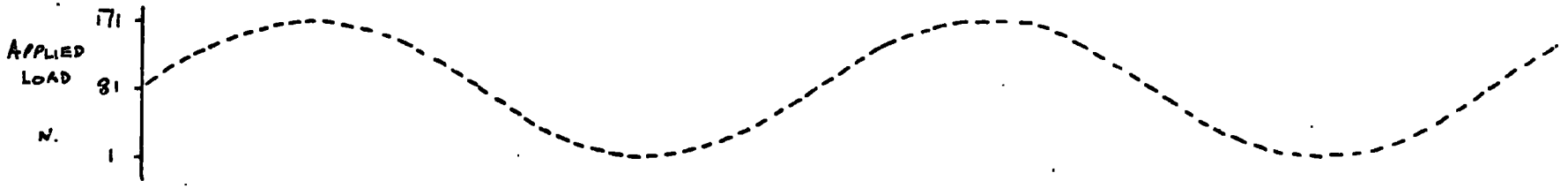

FIGURE 52: THEORETICAL RESPONSE FOR CONSTANT AND OSCILLATING LOADS FOR RADIAL FLOW ONLY.

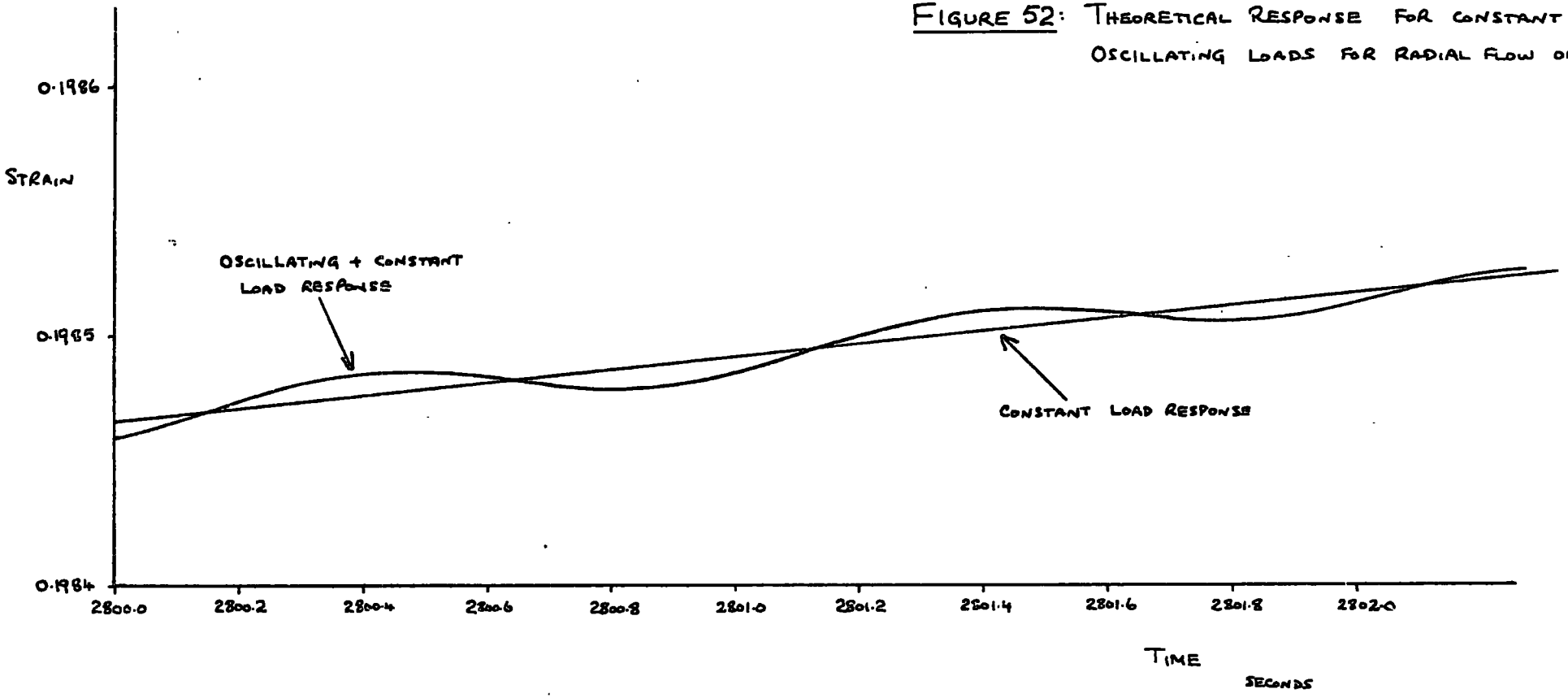

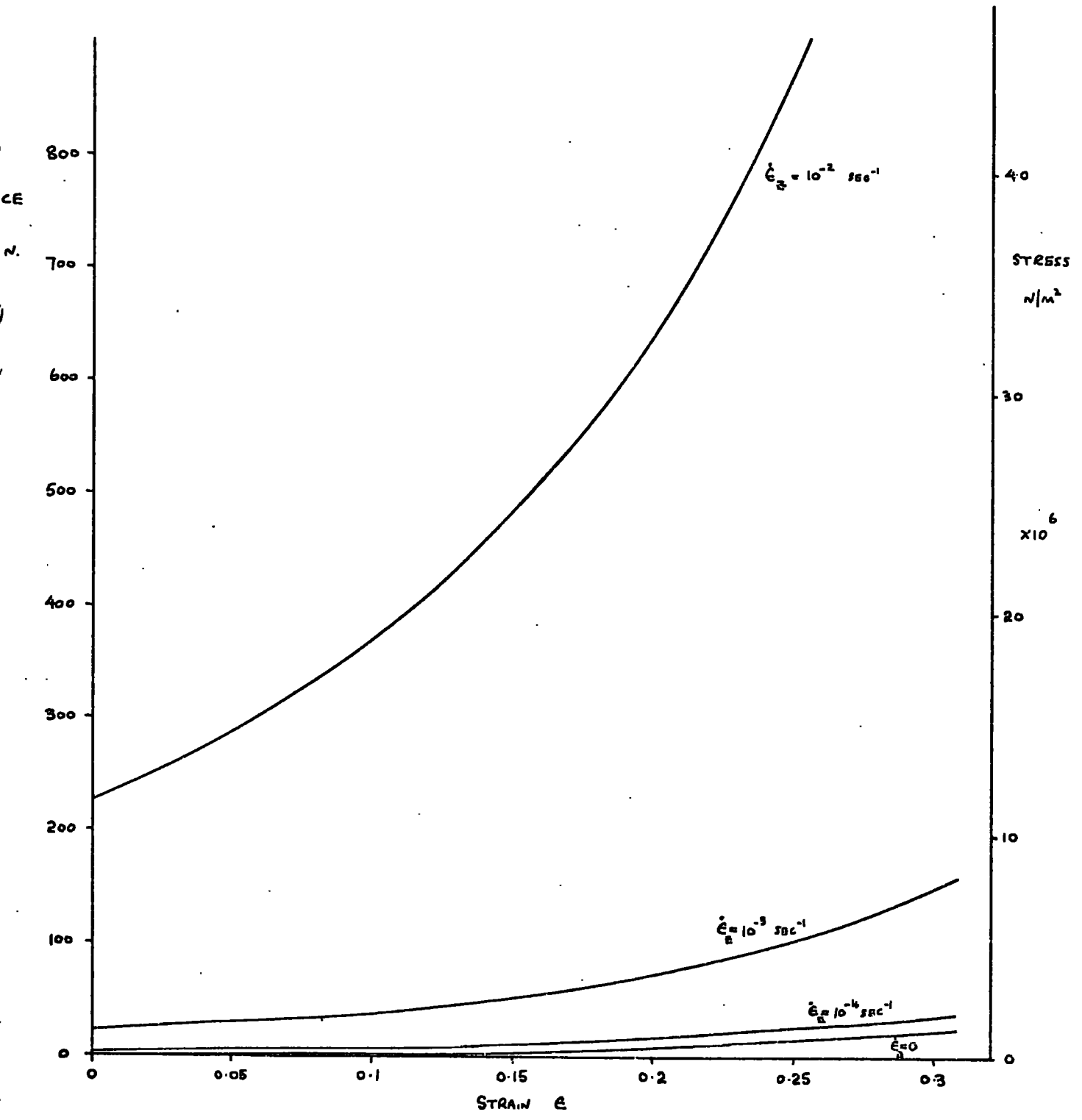

FIGURE 53: VARIATION OF FORCE WITH DEFLECTION FOR CONSTANT STRAIN RATE RADIAL FLOW ONLY.

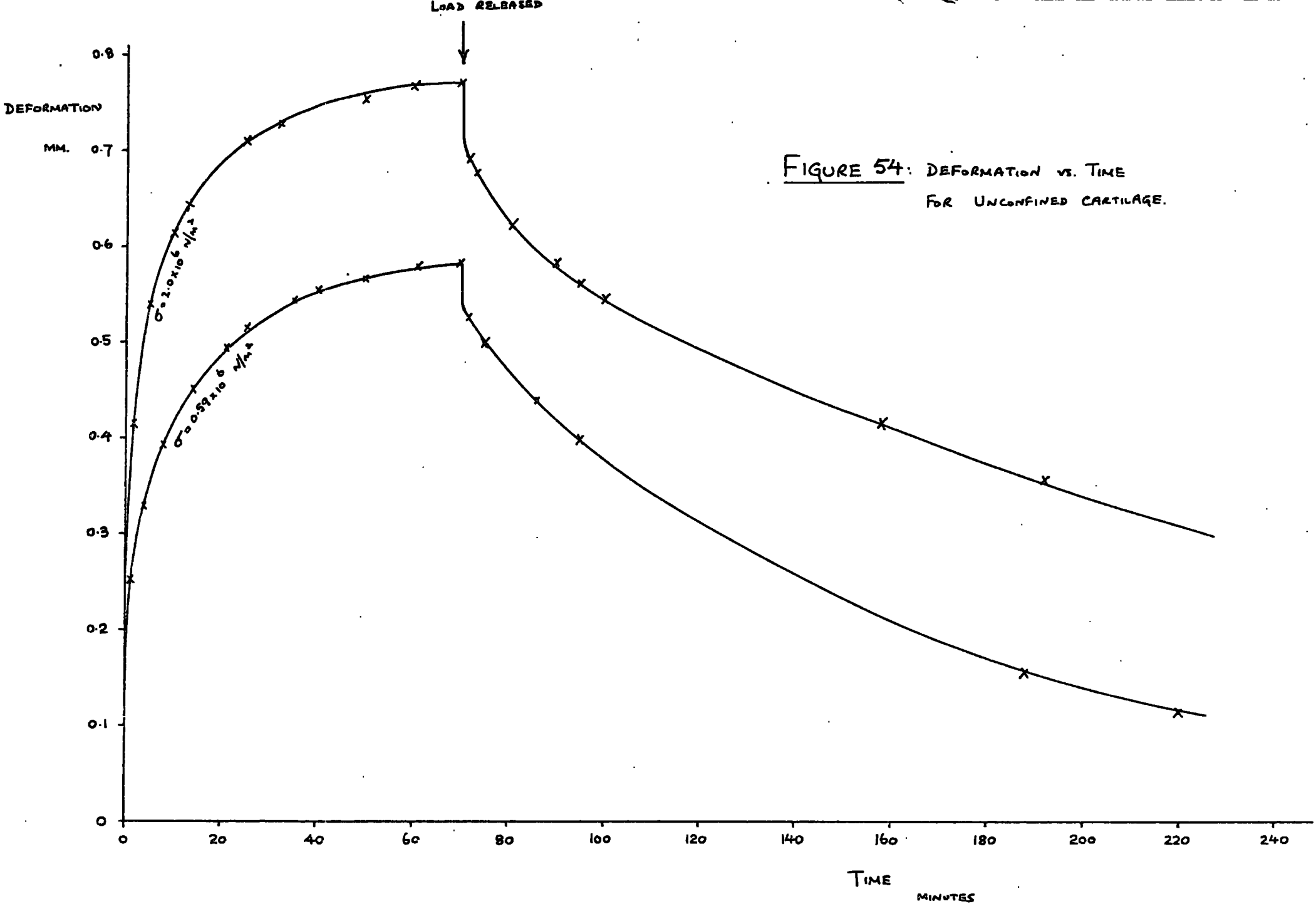

FIGURE 54: DEFORMATION VS. TIME FOR UNCONFINED CARTILAGE.

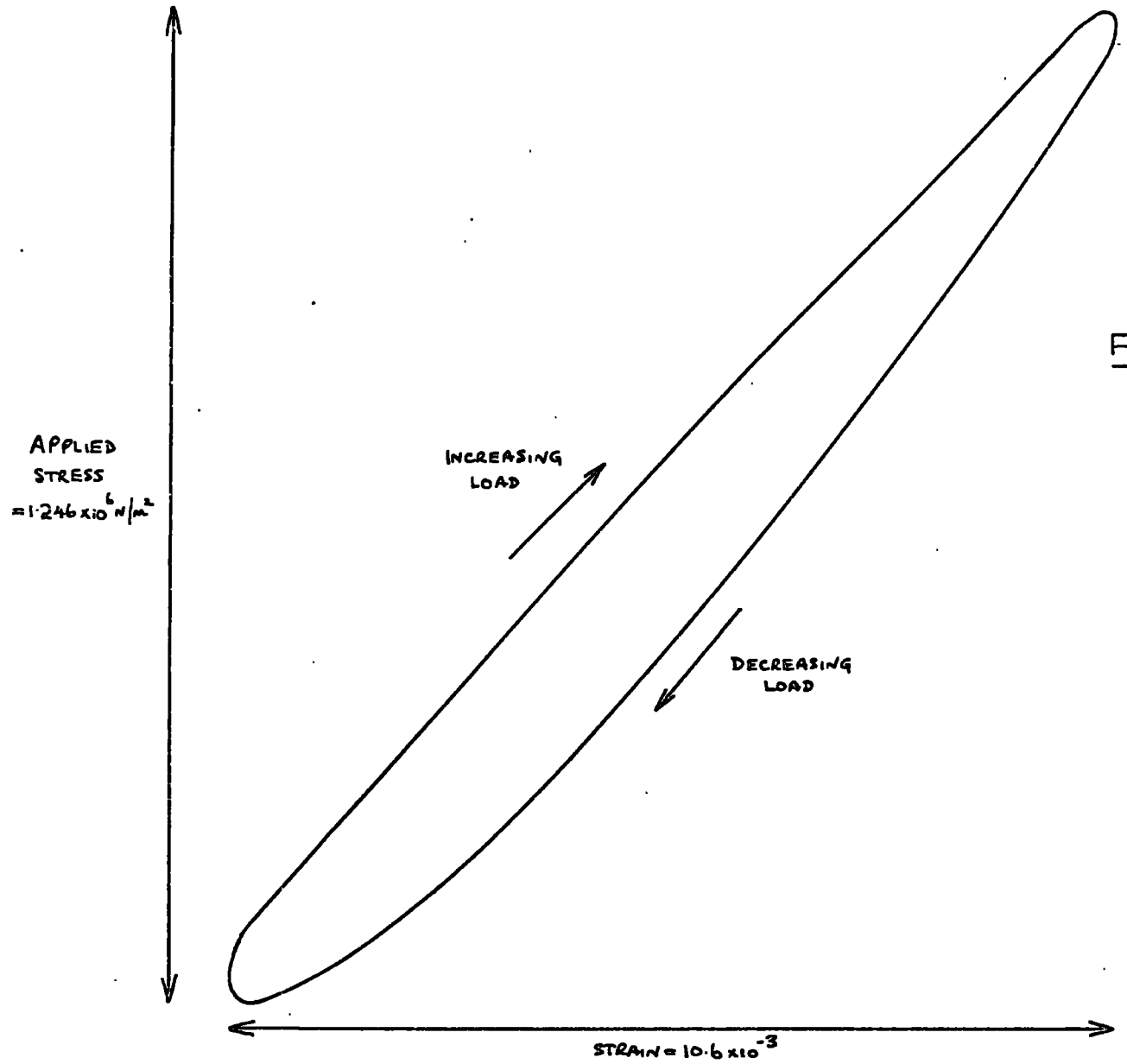

FIGURE 55: HYSTERESIS LOOP FOR SINUSOIDAL OSCILLATION OF UNCONFINED ARTICULAR CARTILAGE

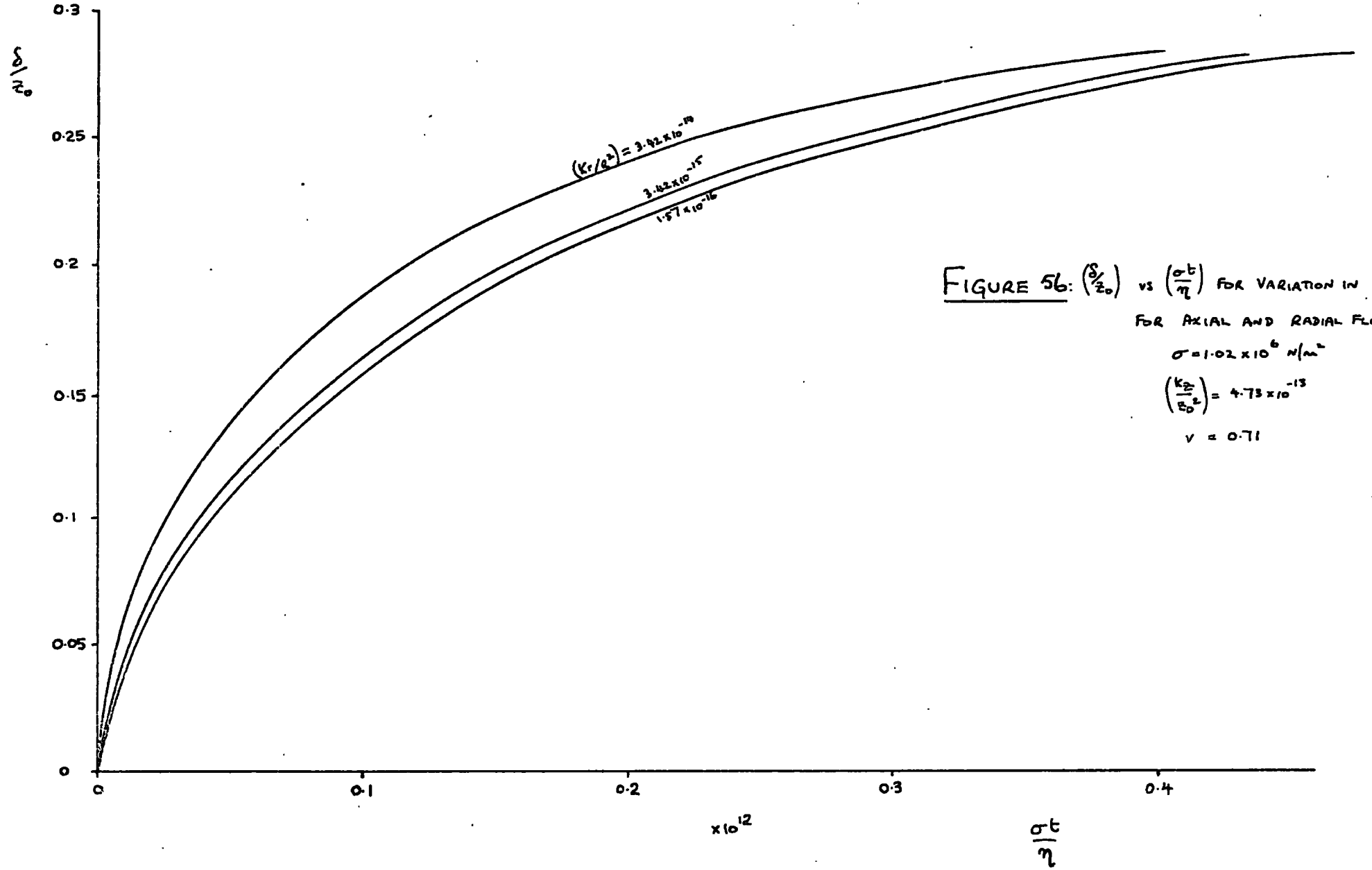

FIGURE 56: (δ/z_0) vs $(\sigma t/\eta)$ FOR VARIATION IN (K_r/R^2)

FOR AXIAL AND RADIAL FLOW

$\sigma = 1.02 \times 10^6$ N/m²

$\left(\frac{k_z}{z_0^2}\right) = 4.73 \times 10^{-13}$

$\nu = 0.71$

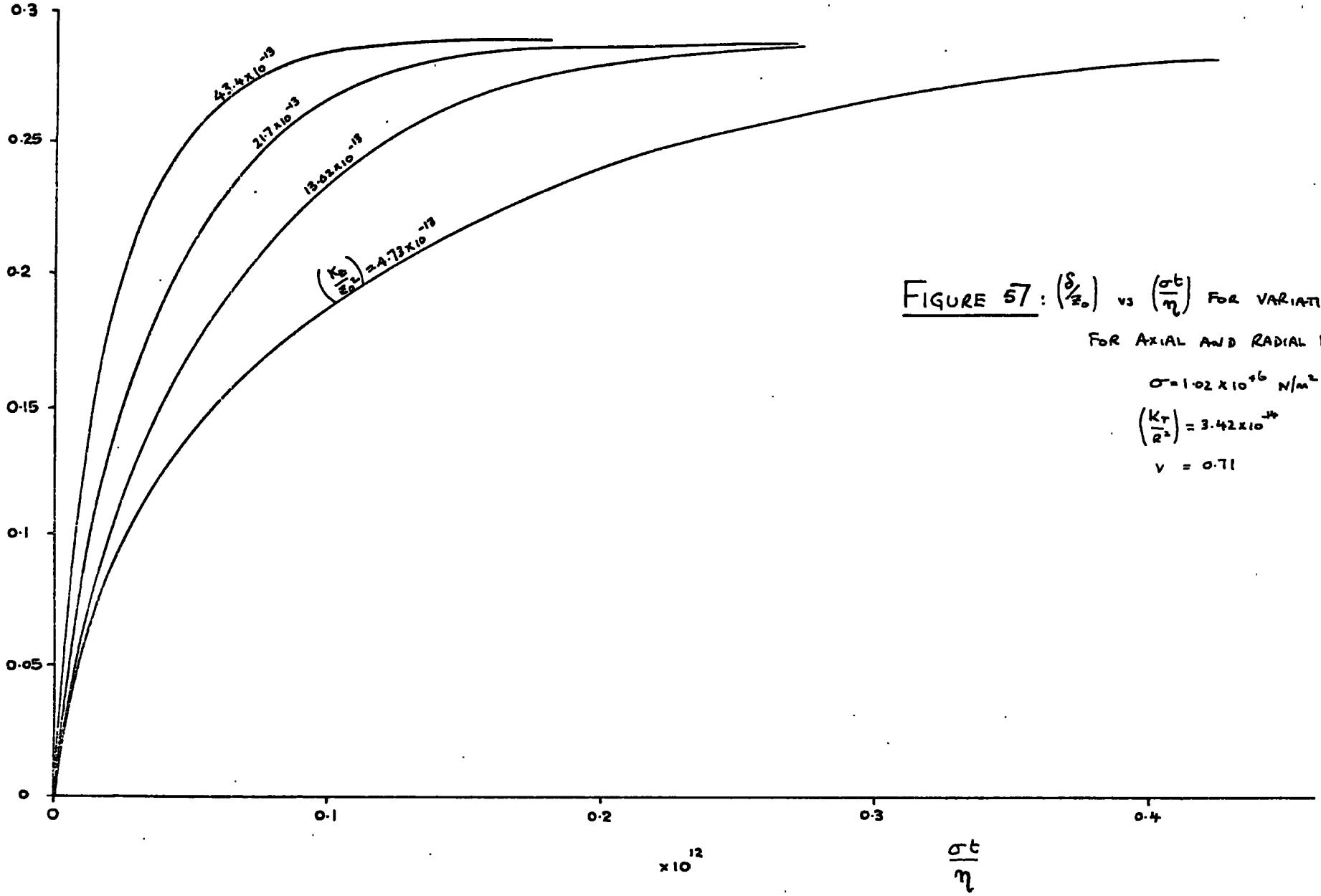

FIGURE 57 : $\left(\frac{\delta}{z_0}\right)$ VS $\left(\frac{\sigma t}{\eta}\right)$ FOR VARIATION IN $\left(\frac{K_0}{z_0^2}\right)$

FOR AXIAL AND RADIAL FLOW

$\sigma = 1.02 \times 10^{+6}$ N/m^2

$\left(\frac{K_T}{R^2}\right) = 3.42 \times 10^{-14}$

$\nu = 0.71$